Engineering a [NiFeSe] Hydrogenases for an efficient hydrogen production

Sónia Alexandra dos Santos Zacarias

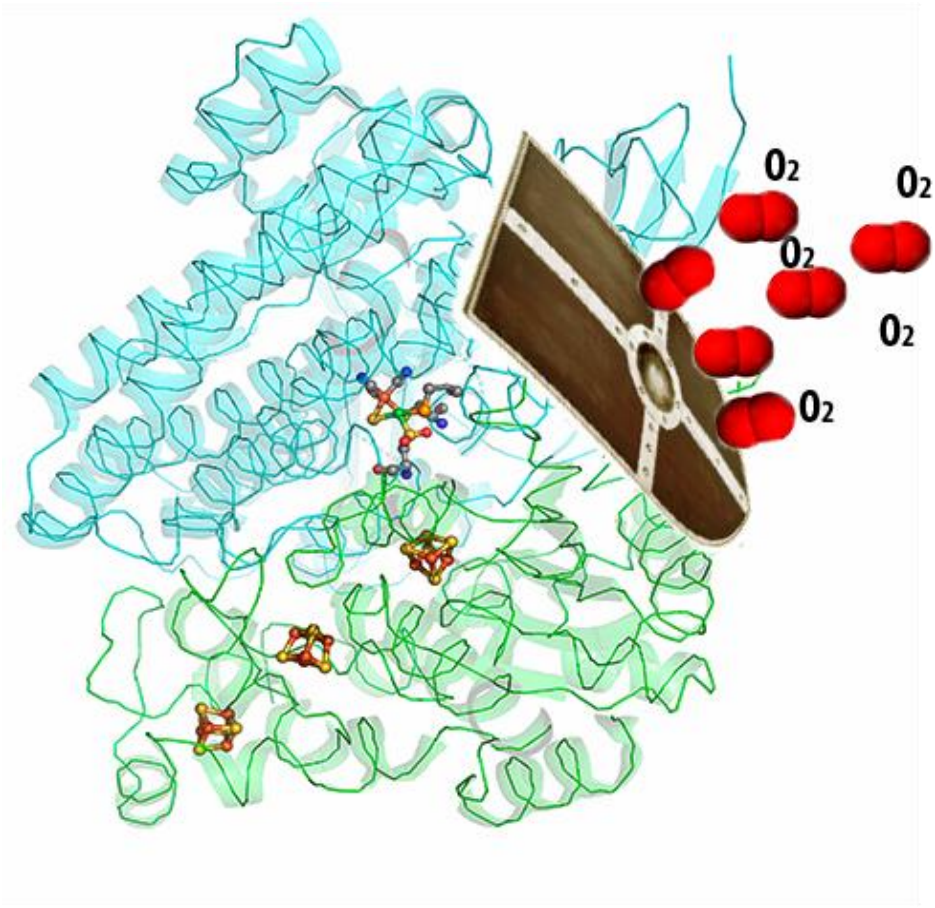

Dissertation presented to obtain the Ph.D degree in Biochemistry

Instituto de Tecnologia Química e Biológica António Xavier | Universidade Nova de Lisboa

Oeiras,
November, 2019

Engineering a [NiFeSe] Hydrogenase for an efficient hydrogen production

Sónia Alexandra dos Santos Zacarias

Dissertation presented to obtain the Ph.D degree in Biochemistry

Instituto de Tecnologia Química e Biológica António Xavier
Universidade Nova de Lisboa

Oeiras, 7th of November 2019

The work presented in this thesis was carried out under the ITQB PhD program at the Instituto de Tecnologia Química e Biológica António Xavier (ITQB NOVA) from Universidade Nova de Lisboa under the supervision of Doctor Inês Cardoso Pereira and Doctor Pedro M. Matias. This work was supported by the PhD fellowship SFRH/BD/100314/2014 from the Fundação para a Ciência e Tecnologia (FCT).

“We are the representatives of the cosmos; we are an example of what hydrogen atoms can do, given 15 billion years of cosmic evolution”.

Carl Sagan

ACKNOWLEDGEMENTS

First, I want to thank my supervisors for integrating me in this great project, for all the availability throughout the years and for the great team spirit. Dra Inês Pereira is an inspiration as a successful portuguese scientist woman, who transmitted to her students a scientific accurate and demanding behavior. To her, a big thanks for all the knowledge and advice, for the friendship and support and for the trust deposited in me. Dr Pedro Matias, for all the support, guidance, kindness throughout the year. For being a demanding and friendly supervisor who as always available. For the enjoyable and pedagogical company in all the synchrotron trips and for all the help with the structural data.

During the course of the PhD the lab was a place of hard work and a place of sharing ideas, experiences and emotions. I was lucky to have very nice labmates to go along in this journey, that made this experience a very joyful one. To Ana Rita Oliveira, for all the speak load ideas, for all the scientific discussion, for all the deep conversations and comprehension. To Cláudia Mourato for the friendship, change of ideas and good vibes. For Mónica Martins for her friendship, tolerance and familiarity. For Margarida Coito, for her energy, desire to learn and for being who she is. To Américo Duarte, for being the funniest person, for all the teaching about traditional portuguese sayings and for all the great scientific discussion. To Delfim Ferreira, who shares with me the great taste of listening music from “death people”, thanks to his good mood and support. To Sofia Venceslau for all the teachings and friendship. To all the others, with whom I shared important moments, Gonçalo Oliveira, Ana Barbosa, Carla Mateus, Marta Marques, Renato Domingos.

To my parents for all the support and comprehension.

And because my words might be insufficient to express my deep feeling of gratitude, I dedicate to all the mentioned people and to my close friends, these words of the portuguese writer António Lobo Antunes:

“Sempre achei que a grandeza dos outros aumentava o meu tamanho: muito obrigado por me terem dado alguns centímetros a mais. Agora vejo mais longe”.

PUBLICATIONS

Zacarias S, Temporão A, Carpentier P, Pereira I A C, Matias P M. krypton and oxygen pressurized crystals of a [NiFeSe] hydrogenase reveal gas access routes to the active site. *In preparation*

Zacarias S, Temporão A, del Barrio M, Fourmond V, Léger C, Matias P M & Pereira I A C. (**2019**). A hydrophilic channel is involved in oxidative inactivation of a [NiFeSe] hydrogenase. 9, 9, 8509-8519. *ACS Catalysis* 10.1021/acscatal.9b02347

Zacarias S, Vélez M, Pita M, De Lacey A, Matias P M & Pereira I A C. (**2018**) Characterization of the [NiFeSe] hydrogenase from *Desulfovibrio vulgaris* Hildenborough.613: 169-201 *Methods in Enzymology*. 10.1016/bs.mie.2018.10.003

Additional Publications Not Included In This Thesis

Zhao F, Wang P, Ruff A, Hartmann V, **Zacarias S**, Pereira I A. C, Nowaczyk M M, Rogner M, Conzuelo F & Schuhmann W (**2019**). A photosystem I monolayer with anisotropic electron flow enables Z-scheme like photosynthetic water splitting. *Energy & Environmental Science.* 12, 3133-3143. 10.1039/C9EE01901D

Szczesny J, Marković N, Conzuelo F, **Zacarias S**, Pereira I A C, Lubitz W, Plumeré N, Schuhmann W & Ruff A. (**2018**). A gas breathing hydrogen/air biofuel cell comprising a redox polymer/hydrogenase-based bioanode. *Nature Communications, 9* (1), 4715. 10.1038/s41467-018-07137-6

Ruff A, Szczesny J, Marković N, Conzuelo F, **Zacarias S**, Pereira I A C, Lubitz W & Schuhmann W. (**2018**). A fully protected hydrogenase/polymer-based bioanode for high-performance hydrogen/glucose biofuel cells. *Nature Communications, 9* (1), 3675. 10.1038/s41467-018-06106-3

Ruff A, Szczesny J, **Zacarias S**, Pereira I A C, Plumeré N & Schuhmann W. (**2017**) Protection and Reactivation of the [NiFeSe] Hydrogenase from Desulfovibrio vulgaris Hildenborough under Oxidative Conditions. *ACS Energy Letters*. 2, 5, 964-968. 10.1021/acsenergylett.7b00167

Tapia C, **Zacarias S**, Pereira I A C, Conesa J C, Pita M, De Lacey A. (**2016**). In Situ Determination of Photobioproduction of H2 by In2S3-[NiFeSe] Hydrogenase from Desulfovibrio vulgaris Hildenborough Using Only Visible Light. *ACS Catalysis*. 6,9, 5691-5697. 10.1021/acscatal.6b01512

Gutiérrez-Sanz Ó, Natale P, Márquez I, Marques M, **Zacarias S**, Pita M, Pereira I, López-Montero I, De Lacey A & Vélez M. (**2016**). H2-fueled ATP synthesis on an electrode: Mimicking cellular respiration. *Angewandte Chemie - International Edition*. 17, 55 (21): 6216 – 6220. 10.1002/anie.201600752

Gutiérrez-Sanz Ó, Tapia C, Marques M, **Zacarias S**, Vélez M, Pereira I A C & De Lacey, Antonio L. (**2015**). Induction of a Proton Gradient across a Gold-Supported Biomimetic Membrane by Electroenzymatic H_2 Oxidation. *Angewandte Chemie - International Edition*, 23, 54 (9): 2684-2687 . 10.1002/anie.201411182

THESIS ABSTRACT

Hydrogen is often described as a potential energy vector because it is a clean burning fuel with high energy density, which might help to reduce the consumption of fossil fuels and consequential global warming. However, the current processes for production hydrogen require fossil fuels, high temperatures and precious-metal catalysts, raising concern about the economic and ambiental viability of what could be the future "hydrogen economy". However, Nature has developed a special class of metalloenzymes called hydrogenases that are capable of catalyzing hydrogen production and oxidation. Hydrogenases are enzymes that contain only earth-abundant transition metals, function at ambient temperatures and pressures with low overpotential, exhibit stable catalytic activity, and can utilize water-derived protons for the synthesis of hydrogen with high turnover frequencies. Their unparalleled catalytic efficiency makes them suitable biocatalysts to use in hydrogen production devices, fuel cell technologies and also as inspiration models for the design of synthetic molecular catalysts. However, there are limitations to the use of hydrogenases, namely their high oxygen sensitivity. There are three main classes of hydrogenases: [FeFe], [NiFe] and [Fe] hydrogenases. The [NiFe] hydrogenases are the most well studied group, and they generally function in nature as hydrogen oxidation catalysts allowing hydrogen to be used as an energy source for microorganisms. Despite being sensitive to oxygen, they exhibit reversible inactivation after exposure. There are several nonstandard [NiFe] hydrogenases that exhibit favorable characteristics, including a degree of oxygen tolerance or a bias towards hydrogen production. The [NiFeSe] hydrogenases are one of these non-standard [NiFe] hydrogenases, which contain a selenocysteine residue as a terminal ligand to the nickel center, in place of a cysteine residue found in the [NiFe] hydrogenases. The [NiFeSe] hydrogenase from *Desulfovibrio vulgaris* Hildenborough, a sulfate reducing bacterium, is the focus of this thesis, since it has very high catalytic activities and some degree of oxygen tolerance, and was already applied with success in hydrogen converting devices. However, several oxygen modifications are found in the protein structure after exposure to O_2, the more dramatic one being an irreversible

oxidation of cysteine 75, a terminal nickel cysteine ligand, which we aimed to prevent. The work presented in this thesis focused on understanding the molecular basis of oxygen diffusion and reactivity in this hydrogenase, aiming to identify key structural elements that might be used to further improve its oxygen tolerance. In chapter I an introduction on the current knowledge of hydrogenase is presented. In chapter II, an overview of the techniques employed to characterize the [NiFeSe] hydrogenase from *Desulfovibrio vulgaris* Hildenborough is described. In chapter III is present the creation of [NiFeSe] hydrogenase variants that constrict a hydrophilic channel that connects the protein surface to cysteine 75 is reported, which led to more oxygen tolerant variants. In chapter IV a study of gas diffusion in the [NiFeSe] hydrogenase was performed, with krypton and oxygen pressurization techniques of protein crystals. Experiments with other [NiFeSe] hydrogenase variants are presented in chapter V. Chaper VI consist on the final conclusion.

RESUMO DA TESE

O hidrogénio é frequentemente descrito como um potencial vector energético pois é um combustível com uma combustão limpa e com elevada densidade energética. Contudo, os processos actualmente usados para produzir hidrogénio necessitam de combustíveis fósseis, temperaturas elevadas e catalisadores feitos de metais raros e preciosos, estes aspectos põem em causa, em termos da sua viabilidade económica e ambiental, o que poderá ser a futura "economia baseada em hidrogénio". Contudo, a Natureza desenvolveu uma classe especial de metaloenzimas designadas por hidrogenases, que têm a capacidade de catalisar tanto a produção como a oxidação de hidrogénio. As hidrogenases são enzimas que contêm como cofactores apenas metais de transição abundantes na crosta terrestre, funcionam à pressão e temperatura ambiente com baixas necessidades energéticas, têm uma estável actividade catalítica e conseguem utilizar protões vindos da água para a síntese de hidrogénio. Não obstante, as hidrogenases também têm limitações, nomeadamente serem muito sensíveis ao oxigénio. Existem três classes principais de hidrogenases: as hidrogenases de [FeFe], de [NiFe] e de [Fe]. O grupo das hidrogenases de [NiFe] é o mais estudado. Estas hidrogenases funcionam geralmente na natureza como biocatalisadores que oxidam hidrogénio, permitindo assim que este seja usado como fonte de energia para os microrganismos. Apesar de serem sensíveis ao oxigénio, a inactivação causada por este é reversível. Existem várias hidrogenases de [NiFe] que fogem ao padrão no que respeita a sensiblidade ao oxigénio, pois têm-lhe alguma tolerância. Adicionalmente também fogem ao padrão pois catalisam preferencialmente a via da produção do hidrogénio. As hidrogenases de [NiFeSe] são uma subclasse especial que pertence ao grupo das hidrogenases de [NiFe]. As hidrogenases de [NiFeSe] contêm uma selenocisteína como resíduo terminal ligado ao níquel no centro activo, em vez de terem uma cisteína como se verifica nas hidrogenases de [NiFe]. A hidrogenase de [NiFeSe] do *Desulfovibrio vulgaris* Hildenborough, uma bactéria reductora de sulfato, é o foco desta tese, uma vez que tem elevada actividade catalítica e algum grau de tolerância ao oxigénio, já tendo sido usada como biocatalisador em dispositivos que convertem hidrogénio. Todavia,

existem modificações oxidativas ao nível da estrutura da proteína causadas pelo oxigénio, sendo a mais dramática uma oxidação irreversível na cisteína 75, cisteína que se encontra ligada ao níquel no centro activo. O objectivo deste trabalho foi compreender e prevenir esta oxidação. Foca-se em compreender as bases moleculares de difusão e reactividade do oxigénio na hidrogenase e assim identificar importantes elementos estruturais que possam ser usados para melhorar a tolerância desta hidrogenase ao oxigénio. O capítulo I consiste numa introdução relativa ao conhecimento actual na área das hidrogenases. O capítulo II, apresenta uma revisão das técnicas usadas para caracterizar a hidrogenase de [NiFeSe] do microrganismo *Desulfovibrio vulgaris* Hildenborough. O capítulo III descreve a criação de variantes desta hidrogenase, que contêm uma constrição no canal hidrofílico que conecta a superfície da proteína à cisteína 75, sendo estes variantes mais tolerantes ao oxigénio. No capítulo IV é apresentado um estudo sobre a difusão de gases na hidrogenase de [NiFeSe], através da pressurização de cristais de proteína com krípton e oxigénio. Experiências com outros variantes da hidrogenase de [NiFeSe] são apresentados no capítulo V. O capítulo VI apresenta as conclusões finais.

ABBREVIATIONS:

A. aeolicus - *Aquifex aeolicus*

AFM - Atomic Force Microscope

AH - Actinobacterial hydrogenase

BSA - Bovine Serum Albumin

D. vulgaris Hildenborough - *Desulfovibio vulgaris* Hildenborough

DDM - n-Dodecyl β-D-maltoside

Dm baculatum - *Desulfomicrobium baculatum*

DLS - Diamond Light Source

E. coli - *Escherichia coli*

EPR - Electron Paramagnetic Resonance

ESRF - European Synchrotron Radiation Facility

FTIR - Fourier-transform infrared spectroscopy

GC – Gas Chromatography

Hm - *Hydrogenovibrio marinus*

IR - Infrared

kDa – kilodalton

MBH - O_2-tolerant membrane bound hydrogenase

MCT - Mercury Cadmium Telluride

Methenyl-H_4MPT^+ - Methenyltetrahydromethanopterin

MV - Methyl Viologen

PCR - Polymerase Chain Reaction

PEG – Polietilenoglicol

PFE - Protein film electrochemical

PGE - Pyrolytic Graphite Edge

PSI - Photosystem I

PSII - Photosystem II

QCM - Quartz Crystal Microbalance

R. eutropha - *Ralstonia eutropha*

RH- Regulatory hydrogenases

ROS - Reactive oxygen species

SAM - Self-Assembled Monolayer

SB3-12 - Zwittergent SB3-12

SCE - Saturated Calomel Reference Electrode

SDS - Sodium Dodecyl Sulfate

SDS-PAGE - Sodium Dodecyl Sulfate-Polyacrylamide Gel Electrophoresis

Sec - Selenocysteine

Sec pathway - General Secretory Pathway

SEIRAS – Surface Enhanced Infrared Absorption Spectroscopy

SH - Soluble $NAD(P)^+$-Reducing hydrogenase

SHE – Standard Hydrogen Electrode

SLIC - sequence ligation independent cloning

TCD - Thermal Conductivity Detector

TpIc_3 - Periplasmic Type-I Cytochrome c_3

TLS – Translation Libration Screw

UV-Vis – Ultraviolet-Visible

4-ATP - 4-aminothiophenol

$[NiFeSe]_m$ hydrogenase - Membrane-associated form of the [NiFeSe] hydrogenase

$[NiFeSe]_r$ hydrogenase - Recombinant version of the soluble [NiFeSe] hydrogenase

$[NiFeSe]_s$ hydrogenase - Soluble native form of the [NiFeSe] hydrogenase

TABLE OF CONTENTS

CHAPTER I

INTRODUCTION

1. Energetic Context

Throughout history, humankind has been exploring natural resources on planet Earth. The trail paved up to modern times has been characterized by energy paradigm shifts. Thousands of years ago, wood was used as the main source of energy. The industrial revolution in the 18th century brought the era of **Fossil Fuels**.

Coal, **oil** and **natural gas** are fossil fuels formed by anaerobic decomposition of buried dead organisms, at high pressures and temperatures in the Earth's crust over millions of years. They are considered non-renewable resources of energy because their rate of formation is far too slower than the rate of their exploitation. (Hubbert 1990) Initially, coal was used predominantly to fuel the steam engine, later oil was used to fuel the internal combustion engine. Nowadays, natural gas consumption is increasing steadily with an expected peak by 2050 (Miranda 2019). All three are still supplying most of the world's energy needs nowadays (Dresselhaus et al. 2001; Coyle et al. 2014; Miranda 2019).

The main problem with fossil fuels is that they all produce carbon dioxide upon combustion; natural gas in less extent, coal in most. Carbon dioxide plus methane and nitrous oxide are the main greenhouse gases. Greenhouse gases can absorb and emit radiation within the infrared (IR) range, trapping significant heat that is warming the planet. The life span of greenhouse gases is diverse, 100 years for CO_2 and 15 years for CH_4 and N_2O (Coyle et al. 2014). Nowadays, the consumption of fossil fuels together with deforestation leads to the liberation of 7×10^{12} kg yr^{-1} of CO_2. Plants and oceans are the two main natural absorbers of CO_2. Plants can absorb 2×10^{12} kg yr^{-1} by photosynthesis and oceans have this same quantity of CO_2 dissolved on it. Therefore, there is a net increase of CO_2 in the atmosphere of approximately 3×10^{12} kg yr^{-1} (Züttel et al. 2010). The excessive burn of fossil fuels is depleting natural resources and causing climate change. Additionally, the global need for energy is predicted to grow in the coming decades, as the world's population is expected to go from about the 7 billion people of today to over 9 billion by 2050, plus the progressive industrialization of developing

nations. Such a scenario demands global efforts in the pursuit for alternative energy sources with a tolerable environmental impact.

2. Hydrogen as an Energy Carrier

The awareness about severe global warming and fossil fuel depletion has prompted an extensive focus on the pursuit of alternative and clean ways of producing and storing energy. Among the various options, hydrogen is regarded as a promising future **energy carrier** (US Department of Energy 2013; European Commission 2019).

The idea of H_2 as a fuel has fascinated humankind for centuries. This pioneering notion was expressed on the science-fiction novel *The Mysterious Island* by Jules Verne (1874): "I believe that water will one day be employed as fuel, that hydrogen and oxygen which constitute it, used singly or together, will furnish an inexhaustible source of heat and light of an intensity of which coal is not capable".

The main positive aspects of H_2 as an energy carrier are its high energy content per unit of mass, between 120 - 142 MJ/kg, approximately 3 times higher than gasoline; its clean combustion, that only produces water; and its easy and efficient conversion into electricity by fuel cells (Veziroglu et al. 2005). Actually, NASA and other space program agencies have long been using H_2 as the fuel for space exploration, both as rocket propellant and in fuel cells to provide electricity during manned space missions.

Due to the scientific and technological interest in H_2 as a clean energy carrier, potential transportation fuel and basic chemical agent, a great enthusiasm regarding H_2 can be found in the scientific literature. However, an opposite feeling of skepticism can also be found, which refuses to adopt an over simplified view over the implementation of an H_2 economy, raising attention to the tremendous challenges that remain to be solved at all levels, namely manufacture, storage and distribution (Bossel 2006).

In fact, despite its abundance on Earth, H_2 must be extracted from other hydrogen-containing compounds, such as water, fossil fuels or biomass. Presently, H_2 is being produced mostly from fossil fuels (Hosseini et al. 2016; Constant et al. 2019) and a small percentage by water electrolysis (Ball et al. 2015). Also, it is difficult to store H_2 given its extremely low density. At atmospheric pressure and room temperature, 1 g of H_2

occupies 11 L of volume and the current storage technologies are either based on high pressures to compress it, or based on low temperatures (-253 °C) to liquefy it, which are very energy demanding processes (Uchida et al. 2018).

For the promise of a green H_2 economy to become a reality, the process to produce it has to be carbon-free or carbon-neutral, in opposition to the current production methods based on fossil fuels (Rand et al. 2008) .Also, for the generalized use of H_2 in a fuel cell, the catalysts used for H_2 oxidation must by cheap and abundant, in opposition to platinum (Pt), an expensive and rare element, used as a standard catalyst in H_2 conversion technologies (Abdalla et al. 2018). In the context of achieving a sustainable H_2 production, it is remarkable that in Nature several microorganisms possess an active H_2 metabolism, able to produce and/or use H_2 as an energy source. Enzymes called hydrogenases are the key catalysts of this metabolism. Given the urgent demand for a clean and sustainable energy system, a deep understanding of the mechanism of action and potential applications of such catalysts must be undertaken.

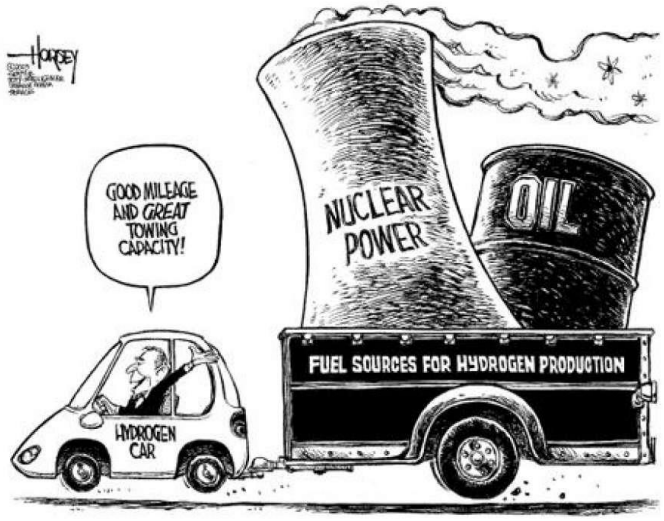

Figure 1: Cartoon satirizing the notion of clean H_2 burning cars, with H_2 made from polluting sources. Author: David Horsey

3. Hydrogenases

3.1 Hydrogenases Overview

Hydrogenases are enzymes that catalyze the interconversion of H_2 into protons and electrons, according to the reaction: $\mathbf{H_2 \Leftrightarrow 2H^+ + 2e^-}$. They were probably "invented" during the earliest stages of life on our planet, in a time when Earth had a reducing atmosphere, with no O_2 and an abundance of volcanic emissions containing H_2, CO_2 and sulfur gases (Kasting et al. 1993). It is believed that through hydrogenases, ancient microbes were able to exploit the reducing power of H_2 for their metabolism (Lane et al. 2010; Sousa et al. 2018). During thousands of millions of years, these natural catalysts were able to develop a strategy to efficiently catalyze H_2 using only earth abundant metals, like Ni and Fe. Since the discovery of hydrogenases by Stephenson and Stickland at the beginning of 20th century (Stephenson and Stickland 1931) these enzymes have scientifically and technologically inspired scientists towards modern time biotechnological solutions.

Hydrogenases are a diverse group of enzymes, distributed among prokaryotic organisms belonging to *Archaea* and *Bacteria* domains of life, but they are also found in *Eukarya* (Vignais et al. 2001; 2004). Their primary functions in the cell are to provide energy by the oxidation of molecular hydrogen, coupling it to energy yielding processes, or to produce H_2 as a way for disposing of excess reducing power during fermentation. Other functions have also been described (see below).

Hydrogenases are generally Fe-containing proteins with one or two metal atoms at their active site. The metal composition of the active site determines the designation and classification of hydrogenases into three main classes: **[FeFe] hydrogenases**, **[NiFe] hydrogenases** and **[Fe] hydrogenases**. The [FeFe] hydrogenases and [NiFe] hydrogenases are the best studied groups. They have a bimetallic active site where the metals are bridged by two thiolates. Carbon monoxide and cyanide groups are bound to Fe ions. (**Figure 2**) Despite catalyzing the same reaction and sharing some structural similarities, the two main groups of hydrogenases, the [FeFe] and [NiFe] types are evolutionarily unrelated, representing a case of convergent evolution (Peters et al. 2015).

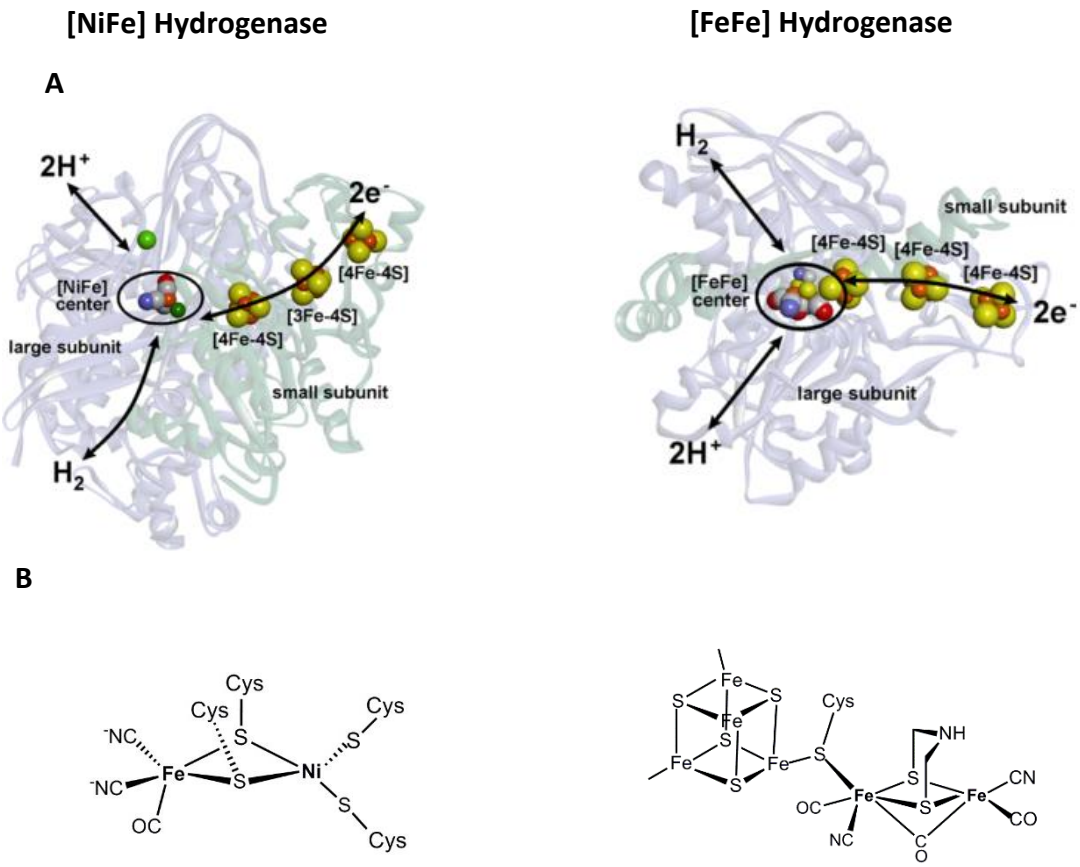

Figure 2: A- Representation of the structures of a [NiFe] hydrogenase (PDB: 1WUL) (Ogata et al. 2005) and of a [FeFe] hydrogenase (PDB: 1HFE) (Nicolet et al. 1999).' with schematic indication of the electron transfer chain (FeS clusters), and some possible pathways for H_2 and the H^+ transfer (figures were adapted from (Lubitz et al. 2014)). B - Chemical structures of the active site of the two types of hydrogenases. The [NiFe] hydrogenase active site is bridged by the thiol groups of two cysteines, and the Fe is coordinated by two cyanides and one carbon monoxide. Ni is also terminally coordinated by two cysteines. The [FeFe] hydrogenase active site is designated as H-cluster, and consists of a canonical cubane-type [4Fe4S] cluster covalently linked to a diiron complex, [2Fe]. Both irons are coordinated by one carbon monoxide and one cyanide, and an additional carbon monoxide ligand bridges the two iron ions. Figures were created in ChemDraw.

The oxidation of H_2 involves the heterolytic cleavage of the H-H bond into a hydride (H^-) (typically bound to a metal) and a proton (H^+), and is assisted by the presence of a basic group in the active site. The formation of H_2 involves the reduction of a proton to a hydride at a metal center and subsequent protonation (Yagy, et al. 1973). Appropriate pathways for protons and H_2 are provided by the protein matrix and the efficient

electron delivery to/from the active site is ensured by the array of FeS clusters (**Figure 2**). The role of the CO and CN^- ligands is to tune the metal centers electronically for optimal reaction.

The bidirectionality of hydrogenases makes them excellent candidates for energy converting devices. Electricity obtained from renewable sources (solar, wind, or hydrothermal) can be stored as H_2 produced from water by electrolysis during low energy demand periods. When this chemically stored energy is required back, H_2 can be oxidized in fuel cells to produce electricity. The catalyst used nowadays to carry out these reactions in an efficient way is platinum. However, because it is a rare precious metal its global scale utilization is limited, and also Pt is poisoned by H_2S and CO, typical contaminants of H_2 produced by steam reforming of fossil fuels (Rand et al. 2008). Hydrogenases can be an alternative to Pt, since they are high-performance biocatalysts, having high turnovers and operating under mild conditions with almost no overpotential (Jones et al. 2002; Hexter et al. 2012; Lubitz et al. 2014). This makes them highly interesting candidates for applications for H_2 production in photo-electrochemical cells or H_2 oxidation in fuel cells (Wakerley et al. 2015; del Barrio et al. 2018; Evans et al. 2018).

Despite being very active catalysts, all hydrogenases are to some extent sensitive to O_2. This represents an obstacle that prevents them from being used in many biotechnological devices, because anaerobic conditions are costly to maintain on an industrial scale. The interaction between hydrogenases and O_2 is very diverse and enzyme-dependent. There is no single definition of O_2 sensitivity nor a number to quantify it. Improving hydrogenase O_2 tolerance is therefore a major contemporary challenge to allow their use in a sustainable hydrogen economy.

Hydrogen evolution and consumption is not catalyzed only by hydrogenases. Nitrogenases, the enzymes which catalyze the production of ammonia from atmospheric nitrogen, also produce H_2 as a byproduct of N_2 fixation (Barahona et al. 2016).

3.2 Types of hydrogenases

The different classes of hydrogenases can have very different catalytic activities and sensitivity to inhibitors. The term catalytic "bias" in hydrogenases is used to describe whether the enzyme exhibits higher catalytic activity for hydrogen consumption or evolution.

The [Fe] hydrogenases are found only in methanogenic archaea. This enzyme class catalyzes a reaction involved in the methanogenic energy conversion pathway from CO_2 to methane (Thauer et al. 2010). The enzyme harbors a unique Fe cofactor and does not contain any FeS clusters. The [Fe] hydrogenase catalyzes the reversible reduction of the substrate methenyltetrahydromethanopterin (methenyl-H_4MPT^+) with H_2. Its activity is dependent on the presence of its substrate, methenyl-H_4MPT^+, not being able to reduce other electron acceptors, like artificial dyes. Also, [Fe] hydrogenases are not able to catalyze H^+ reduction (Lyon et al. 2004). Their structure and catalytic reaction mechanism differ significantly from [NiFe] and [FeFe] hydrogenases, so this class of hydrogenase will not be discussed further in this thesis.

The [FeFe] hydrogenases are physiologically primarily involved in H_2 production. This type of hydrogenase is found in anaerobic prokaryotes such as *Clostridia* and sulfate reducers (Vignais et al. 2001; 2004). Also, it is the only type of hydrogenase that appears in eukaryotes, where it is located exclusively in membrane-limited organelles, such as the chloroplasts of green algae (Happe et al. 1993) or hydrogenosomes in protozoa (Horner et al. 2002). The [FeFe] hydrogenases have very high catalytic activities for H_2 production, (Hexter et al. 2012) especially the ones from bacteria, which are able to produce $\sim 10^4$ molecules of H_2 per second (Hatchikian et al. 1992; Birrell et al. 2016). Despite being very active in H_2 production, the [FeFe] hydrogenases are in general very sensitive to O_2, being irreversibly inactivated by it on a time scale of seconds, due to a partial degradation of the active site, via a multistep process (Stripp et al. 2009; Lambertz et al. 2011; Swanson et al. 2015). The first reported structures of [FeFe] hydrogenases were from *Clostridium pasteurianum* (Peters et al. 1998) and *Desulfovibrio desulfuricans* (Nicolet et al. 1999). More recently, the [FeFe] hydrogenase from the green algae *Chlamydomonas reinhardtii* was heterologously expressed in *Escherichia coli* without the maturation factors (Mulder et al. 2010). The active site of

[FeFe] hydrogenases is designated as H-cluster and consists of a di-iron subcluster [2Fe] and a [4Fe4S] cluster (**Figure 2**). The H-cluster is well conserved among different [FeFe] hydrogenases. At the molecular level, its O_2 sensitivity occurs once O_2 binds to the distal Fe of the [2Fe] subcluster (the distal Fe on the [2Fe] is the Fe farthest from the [4Fe4S] in the H-cluster) a reactive oxygen species (ROS) will then destroys the [4Fe4S] cluster (Stripp et al. 2009; Stiebritz et al. 2009; Lambertz et al. 2011). The distal Fe on the [2Fe] cluster is also the hydrogen binding site and the site of reversible carbon monoxide binding and inhibition (Lemon et al. 1999; De Lacey et al. 2007). Many [FeFe] hydrogenases are composed of a single subunit, containing only the H-cluster, while some [FeFe] hydrogenases are composed of multi-subunits up to heterotetramers. The [FeFe] hydrogenases from green algae, such as *C. reinhardtii* contain only the catalytic H-cluster and no accessory clusters, thus representing the simplest form of [FeFe] hydrogenases yet identified. Hydrogenases from photosynthetic microbes receive much attention as these organisms provide the means to generate H_2 using sunlight (Gaffron et al. 1942; Weaver et al. 1980; Brand et al. 1989), since the H_2 production by [FeFe] hydrogenases is coupled directly to water oxidation through photosystem II (PSII) (Melis et al. 2001; Stripp et al. 2009). In this reaction, the water is a source of electrons and the sunlight a source of energy. In the PSII water is oxidized and O_2 is evolved, and the electrons are transferred to photosystem I (PSI). In PSI a second light event increases the energy of the transferred electrons. In species like *C. reinhardtii*, a ferredoxin takes the electrons and directs them either to CO_2 fixation or to the hydrogenase for H_2 evolution under sulfur deprived conditions (Hemschemeier et al. 2008; 2011). One strategy used to harvest H_2 from light and water aims to genetically engineer algae or cyanobacteria in order to enhance their H_2 production. Another major challenge is that the hydrogenases of these organisms are very O_2 sensitive, and as the H_2 production process is coupled to O_2 production, the process is not viable on the long term as the hydrogenase becomes inactivated (Esper et al. 2006).

The [NiFe] hydrogenases are the best studied class of hydrogenases. They are found only in archaea and bacteria, and in many cases catalyze H_2 oxidation. The standard [NiFe] hydrogenases are O_2-sensitive and comprise two subunits, the large and the small subunit (**Figure 2**). The large subunit has a molecular mass of ~60 kDa subunit housing the di-metal active site of Ni and Fe, where the Fe is ligated by two CN^- ligands and a CO

ligand. The Ni and the Fe are bridged via the thiol group of two cysteines, and the Ni is coordinated by two additional terminal Cys ligands. The small subunit has a molecular mass of ~30 kDa and usually contains three FeS clusters that transfer electrons between the protein surface and the [NiFe] active site (**Figure 2**). The FeS clusters are termed as distal, medial and proximal, based on their distance to the active site. The distal cluster is exposed to solvent, and electron transfer occurs from the distal FeS cluster to the physiological partner or to an artificial electron acceptor. A standard [NiFe] hydrogenase, isolated from *Desulfovibrio gigas* (Volbeda et al. 1995) was the first hydrogenase to be crystallized, followed by a [NiFe] hydrogenase of *Desulfovibrio vulgaris* Miyazaki (Higuchi et al. 1997). A few years later, the first structure of a subclas of the [NiFe] hydrogenases was published (Garcin et al. 1999), the **[NiFeSe] hydrogenase**. In contrast to the [FeFe] hydrogenases, the [NiFe] hydrogenases are usually more prone to H_2 oxidation and their reported catalytic activities are usually lower. However, the [NiFeSe] hydrogenases are remarkable exceptions, since they are biased for H_2 production and have very high catalytic activities (Parkin et al. 2008; Marques et al. 2017).

[NiFe] hydrogenases are a diverse group of enzymes with respect to their modular composition and physiological function, leading to their subdivision into four groups, according to the revised system of Vignais and co-workers (Vignais et al. 2001; 2004; 2007):

Group 1 - Energy-transducing hydrogenases;

Group 2 - Cyanobacterial uptake hydrogenases and cytoplasmic H_2 sensors;

Group 3 - Bidirectional cytoplasmic hydrogenases;

Group 4 - Membrane-associated energy-converting hydrogenases.

A recent comprehensive survey on the distribution of hydrogenases provided evidence that microbial H_2 metabolism is significantly more extensive and elaborate than previously anticipated (Greening et al. 2016). This analysis of the phylogeny, genetic organization and metal-binding motifs, demonstrated that hydrogenases have evolved into numerous functionally distinct subgroups/subtypes. New definitions and subgroups of [NiFe] hydrogenases were introduced.

A more general and broad classification can be described as follow:

[NiFe] hydrogenases from **group 1** allow microorganisms to use H_2 as an energy source, and are also designated as H_2 uptake hydrogenases. They are key components of the electron transport chain, channelling electrons to the quinone pool, via a membrane integral cytochrome *b* to which the core hydrogenase dimer is anchored. However, in periplasmic hydrogenases of *Desulfovibrio spp*. and other sulfate reducers the redox partner is instead a soluble low-potential cytochrome *c* that transfers electrons to membrane-associated complexes (Pereira et al. 2011). Group 1 [NiFe] hydrogenases are characterized by the presence of a signal peptide in the small subunit, involved in translocation of the mature protein to the periplasm. The subclass of [NiFeSe] hydrogenases are part of this group.

The **group 2** [NiFe] hydrogenases do not contain a signal peptide, and they are localized in the cytoplasm. Some hydrogenases of this group function as H_2 sensors that respond to H_2 concentration, triggering the biosynthesis of the energy-transducing [NiFe] hydrogenases. This group also comprises the cyanobacterial uptake enzymes, which are induced under N_2 fixing conditions (Constant et al. 2019).

The **group 3** are also cytoplasmic enzymes, in which the hydrogenase dimer core is associated with additional subunits able to bind soluble cofactors such as NAD(P) and cofactor 420 (F420). This group includes many enzymes from methanogens, but some enzymes are also present in bacteria (Schwartz et al. 2006). Their activity is bidirectional *in vivo*, and they are involved in electron transport, ensuring redox balance in the cells.

Hydrogenases belonging to **group 4** are highly divergent from the other groups. These proteins are involved in energy conservation, and their subunits are closely related to subunits of complex I (Schwartz et al. 2006).

H_2 occurs ubiquitously in the environment, and the amount of molecular H_2 in the atmosphere is about 0.5 ppmv (Constant et al. 2009), produced from biological, geothermal and atmospheric sources (stratospheric photochemistry) (Schwartz et al. 2006), but mostly being produced by anthropogenic processes, including fossil fuel combustion and biomass burning (Novelli et al. 1999). This great diversification of hydrogenases has enabled H_2 metabolism to sustain the growth of microorganisms in a wide range of ecosystems to the present day (Greening et al. 2016). This group system classification clearly demonstrates the variety of forms and roles that [NiFe]

hydrogenases can have, from membrane-bound to soluble types, different degrees of catalytic activities, as well as different degrees of sensitivity to inhibitors.

3.3 [NiFe] Hydrogenases reactions with O_2

All hydrogenases have some degree of sensitivity to O_2. While the majority of [FeFe] hydrogenases are always irreversibly inactivated by O_2, the [NiFe] hydrogenases can be reversibly inactivated. Depending on the availability of electrons, different reactive oxygen species (ROS) can be generated at the active site of hydrogenases by an incomplete reduction of O_2:

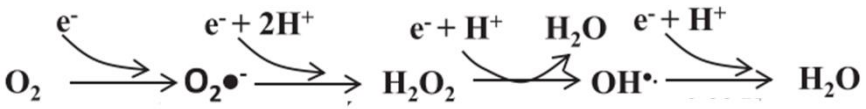

Figure 3: Reduction of O_2 to H_2O and its free radical intermediates. O_2 can only accept one electron at a time when it is being reduced to H_2O which generates several free radical intermediates namely, superoxide ($O_2^{-\bullet}$), hydrogen peroxide (H_2O_2), and hydroxyl radical ($OH^{\bullet}$). Figure adapted from (Mailloux 2015).

Hydroxyl radicals represent the most dangerous ROS, followed by superoxide and hydrogen peroxide (Lauterbach et al. 2013). Harmless water is produced only by the four-electron reduction of O_2. Indeed, O_2 is highly toxic towards anaerobic organisms, its damaging effects are associated mainly with its free radical properties which depleted essential thiols and dismantle FeS clusters required for metabolism and the biosynthesis of macromolecular structures (Mailloux 2015). The likely reason for hydrogenase inactivation cause by O_2 is the reaction of ROS with hydrogenase cofactors, damaging their integrity.

During catalysis, H_2 is heterolytically cleaved at the dimetal active site, resulting in the release of a proton to a nearby proton acceptor with the formation of a state named NiR, characterized by a bridging hydride between the two metals (Ogata et al. 2015).

The low-spin Fe(II) ion is redox-inactive throughout the catalysis, whereas the Ni changes its oxidation state. When O_2 attacks the active site it can lead to the formation of a mixture of two inactive states named Ni-A and Ni-B, characterized by their electron paramagnetic resonance (EPR) spectroscopic signatures and different rates of reactivation under reducing conditions (Fernández, et al. 1985). Ni-B is also termed "ready" and can be activated within seconds, whereas Ni-A is named "unready" and requires longer times (up to several hours) to activate (Kurkin et al. 2004; De Lacey et al. 2007). In both Ni-A and Ni-B, nickel is in a Ni(III) oxidation state and an oxygen species is bridging the metals in the active site. The nature of the oxygen species has been reported to be hydroperoxide (Volbeda et al. 2005; Ogata et al. 2005), a hydroxide (Volbeda et al. 2005; Ogata et al. 2005), a oxide (Volbeda et al. 1996) or a sulphide (Higuchi et al. 1997;1999). While it is now consensual that Ni-B contains a hydroxyl bridging group, the nature of the bridging ligand in Ni-A is still under debate (Barilone et al. 2015). The general assumption that Ni-A and Ni-B formation results from partial reduction of O_2 was questioned when it was observed that Ni-A and Ni-B could also be formed under anaerobic oxidizing conditions, indicating that different mechanisms may operate under oxidizing aerobic and oxidizing anaerobic conditions, leading to the same inactivation states (Abou Hamdan et al. 2013). One-electron reduction of Ni-A and Ni-B generates EPR silent intermediates like the Ni-SIr. The Ni-SIr state is converted to Ni-SIa, the EPR silent state representing the oxidized form of the enzyme that is active in catalysis and lost the bridging OH^- group. One-electron reduction of Ni-SIa leads to Ni-C, which exhibits a Ni(III) EPR signal and contains a bridging hydride ligand (Brecht et al. 2003). The fully reduced Ni-R state can be obtained via one-electron reduction of Ni-C, and features both the bridging hydride and protonation of one of the Cys terminal Ni ligands (Ogata, et al. 2015). In brief, the standard [NiFe] hydrogenases are inactivated by O_2 but can recover after some time under reducing conditions.

In the past years, some [NiFe] hydrogenases were identified as containing some degree of tolerance to O_2 (Fritsch, et al. 2013). These hydrogenases are predominantly identified in aerobic or facultative aerobic H_2-oxidizing bacteria, with the chemolithoautotroph H_2 oxidizer *Ralstonia eutropha* as a good model organism to study them, since it contains four types of [NiFe] hydrogenases known to have some degree of O_2 tolerance: the **O_2-tolerant membrane bound hydrogenase** (**O_2-tolerant MBH**),

the **Regulatory hydrogenase** (**RH**), the soluble **NAD(P)$^+$-Reducing hydrogenase** (**SH**) and the **actinobacterial hydrogenase** (**AH**).

The O_2-tolerant MBHs belong to group 1 and are the best characterized group of O_2-tolerant hydrogenases. These enzymes are able to catalyze H_2 oxidation in the presence of O_2 (Vincent et al. 2005; Cracknell et al. 2009). The best studied proteins of this class are the HoxGK from *R. eutropha*, the Hyd-1 from *E. coli*, Hase I protein from *Aquifex aeolicus* and the MBH from *Hydrogenovibrio marinus*. Typical O_2-tolerant MBHs are composed of the heterodimeric hydrogenase subunits and the integral membrane protein cytochrome *b*. As a general picture, when O_2 attacks the [NiFe] active site of O_2-tolerant MBHs, the O_2 is rapidly reduced, producing an H_2O molecule and a bridging hydroxide (Ni-B). In fact, the unready state Ni-A found in standard [NiFe] hydrogenases is absent in all O_2-tolerant MBHs, and the oxidized protein forms only the Ni-B state, (Pandelia et al. 2010; Saggu et al. 2009) which reactivates very fast at more positive potentials than standard [NiFe] hydrogenases (Cracknell et al. 2009; Pandelia et al. 2010; Fourmond et al. 2010). The most significant difference between the O_2-tolerant MBHs and O_2-sensitive [NiFe] hydrogenases is found in the proximal FeS cluster. Standard O_2-sensitive [NiFe] hydrogenases have a typical cubane [4Fe4S] cluster coordinated by four cysteines (**Figure 4**), while the O_2-tolerant MBHs have an unusual cluster coordinated by six cysteines, where the two additional cysteines are known as supernumerary cysteines. While four of the six cysteine residues coordinate the cluster in a classical way, the thiolate of one of the supernumerary cysteine (Cys19 in *R. eutropha* and *E. coli, or* Cys25 in *H. marinus*) replaces the inorganic sulfide in the cubane core, forming a [4Fe3S] cluster, allowing it to adopt a cubane shape in the reduced form (Fritsch et al. 2011; Shomura et al. 2011; Volbeda et al. 2012). The other supernumerary cysteine (Cys120 in *R. eutropha* and *E. coli,* or Cys126 in *H. marinus*) is terminally coordinated to one of the Fe atoms.

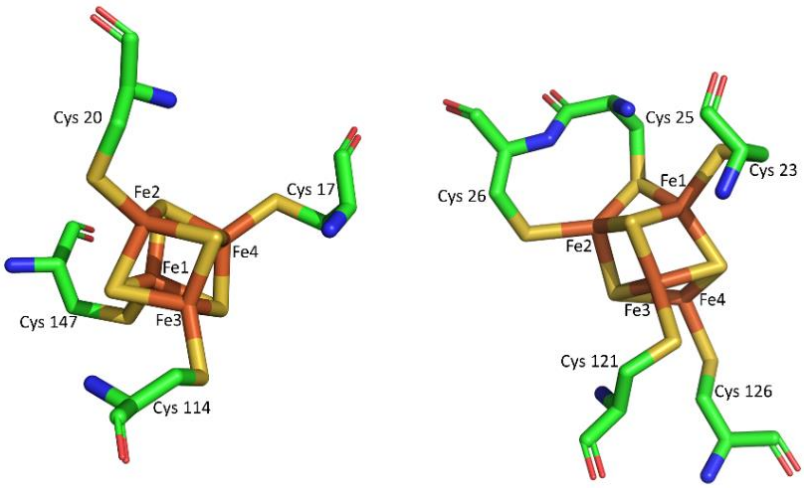

Figure 4: Comparison of the proximal FeS clusters in the standard O_2-sensitive [NiFe] hydrogenase of *Desulfovibrio fructosovorans* (1YQW) (left) and in the reduced form of the O_2-tolerant [NiFe] hydrogenase from *H. marinus* (3AYX), with the supernumerary cysteines, Cys25 and Cys126 (right).

The supernumerary cysteines give the proximal [4Fe3S] cluster the capability to access three redox states under physiological potentials, efficiently assisting in the complete reduction of O_2 (Pandelia et al. 2011; Goris et al. 2011; Roessler et al. 2012). Removal of the additional cysteines alters the electronic structure of the proximal FeS cluster and renders the protein O_2 sensitive (Goris et al. 2011). Based on protein film electrochemical (PFE) experiments one of the cysteines (Cys19 in *E. coli*) was found to be critical for O_2-tolerance, while the Cys120 has less effect (Lukey et al. 2011). However, *in vivo* studies demonstrated on the contrary that Cys120 is more important in the O_2-tolerant MBH of *R. eutropha* (Goris et al. 2011). This suggests that under physiological conditions, both supernumerary cysteine residues seem to be fundamental for either electron transfer during H_2 catalysis or electron storage for the rapid reactivation of the [NiFe] site following O_2 attack (Fritsch, et al. 2013). While classical [4Fe4S] clusters are involved in one electron transfer, the proximal [4Fe3S] clusters can attain three redox states, reduced (3+), oxidized (4+) and superoxidized (5+), within a narrow redox potential range of 150 mV, being involved in two electron transfer reactions (Pandelia et al. 2011; Lukey et al. 2011). The superoxidized state is stabilized by a structural change created by the break between the Fe2 and the sulfur and the new bond of Fe2 with the

deprotonated amide of Cys26 (**Figure 5**). A nearby glutamate residue is proposed to act as a base for the deprotonation of the amide (Volbeda et al. 2012). Thus, the complete reduction of O_2 to water is assisted by: *i)* the proximal [4Fe3S] cluster able to supply two electrons in a narrow potential range ($[4Fe3S]^{5+/4+/3+}$, +230 mV and +30 mV *vs* SHE in *E. coli* or -60 mV and -160 mV *vs* SHE in *R. eutropha*); *ii)* the medial [3Fe4S] cluster, that can deliver one electron ($[3Fe4S]^{+/0}$, +180 mV in *E. coli*) (Roessler et al. 2012; Evans et al. 2013); and *iii)* the [NiFe] active site that can supply one electron, in the Ni(II) transition to Ni(III). However, the exact origin of the four electrons depends on the oxidation state of the hydrogenase at the time of the O_2 attack.

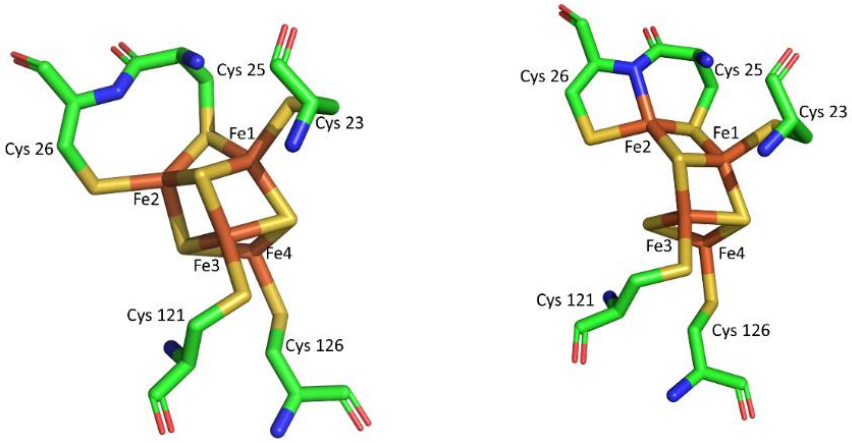

Figure 5: Representation of the proximal [4Fe3S] cluster of the O_2-tolerant MBH from *H. marinus* in its reduced (3AYX) (left) and superoxidized form (85Y34), illustrating the structural reargements that stabilize the cluster in the superoxidized form (right).

However, it is important to mention that the role played by the proximal FeS cluster in the O_2-tolerant MBHs is not enough to fully explain their O_2 tolerance, since the variants with the supernumerary cysteines mutated, still exhibited some degree of O_2 tolerance (Goris et al. 2011; Lukey et al. 2011). Also, a new type of O_2-tolerant MBH from Citrobacter sp. S-77 does not have supernumerary cysteines, suggesting that it has an alternative mechanism for O_2-tolerance (Eguchi et al. 2012; Noor et al. 2018).

Besides their remarkable O_2 tolerance, these enzymes likewise show no inactivation by carbon monoxide, (Vincent et al. 2005; Lukey et al. 2010) which is also a strong inhibitor of standard hydrogenases. However, despite their remarkable tolerance these

enzymes are biased to H_2 oxidation with no or very low H^+ reduction activities. They are also strongly inhibited by the H_2 product (Goldet et al. 2008; Pandelia et al. 2010; Lukey et al. 2010), which limits their application in H_2 producing devices.

Another class of nonstandard [NiFe] hydrogenases are the sensory or regulatory hydrogenases (RH). These hydrogenases mediate H_2-dependent signal transduction leading to the regulation of metabolic hydrogenases (Bernhard et al. 2001; Buhrke et al. 2004). There are no X-ray crystallography structures of RHs, but techniques like homology modelling and amino acid exchange have provided the much information regarding RH's oxygen tolerance. Bulky amino acid residues, isoleucine and phenylalanine placed between the active site and the entrance of a hydrophobic channel were identified as the reason for O_2 tolerance (Volbeda et al. 2002), since replacement of these aminoacids by smaller ones like valine and leucine lead to some level of O_2 sensitivity in RH (Duché et al. 2005; Buhrke et al. 2005). However, it should be noted that restricting O_2 access to the active site only lowers the probability of reaction between both, and it does not prevent the reaction to take place (Liebgott, Dementin, et al. 2011).

A new group of [NiFe] hydrogenases that can oxidize hydrogen in the presence of oxygen at the atmospheric level was identified in soil-living actinobacteria and these enzymes have therefore been designated as actinobacterial hydrogenases (AH) (Constant et al. 2008; 2011). These bacteria are able to scavenge H_2 from the lower atmosphere, challenging the notion that H_2 metabolism is restricted to low O_2 and high H_2 concentration environments (Greening et al. 2014). These enzymes are insensitive to oxygen, as no decrease of activity is detected in the presence of O_2, in contrast to the other O_2-tolerant hydrogenases that show a small decrease in activity upon O_2 exposure. The O_2 tolerance of AH it not fully understood, but might be related to special properties of the proximal cluster that shows nonstandard coordination, carrying an aspartate ligand (Schäfer et al. 2013; 2016).

Another member of the O_2-tolerant hydrogenases are the soluble NAD^+-reducing [NiFe]-hydrogenases (SH) (Schneider et al. 1981). These enzymes directly couple H_2 oxidation with the reduction of NAD^+, producing NADH, which is used both for energy conservation (through Complex I and the respiratory chain) and for CO_2 fixation via the Calvin cycle. Under certain conditions, the enzyme is also capable of catalyzing the

reverse reaction, the NADH mediated reduction of protons to H_2 (Kuhn et al. 1984). From a structural and functional perspective, the SHs are closely related to the peripheral arm of Complex I (Albracht et al. 2000). The O_2 tolerance is believed to come from the ability of SH to perform a complete reduction of O_2 to H_2O (Lauterbach et al. 2013; Preissler et al. 2018). However, the exact mechanism by which these enzymes operate under O_2 remains unclear.

3.4 [NiFeSe] hydrogenases

Selenium is a non-metal with intermediate properties between the elements above and below it in the periodic table, sulfur and tellurium, respectively. In proteins, selenium is present in the amino acid selenocysteine (Sec). Sec has a chemical structure similar to cysteine, with a selenium atom replacing the sulfur (**Figure 6**) (Böck et al. 1991).

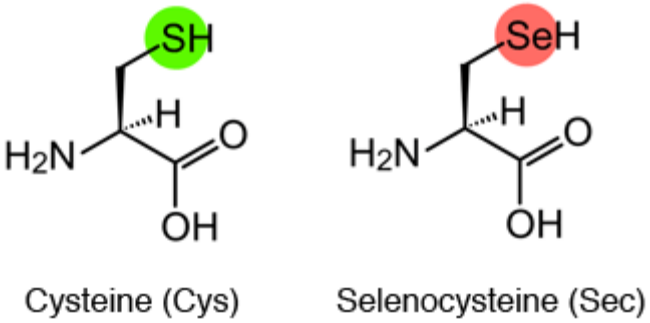

Figure 6: Chemical structure of the aminoacids cysteine and selenocysteine, emphasizing the thiol and selenol group, respectively.

In 1986 it was discovered that under special circumstances the translation of the stop codon UGA could be changed to specify the 21st amino acid, selenocysteine. Only some organisms have Sec-containing proteins, because a specific translation machinery is needed for Sec incorporation. A stem loop on the mRNA immediately near the UGA codon enables the binding of a protein complex responsible to bring a specific tRNA carrying the Sec (Böck 2000). This process is bioenergetically costly, and therefore the

Sec aminoacid must bring advantages to a protein that the sulfur-containing analog, Cys, could not accomplish.

The [NiFeSe] hydrogenase is a paradigmatic example of nature's use of selenium. Its active site is identical to that of the [NiFe] hydrogenases except for the replacement of a terminally coordinating Cys residue by Sec (Baltazar et al. 2011; Wombwell et al. 2015). The presence of selenium in certain hydrogenases was first demonstrated in 1989 by X-ray absorption experiments at both the nickel and selenium absorption energies (Eidsness et al. 1989). This was later confirmed by global incorporation of the magnetic isotope ^{77}Se and subsequent EPR experiments that demonstrated that selenium is a ligand to the nickel (Sorgenfrei et al. 1993).

[NiFeSe] hydrogenases have been found exclusively in sulfate-reducing and methanogenic microorganisms and belong to Group 1 (periplasmic membrane associated, designated Hys), Group 3a (F420 reducing enzymes, designated Fru) and Group 3c (methyl viologen reducing enzymes, designated Vhu) (Baltazar et al. 2011). Crystal structures of [NiFeSe] hydrogenases are available from two organisms, *Desulfomicrobium baculatum* (Garcin et al. 1999) and *Desulfovibio vulgaris* Hildenborough (Marques et al. 2010), both of which are sulfate reducers. These two [NiFeSe] hydrogenases belong to Group 1 and feature the heterodimeric quaternary structure that resemble the [NiFe] hydrogenases (**Figure 7**). The group 3 enzymes, for which there are no crystallographic structures, have a more complicated quaternary structure.

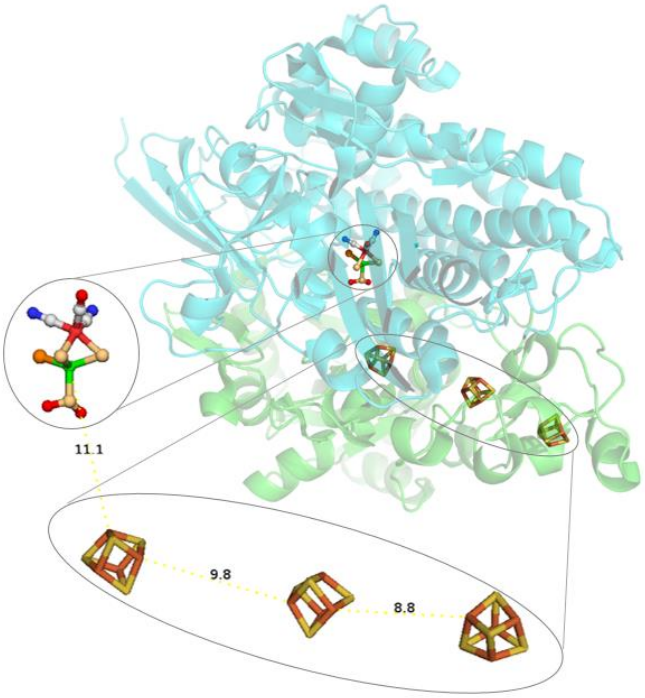

Figure 7: Heterodimeric structure of the [NiFeSe] hydrogenase from *D. vulgaris Hildenborough* emphasizing its cofactors. The large subunit (cyan) contains the active site of the protein. In the small subunit there is an array of three cubane FeS clusters, responsible for electron transfer. (PDB:5JSH)

Throughout the years several catalytic properties of [NiFeSe] hydrogenases have been described, evidencing its superior catalytic behavior in comparison with [NiFe] hydrogenases. [NiFeSe] hydrogenases have very high catalytic activities, ~8000 s^{-1} for H_2 production (Valente et al. 2005; Marques et al. 2017) and ~4500 s^{-1} for H_2 oxidation (Parkin et al. 2008; Zacarias et al. 2018), showing an *in vitro* bias for H_2 production. Also, [NiFeSe] hydrogenases suffer from less product inhibition than [NiFe] hydrogenases (Parkin et al. 2008; Riethausen et al. 2013).

Like [NiFe] hydrogenases, they are reversibly inactivated either by O_2 or by positive electrochemical potentials in anaerobic conditions, and to become active they have to be reactivated through reduction, either by exposure to H_2 or by the application of a negative electrochemical potential (Teixeira et al. 1987; Valente et al. 2005; Parkin et al. 2008; Ceccaldi et al. 2015; Marques et al. 2017). However, in opposition to [NiFe] hydrogenases, aerobic isolation of the [NiFeSe] hydrogenases from both *Dm. baculatum* and *D. vulgaris* Hildenborough results in EPR-silent states, where no Ni-A or Ni-B are

detected, which led to the initial suggestion that these proteins might be oxygen tolerant (Teixeira et al. 1987; Valente et al. 2005). Also, the [NiFeSe] hydrogenases are much more rapidly reactivated than [NiFe] hydrogenases, but require low potentials (Medina et al. 1996; Parkin et al. 2008; Ceccaldi et al. 2015). Because reactivation of the O_2-specific inactive species only occurs rapidly at electrode potentials close to the thermodynamic potential of the H^+/H_2 couple, there is no possibility that [NiFeSe] hydrogenase could oxidize H_2 in the presence of O_2, like O_2-tolerant MBHs. However, it was demonstrated that sustainable H_2 production in the presence of small quantities of O_2 is possible (Parkin et al. 2008; Riethausen et al. 2013). It is important to note that a rapid reactivation after O_2 attack is also a characteristic of the O_2-tolerant MBHs, but because in these enzymes this process occurs at a high potential, it allows H_2 oxidation to proceed in air (Vincent et al. 2005).

When standard [NiFe] hydrogenases react with O_2, the nickel center is oxidized to Ni(III) and an oxygen-containing ligand takes the bridging position between the nickel and the iron centers (Volbeda et al. 1995; Ogata et al. 2005; Volbeda et al. 2005; van Gastel et al. 2005). In the O_2-oxidized [NiFeSe] hydrogenases, the nickel center is not oxidized to Ni(III) and no bridging ligand is observed between the two metal centers (Teixeira et al. 1987; Medina et al. 1996; Valente et al. 2005; Marques et al. 2010; Riethausen et al. 2013; Volbeda et al. 2013).

The enhanced catalytic properties of the [NiFeSe] hydrogenases can be rationalized to a large extent in terms of the chemistry of selenocysteine. In comparison with sulfur, selenium is more acidic, making it a better source of protons; its lower pKa (5.24 for Sec *vs.* 8.25 for Cys) (Birringer et al. 2002) favors H_2 production at physiological pH by donation of a proton to the hydride that is formed at the active site. Also, the increased nucleophilicity and polarizability of the Sec ligand with respect to Cys increases the electron density on the cluster through an increased covalency of the Ni-Se bond, favoring the formation of H^-. All these properties can explain the high catalytic activities observed for [NiFeSe] hydrogenases in comparison with [NiFe] hydrogenases (Reich et al. 2016; Marques et al. 2017; Maroney et al. 2018). In regard to reactions with O_2, selenium is more easily oxidized than sulfur but the Se-O bond is weaker than the S-O bond, resulting in selenium oxides that are much more unstable than their sulfur analogs and therefore easier to reduce back. Thus, oxidation of the Sec residue to the

corresponding selenenic or seleninic acids is easily reversible, whereas reduction of a sulfenic or sulfinic acid is more difficult or even impossible for the latter (Reddie et al. 2008). This property apparently enables selenoenzymes to better resist irreversible oxidative inactivation than their cysteine counterparts (Maroney et al. 2018). Actually, evolutionary studies of selenoproteins have indicated that their numbers have gone up after the oxygen levels in the atmosphere increased, suggesting that selenocysteine is helpful in adaptation to an aerobic environment (Zhang et al. 2006). These properties of the selenium reaction with O_2 can explain why the inactive oxygen-bound states are more easily restored in [NiFeSe] than in [NiFe] hydrogenases.

The importance of Se in the [NiFeSe] hydrogenases was demonstrated when a a selenocysteine-to-cysteine (Sec489Cys) variant was created in *D. vulgaris* Hildenborough, transforming for the first time the active site of a [NiFeSe] hydrogenase into a [NiFe] type (Marques et al. 2017). This modification led to a severely reduced Ni incorporation, revealing the direct involvement of this residue in the maturation process. However, the Ni-depleted protein could be partly reconstituted to generate an enzyme showing much lower activity and displaying the characteristic Ni-A and Ni-B inactive states of [NiFe] hydrogenases. This means that the presence of selenium in the active site of this enzyme has a crucial role in the high catalytic activities of the [NiFeSe] hydrogenases and in its protection against oxidative damage (Marques et al. 2017). In the case of [NiFeSe] hydrogenase the superiority of Se has been demonstrated, but it is not always so clear. Several cysteine homologs of selenocysteine-containing enzymes can catalyze their enzymatic reactions with high catalytic efficiency, probably employing mechanisms that increase the reactivity of Cys (Hondal et al. 2011; Hondal et al. 2013). This suggests that the main advantage of using Sec may lie in its protection from oxidative inactivation.

Apart from the active site, other differences are found between the [NiFeSe] hydrogenases and [NiFe] hydrogenases that could contribute to their improved catalytic properties. In [NiFeSe] hydrogenases the medial cluster is a [4Fe4S] cluster with a midpoint potential of - 315 mV at pH 7.6. This cluster is flanked by the proximal and distal [4Fe4S] clusters, both having the same low redox potential (Teixeira et al. 1990). In [NiFe] hydrogenases a [3Fe-4S] cluster occupies the medial position and has higher reduction potential than its surrounding clusters. In *D. gigas* [NiFe] hydrogenase the

reduction potentials for the proximal [4Fe4S], medial [3Fe4S], and distal [4Fe4S] clusters are -290 mV, -70 mV and -340 mV, respectively (Rousset et al. 1998) and in *D. frutusovorans* [NiFe] hydrogenase the corresponding values are -340 mV, +65 mV and -340 mV (Dementin et al. 2006)). The high midpoint potential of the medial [3Fe4S] cluster cast doubts about its involvement in an efficient electron transfer. A mutation performed to convert the [3Fe4S] into a [4Fe4S] cluster resulted in a lowering of the midpoint potential by approximately 300 mV (Rousset et al. 1998). However, it did not have a significant impact on the catalytic activity of the enzyme, indicating that the electron transfer is not the rate-limiting step of the catalytic reaction (Rousset et al. 1998). The more negative midpoint redox potential of the medial cluster in [NiFeSe] hydrogenases may contribute to tuning the catalytic properties of these hydrogenases in comparison to the [NiFe] hydrogenases.

Also, other ligands have been identified in the protein structure of the [NiFeSe] hydrogenases, namely a $Fe^{2+/3+}$ (Garcin et al. 1999; Marques et al. 2010) (**Figure 7**) which is a Mg^{2+} ion in standard [NiFe] hydrogenases (Higuchi et al. 1997). The functional role of this site is unclear. Also, a Cl^- or a HS^- have been assigned in another protein site, 7 Å away from the active site. Both species are isoelectronic so they can't be distinguished by X-ray crystallography (Marques et al. 2010). The presence of a HS^- reservoir makes sense, since [NiFeSe] hydrogenases from sulfate reducers may have evolved to use the H_2S produced from sulfate reduction to repair oxidative damages. An exogenous sulfur is found as a Ni ligand in the oxidized states of [NiFeSe] hydrogenase from *D. vulgaris* Hildenborough*,* which might work as protective mechanism to avoid oxygen species to be placed between the two metals, also agrees with the existence of this HS^- reservoir in the protein structure.

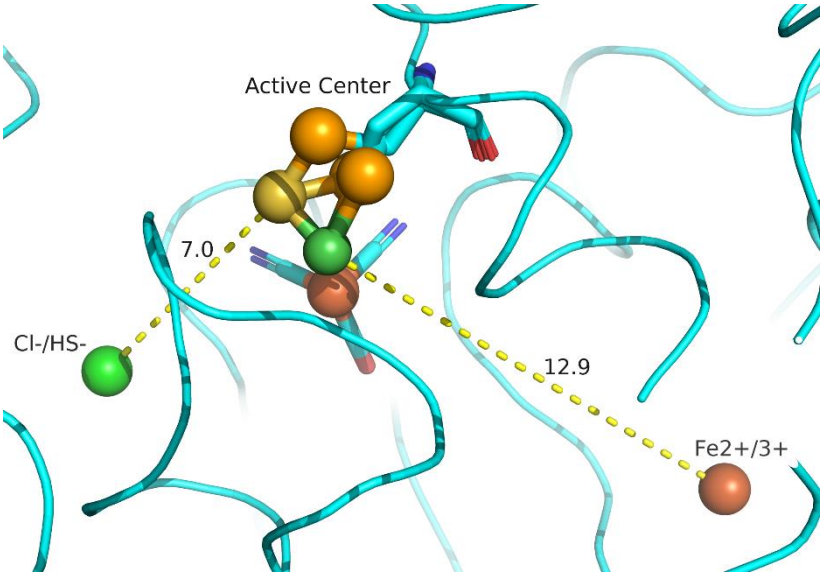

Figure 7: Position of other ligands in relation to the active site in the [NiFeSe] hydrogenase from *D. vulgaris* Hildenborough. The Cl^-/HS^- is 7 Å away and the $Fe^{2+/3+}$ is ~13 Å away from the active site. (PDB:5JSH)

Developing strategies to enhance hydrogenase O_2 tolerance is a major field of research that has been pursued by several groups with different degrees of success. Engineering an enzyme by mutating key residues in its structure has led to already improved variants of [NiFe] (Dementin et al. 2009; Liebgott, de Lacey, et al. 2011) and [NiFeSe] hydrogenases (Zacarias et al. 2019), in terms of O_2 resistance. Shielding the enzyme active site from O_2 is also a way to overcome its effects. In these strategies, O_2 is reduced before it reaches the enzyme. There are several examples in the literature of this kind of protection strategy. For example, in Sakay and colleagues (Sakai et al. 2013) protected a [NiFeSe] hydrogenase from *Dm. baculatum* from O_2 in a photocatalytic H_2 production system through an organic dye, Eosin Y. Shielding strategies have also been applied to H_2 oxidizing systems. Redox-active polymers containing viologen moieties (Plumeré et al. 2014) are capable of simultaneously immobilizing and protecting hydrogenases, working as self-activated catalytic O_2-scavenging mechanisms, allowing successful H_2 oxidation in the presence of O_2. This strategy was already tested with success for different classes of hydrogenases possessing different sensibilities to O_2, including NiFeSe hydrogenases (Plumeré et al. 2014; Oughli et al. 2015; Ruff et al. 2017).

Bibliography:

Abdalla, A. M., Hossain, S., Nisfindy, O. B., Azad, A. T., Dawood, M., & Azad, A. K. (2018). Hydrogen production, storage, transportation and key challenges with applications: A review. *Energy Conversion and Management*, *165*(January), 602–627. https://doi.org/10.1016/j.enconman.2018.03.088

Abou Hamdan, A., Burlat, B., Gutiérrez-Sanz, Ó., Liebgott, P.-P., Baffert, C., De Lacey, A. L., … Dementin, S. (2013). O2-independent formation of the inactive states of NiFe hydrogenase. *Nature Chemical Biology*, *9*(1), 15–17. https://doi.org/10.1038/nchembio.1110

Albracht, S. P. J., & Hedderich, R. (2000). Learning from hydrogenases: location of a proton pump and of a second FMN in bovine NADH--ubiquinone oxidoreductase (Complex I). *FEBS Letters*, *485*(1), 1–6. https://doi.org/10.1016/s0014-5793(00)02172-4

Ball, M., & Weeda, M. (2015). The hydrogen economy - Vision or reality? *International Journal of Hydrogen Energy*, *40*(25), 7903–7919. https://doi.org/10.1016/j.ijhydene.2015.04.032

Baltazar, C. S. A., Marques, M., Soares, C. M., De Lacey, A. L., Pereira, I. A. C., & Matias, P. M. (2011). Nickel-Iron-Selenium Hydrogenases - An Overview. *European Journal of Inorganic Chemistry*, *2011*(7), 948–962. https://doi.org/10.1002/ejic.201001127

Barahona, E., Jiménez-Vicente, E., & Rubio, L. M. (2016). Hydrogen overproducing nitrogenases obtained by random mutagenesis and high-throughput screening. *Scientific Reports*, *6*. https://doi.org/10.1038/srep38291

Barilone, J. L., Ogata, H., Lubitz, W., & van Gastel, M. (2015). Structural differences between the active sites of the Ni-A and Ni-B states of the [NiFe] hydrogenase: an approach by quantum chemistry and single crystal ENDOR spectroscopy. *Phys. Chem. Chem. Phys.*, *17*(24), 16204–16212. https://doi.org/10.1039/C5CP01322D

Bernhard, M., Buhrke, T., Bleijlevens, B., De Lacey, A. L., Fernandez, V. M., Albracht, S. P. J., & Friedrich, B. (2001). The H2 sensor of Ralstonia eutropha. *Journal of Biological Chemistry*, *276*(19), 15592–15597. https://doi.org/10.1074/jbc.M009802200

Birrell, J. A., Wrede, K., Pawlak, K., Rodríguez-Maciá, P., Rüdiger, O., Reijerse, E. J., & Lubitz, W. (2016). Artificial Maturation of the Highly Active Heterodimeric [FeFe] Hydrogenase from Desulfovibrio desulfuricans ATCC 7757. *Israel Journal of Chemistry*, 1–13. https://doi.org/10.1002/ijch.201600035

Birringer, M., Pilawa, S., & Flohé, L. (2002). Trends in selenium biochemistry. *Natural Product Reports*, *19*(6), 693–718. Retrieved from http://www.ncbi.nlm.nih.gov/pubmed/12521265

Böck, A, Forchhammer, K., Heider, J., Leinfelder, W., Sawers, G., Veprek, B., & Zinoni, F. (1991). Selenocysteine: the 21st amino acid. *Molecular Microbiology*, *5*(3), 515–520.

Böck, August. (2000). Biosynthesis of selenoproteins - An overview. *BioFactors*. IOS Press. https://doi.org/10.1002/biof.5520110122

Bossel, U. (2006). Does a Hydrogen Economy Make Sense? *Proceedings of the IEEE*, *94*(10).

Brand, J. J., Wright, J. N., & Lien, S. (1989). Hydrogen production by eukaryotic algae. *Biotechnology and Bioengineering*, *33*(11), 1482–1488. https://doi.org/10.1002/bit.260331116

Brecht, M., Van Gastel, M., Buhrke, T., Friedrich, B., & Lubitz, W. (2003). Direct Detection of a Hydrogen Ligand in the [NiFe] Center of the Regulatory H2-Sensing Hydrogenase from Ralstonia eutropha in Its Reduced State by HYSCORE and ENDOR Spectroscopy. *Journal of the American Chemical Society*, *125*(43), 13075–13083. https://doi.org/10.1021/ja036624x

Buhrke, T., Lenz, O., Krauss, N., & Friedrich, B. (2005). Oxygen tolerance of the H2-sensing [NiFe] hydrogenase from Ralstonia eutropha H16 is based on limited access of oxygen to the active site. *Journal of Biological Chemistry*, *280*(25), 23791–23796. https://doi.org/10.1074/jbc.M503260200

Buhrke, T., Lenz, O., Porthun, A., & Friedrich, B. (2004). The H2-sensing complex of Ralstonia eutropha: interaction between a regulatory [NiFe] hydrogenase and a histidine protein kinase. *Molecular Microbiology*, *51*(6), 1677–1689. https://doi.org/10.1046/j.1365-2958.2003.03933.x

Ceccaldi, P., Marques, M., Fourmond, V., Pereira, I. A. C., & Léger, C. (2015). Oxidative inactivation of NiFeSe hydrogenase. *Chemical Communications (Cambridge, England)*, *51*, 14223–14226. https://doi.org/10.1039/C5CC05930E

Constant, P., Chowdhury, S. P., Hesse, L., Pratscher, J., & Conrad, R. (2011). Genome data mining and soil survey for the novel group 5 [NiFe]-hydrogenase to explore the diversity and ecological importance

of presumptive high-affinity H 2-oxidizing bacteria. *Applied and Environmental Microbiology*, *77*(17), 6027–6035. https://doi.org/10.1128/AEM.00673-11

Constant, P., & Hallenbeck, P. C. (2019). Hydrogenase. In *Biohydrogen* (pp. 49–78). https://doi.org/10.1016/B978-0-444-64203-5.00003-4

Constant, P., Poissant, L., & Villemur, R. (2008). Isolation of Streptomyces sp. PCB7, the first microorganism demonstrating high-affinity uptake of tropospheric H2. *ISME Journal*, *2*(10), 1066–1076. https://doi.org/10.1038/ismej.2008.59

Constant, P., Poissant, L., & Villemur, R. (2009). Tropospheric H(2) budget and the response of its soil uptake under the changing environment. *The Science of the Total Environment*, *407*(6), 1809–1823. https://doi.org/10.1016/j.scitotenv.2008.10.064

Coyle, E. D., & Simmons, R. A. (2014). *Understanding the Global Energy Crisis*. Purdue University Press Lafayette.

Cracknell, J. A., Wait, A. F., Lenz, O., Friedrich, B., & Armstrong, F. A. (2009). A kinetic and thermodynamic understanding of O2 tolerance in [NiFe]-hydrogenases. *Proceedings of the National Academy of Sciences of the United States of America*, *106*(49), 20681–20686. https://doi.org/10.1073/pnas.0905959106

De Lacey, A. L., Fernández, V. M., Rousset, M., & Cammack, R. (2007). Activation and inactivation of hydrogenase function and the catalytic cycle: spectroelectrochemical studies. *Chemical Reviews*, *107*(10), 4304–4330. https://doi.org/10.1021/cr0501947

del Barrio, M., Sensi, M., Orain, C., Baffert, C., Dementin, S., Fourmond, V., & Léger, C. (2018). Electrochemical Investigations of Hydrogenases and Other Enzymes That Produce and Use Solar Fuels. *Accounts of Chemical Research*, *51*(3), 769–777. https://doi.org/10.1021/acs.accounts.7b00622

Dementin, S., Belle, V., Bertrand, P., Guigliarelli, B., Adryanczyk-Perrier, G., De Lacey, A. L., … Léger, C. (2006). Changing the ligation of the distal [4Fe4S] cluster in NiFe hydrogenase impairs inter- and intramolecular electron transfers. *Journal of the American Chemical Society*, *128*(15), 5209–5218. https://doi.org/10.1021/ja060233b

Dementin, S., Leroux, F., Cournac, L., de Lacey, A. L., Volbeda, A., Léger, C., … Rousset, M. (2009). Introduction of methionines in the gas channel makes [NiFe] hydrogenase aero-tolerant. *Journal of the American Chemical Society*, *131*(29), 10156–10164. https://doi.org/10.1021/ja9018258

Dresselhaus, M. S., & Thomas, I. L. (2001). Alternative energy technologies. *Nature*, *414*(6861), 332–337. https://doi.org/https://doi.org/10.1038/35104599

Duché, O., Elsen, S., Cournac, L., & Colbeau, A. (2005). Enlarging the gas access channel to the active site renders the regulatory hydrogenase HupUV of Rhodobacter capsulatus O2 sensitive without affecting its transductory activity. *FEBS Journal*, *272*, 3899–3908. https://doi.org/10.1111/j.1742-4658.2005.04806.x

Eguchi, S., Yoon, K. S., & Ogo, S. (2012). O2-stable membrane-bound [NiFe] hydrogenase from a newly isolated Citrobacter sp. S-77. *Journal of Bioscience and Bioengineering*, *114*(5), 479–484. https://doi.org/10.1016/j.jbiosc.2012.05.018

Eidsness, M. K., Scott, R. A., Prickril, B. C., DerVartanian, D. V., Legall, J., Moura, I., … Peck, H. D. (1989). Evidence for selenocysteine coordination to the active site nickel in the [NiFeSe]hydrogenases from Desulfovibrio baculatus. *Proceedings of the National Academy of Sciences*, *86*(1), 147–151. https://doi.org/10.1073/pnas.86.1.147

Esper, B., Badura, A., & Rögner, M. (2006). Photosynthesis as a power supply for (bio-)hydrogen production. *Trends in Plant Science*, *11*(11), 543–549. https://doi.org/10.1016/j.tplants.2006.09.001

European Commission. Hydrogen Energy and Fuel Cells (2019).

Evans, R. M., Parkin, A., Roessler, M. M., Murphy, B. J., Adamson, H., Lukey, M. J., … Armstrong, F. A. (2013). Principles of sustained enzymatic hydrogen oxidation in the presence of oxygen -the crucial influence of high potential Fe-S clusters in the electron relay of [NiFe]-hydrogenases. *Journal of the American Chemical Society*, *135*(7), 2694–2707. https://doi.org/10.1021/ja311055d

Evans, R. M., Siritanaratkul, B., Megarity, C. F., Pandey, K., Esterle, T. F., Badiani, S., & Armstrong, F. A. (2018). The value of enzymes in solar fuels research – efficient electrocatalysts through evolution. *Chemical Society Reviews*. https://doi.org/10.1039/C8CS00546J

Fernández, V. M., Hatchikian, E. C., & Cammack, R. (1985). Properties and reactivation of two different deactivated forms of Desulfovibrio gigas hydrogenase. *Biochimica et Biophysica Acta*, *832*(1), 69–79.

Fourmond, V., Infossi, P., Giudici-Orticoni, M. T., Bertrand, P., & Léger, C. (2010). "two-Step" chronoamperometric method for studying the anaerobic inactivation of an oxygen tolerant nife hydrogenase. *Journal of the American Chemical Society*, *132*(13), 4848–4857. https://doi.org/10.1021/ja910685j

Fritsch, J., Lenz, O., & Friedrich, B. (2013). Structure, function and biosynthesis of O2-tolerant hydrogenases. *Nature Reviews. Microbiology*, *11*(2), 106–114. https://doi.org/10.1038/nrmicro2940

Fritsch, J., Scheerer, P., Frielingsdorf, S., Kroschinsky, S., Friedrich, B., Lenz, O., & Spahn, C. M. T. (2011). The crystal structure of an oxygen-tolerant hydrogenase uncovers a novel iron-sulphur centre. *Nature*, *479*(7372), 249–252. https://doi.org/10.1038/nature10505

Gaffron, H., & Rubin, J. (1942). FERMENTATIVE AND PHOTOCHEMICAL PRODUCTION OF HYDROGEN IN ALGAE. *The Journal of General Physiology*, *26*(2), 219–240. https://doi.org/10.1085/jgp.26.2.219

Garcin, E., Vernede, X., Hatchikian, E. C., Volbeda, A., Frey, M., & Fontecilla-Camps, J. C. (1999). The crystal structure of a reduced [NiFeSe] hydrogenase provides an image of the activated catalytic center. *Structure*, *7*(5), 557–566. Retrieved from http://www.ncbi.nlm.nih.gov/pubmed/10378275

Goldet, G., Wait, A. F., Cracknell, J. A., Vincent, K. A., Ludwig, M., Lenz, O., … Armstrong, F. A. (2008). Hydrogen production under aerobic conditions by membrane-bound hydrogenases from Ralstonia species. *Journal of the American Chemical Society*, *130*(33), 11106–11113. https://doi.org/10.1021/ja8027668

Goris, T., Wait, A. F., Saggu, M., Fritsch, J., Heidary, N., Stein, M., … Lenz, O. (2011). A unique iron-sulfur cluster is crucial for oxygen tolerance of a [NiFe]-hydrogenase. *Nature Chemical Biology*, *7*(5), 310–318. https://doi.org/10.1038/nchembio.555

Greening, C., Biswas, A., Carere, C. R., Jackson, C. J., Taylor, M. C., Stott, M. B., … Morales, S. E. (2016). Genomic and metagenomic surveys of hydrogenase distribution indicate H 2 is a widely utilised energy source for microbial growth and survival. *ISME Journal*, *10*(3), 761–777. https://doi.org/10.1038/ismej.2015.153

Greening, C., & Cook, G. M. (2014, April). Integration of hydrogenase expression and hydrogen sensing in bacterial cell physiology. *Current Opinion in Microbiology*. https://doi.org/10.1016/j.mib.2014.02.001

Happe, T., & Naber, J. D. (1993). Isolation, characterization and N-terminal amino acid sequence of hydrogenase from the green alga Chlamydomonas reinhardtii. *European Journal of Biochemistry / FEBS*, *214*(2), 475–481. https://doi.org/10.1111/j.1432-1033.1993.tb17944.x

Hatchikian, E. C., Forget, N., Fernandez, V. M., Williams, R., & Cammack, R. (1992). Further characterization of the [Fe]-hydrogenase from Desulfovibrio desulfuricans ATCC 7757. *European Journal of Biochemistry*, *209*(1), 357–365. https://doi.org/10.1111/j.1432-1033.1992.tb17297.x

Hemschemeier, A., Fouchard, S., Cournac, L., Peltier, G., & Happe, T. (2008). Hydrogen production by Chlamydomonas reinhardtii: an elaborate interplay of electron sources and sinks. *Planta*, *227*(2), 397–407. https://doi.org/10.1007/s00425-007-0626-8

Hemschemeier, A., & Happe, T. (2011). Alternative photosynthetic electron transport pathways during anaerobiosis in the green alga Chlamydomonas reinhardtii. *Biochimica et Biophysica Acta*, *1807*(8), 919–926. https://doi.org/10.1016/j.bbabio.2011.02.010

Hexter, S. V., Grey, F., Happe, T., Climent, V., & Armstrong, F. A. (2012). Electrocatalytic mechanism of reversible hydrogen cycling by enzymes and distinctions between the major classes of hydrogenases (Proceedings of the National Academy of Sciences of the United States of America (2012) 109 (11516-11521)). *Proceedings of the National Academy of Sciences of the United States of America*, *109*(44), 18232–18233. https://doi.org/10.1073/pnas.1216081109

Higuchi, Y., Ogata, H., Miki, K., Yasuoka, N., & Yagi, T. (1999). Removal of the bridging ligand atom at the Ni-Fe active site of [NiFe] hydrogenase upon reduction with H2, as revealed by X-ray structure analysis at 1.4 Å resolution. *Structure*, *7*(5), 549–556. https://doi.org/10.1016/S0969-2126(99)80071-9

Higuchi, Y., Yagi, T., & Yasuoka, N. (1997). Unusual ligand structure in Ni – Fe active center and an additional Mg site in hydrogenase revealed by high resolution X-ray structure analysis. *Structure*, *5*(2), 1671–1680.

Hondal, R. J., Marino, S. M., & Gladyshev, V. N. (2013, May 1). Selenocysteine in thiol/disulfide-like exchange reactions. *Antioxidants and Redox Signaling*. https://doi.org/10.1089/ars.2012.5013

Hondal, R. J., & Ruggles, E. L. (2011, June). Differing views of the role of selenium in thioredoxin reductase. *Amino Acids*. https://doi.org/10.1007/s00726-010-0494-6

Horner, D. S., Heil, B., Happe, T., & Embley, T. M. (2002). Iron hydrogenases - Ancient enzymes in modern eukaryotes. *Trends in Biochemical Sciences*, *27*(3), 148–153. https://doi.org/10.1016/S0968-0004(01)02053-9

Hosseini, S. E., & Wahid, M. A. (2016). Hydrogen production from renewable and sustainable energy resources: Promising green energy carrier for clean development. *Renewable and Sustainable Energy Reviews*, *57*, 850–866. https://doi.org/10.1016/j.rser.2015.12.112

Hubbert, K. (1990). Energy From Fossil Fuels. *Scientific American*, *262–9*(February), 129–135.

Jones, A. K., Sillery, E., Albracht, S. P. J., & Armstrong, F. A. (2002). Direct comparison of the electrocatalytic oxidation of hydrogen by an enzyme and a platinum catalyst. *Chemical Communications*, (8), 866–867. https://doi.org/10.1039/b201337a

Kasting, J. F., Ackerman, T. P., Series, N., & Jan, N. (1993). Earth ' s Early Atmosphere : Response. *Science*, *235*(4787), 2341–2343.

Kuhn, M., Steinbüchel, A., & Schlegel, H. G. (1984). Hydrogen evolution by strictly aerobic hydrogen bacteria under anaerobic conditions. *Journal of Bacteriology*, *159*(2), 633–639. Retrieved from http://www.ncbi.nlm.nih.gov/pubmed/6378884

Kurkin, S., George, S. J., Thorneley, R. N. F., & Albracht, S. P. J. (2004). Hydrogen-induced activation of the [NiFe]-hydrogenase from Allochromatium vinosum as studied by stopped-flow infrared spectroscopy. *Biochemistry*, *43*(21), 6820–6831. https://doi.org/10.1021/bi049854c

Lambertz, C., Leidel, N., Havelius, K. G. V., Noth, J., Chernev, P., Winkler, M., … Haumann, M. (2011). O2 reactions at the six-iron active site (H-cluster) in [FeFe]-hydrogenase. *Journal of Biological Chemistry*, *286*(47), 40614–40623. https://doi.org/10.1074/jbc.M111.283648

Lane, N., Allen, J. F., & Martin, W. (2010). How did LUCA make a living? Chemiosmosis in the origin of life. *BioEssays*, *32*(4), 271–280. https://doi.org/10.1002/bies.200900131

Lauterbach, L., & Lenz, O. (2013). Catalytic production of hydrogen peroxide and water by oxygen-tolerant [NiFe]-hydrogenase during H2 cycling in the presence of O2. *Journal of the American Chemical Society*, *135*(47), 17897–17905. https://doi.org/10.1021/ja408420d

Lemon, B. J., & Peters, J. W. (1999). Binding of exogenously added carbon monoxide at the active site of the iron-only hydrogenase (CpI) from Clostridium pasteurianum. *Biochemistry*, *38*(40), 12969–12973. https://doi.org/10.1021/bi9913193

Liebgott, P.-P., de Lacey, A. L., Burlat, B., Cournac, L., Richaud, P., Brugna, M., … Dementin, S. (2011). Original design of an oxygen-tolerant [NiFe] hydrogenase: major effect of a valine-to-cysteine mutation near the active site. *Journal of the American Chemical Society*, *133*(4), 986–997. https://doi.org/10.1021/ja108787s

Liebgott, P.-P., Dementin, S., Léger, C., & Rousset, M. (2011). Towards engineering O2-tolerance in [Ni–Fe] hydrogenases. *Energy & Environmental Science*, *4*(1), 33. https://doi.org/10.1039/c0ee00093k

Lubitz, W., Ogata, H., Rudiger, O., & Reijerse, E. (2014). Hydrogenases. *Chemical Reviews*, *114 (8)*, 4081–4148. https://doi.org/10.1021/cr4005814

Lukey, M. J., Parkin, A., Roessler, M. M., Murphy, B. J., Harmer, J., Palmer, T., … Armstrong, F. A. (2010). How Escherichia coli is equipped to oxidize hydrogen under different redox conditions. *Journal of Biological Chemistry*, *285*(6), 3928–3938. https://doi.org/10.1074/jbc.M109.067751

Lukey, M. J., Roessler, M. M., Parkin, A., Evans, R. M., Davies, R. a, Lenz, O., … Armstrong, F. a. (2011). Oxygen-tolerant [NiFe]-hydrogenases: the individual and collective importance of supernumerary cysteines at the proximal Fe-S cluster. *Journal of the American Chemical Society*, *133*(42), 16881–16892. https://doi.org/10.1021/ja205393w

Lyon, E. J., Shima, S., Boecher, R., Thauer, R. K., Grevels, F. W., Bill, E., … Albracht, S. P. J. (2004). Carbon monoxide as an intrinsic ligand to iron in the active site of the iron-sulfur-cluster-free hydrogenase H2-forming methylenetetrahydromethanopterin dehydrogenase as revealed by infrared spectroscopy. *Journal of the American Chemical Society*, *126*(43), 14239–14248. https://doi.org/10.1021/ja046818s

Mailloux, R. J. (2015). Teaching the fundamentals of electron transfer reactions in mitochondria and the production and detection of reactive oxygen species. *Redox Biology*, *4*(March), 381–398. https://doi.org/10.1016/j.redox.2015.02.001

Maroney, M. J., & Hondal, R. J. (2018). Selenium versus sulfur: Reversibility of chemical reactions and resistance to permanent oxidation in proteins and nucleic acids. *Free Radical Biology and Medicine*, *127*, 228–237. https://doi.org/10.1016/j.freeradbiomed.2018.03.035

Marques, M., Coelho, R., De Lacey, A. L., Pereira, I. A. C., & Matias, P. M. (2010). The three-dimensional structure of [NiFeSe] hydrogenase from Desulfovibrio vulgaris Hildenborough: a hydrogenase

without a bridging ligand in the active site in its oxidised, "as-isolated" state. *Journal of Molecular Biology*, *396*(4), 893–907. https://doi.org/10.1016/j.jmb.2009.12.013

Marques, M., Tapia, C., Gutiérrez-Sanz, Ó., Ramos, A. R., Keller, K. L., Wall, J. D., … Pereira, I. A. C. (2017). The direct role of selenocysteine in [NiFeSe] hydrogenase maturation and catalysis. *Nature Chemical Biology*, *13*(5), 554–550. https://doi.org/10.1038/nchembio.2335

Medina, M., Hatchikian, E. C., & Cammack, R. (1996). Studies of light-induced nickel EPR signals in hydrogenases: comparation of enzymes with and without selenium. *Biochimica et Biophysica Acta*, *1275*, 227–236.

Melis, A., & Happe, T. (2001). Hydrogen Production . Green Algae as a Source of Energy. *Plant Physiology*, *127*, 740–748. https://doi.org/10.1104/pp.010498.740

Miranda, P. (2019). Hydrogen Energy. In *Science and Engineering of Hydrogen-Based Energy Technologies* (pp. 1–38). Elsevier Inc. https://doi.org/10.1016/B978-0-12-809597-3.00113-9

Mulder, D. W., Boyd, E. S., Sarma, R., Lange, R. K., Endrizzi, J. A., Broderick, J. B., & Peters, J. W. (2010). Stepwise FeFe-hydrogenase H-cluster assembly revealed in the structure of HydA ΔeFG. *Nature*, *465*(7295), 248–251. https://doi.org/10.1038/nature08993

Nicolet, Y., Piras, C., Legrand, P., Hatchikian, E. C., & Fontecilla-camps, J. C. (1999). Desulfovibrio desulfuricans iron hydrogenase: the structure shows unusual coordination to an active site Fe binuclear center. *Structure*, 13–23. Retrieved from http://www.sciencedirect.com/science/article/pii/S0969212699800057

Noor, D., Matsuura, H., Nishikawa, K., Tai, H., Hirota, S., Kim, J., … Higuchi, Y. (2018). Redox-dependent conformational changes of a proximal [4Fe-4S] cluster in Hyb-type [NiFe]-hydrogenase to protect the active site from O2. *ChemComm*, 12385–12388. https://doi.org/10.1039/c8cc06261g

Novelli, P. C., Masaric, K., Hurst, D., Myers, R., & Elkins, J. (1999). Molecular hydrogen in the troposphere: Global distribution and budget. *Journal of Geophysical Research Atmospheres*, *104*(D23), 30427–30444. https://doi.org/10.1029/1999JD900788

Ogata, H., Hirota, S., Nakahara, A., Komori, H., Shibata, N., Kato, T., … Higuchi, Y. (2005). Activation process of [NiFe] hydrogenase elucidated by high-resolution X-ray analyses: Conversion of the ready to the unready state. *Structure*, *13*(11), 1635–1642. https://doi.org/10.1016/j.str.2005.07.018

Ogata, H., Nishikawa, K., & Lubitz, W. (2015). Hydrogens detected by subatomic resolution protein crystallography in a [NiFe] hydrogenase. *Nature*, 571–574. https://doi.org/10.1038/nature14110

Pandelia, M.-E., Fourmond, V., Tron-Infossi, P., Lojou, E., Bertrand, P., Léger, C., … Lubitz, W. (2010). Membrane-bound hydrogenase I from the hyperthermophilic bacterium aquifex aeolicus: Enzyme activation, redox intermediates and oxygen tolerance. *Journal of the American Chemical Society*, *132*(20), 6991–7004. https://doi.org/10.1021/ja910838d

Pandelia, M.-E., Nitschke, W., Infossi, P., Giudici-Orticoni, M.-T., Bill, E., & Lubitz, W. (2011). Characterization of a unique [FeS] cluster in the electron transfer chain of the oxygen tolerant [NiFe] hydrogenase from Aquifex aeolicus. *Proceedings of the National Academy of Sciences of the United States of America*, *108*(15), 6097–6102. https://doi.org/10.1073/pnas.1100610108

Parkin, A., Goldet, G., Cavazza, C., Fontecilla-Camps, J. C., & Armstrong, F. a. (2008). The difference a Se makes? Oxygen-tolerant hydrogen production by the [NiFeSe]-hydrogenase from Desulfomicrobium baculatum. *Journal of the American Chemical Society*, *130*(40), 13410–13416. https://doi.org/10.1021/ja803657d

Pereira, I. A. C., Ramos, A. R., Grein, F., Marques, M., da Silva, S. M., & Venceslau, S. S. (2011). A comparative genomic analysis of energy metabolism in sulfate reducing bacteria and archaea. *Frontiers in Microbiology*, *2*(April), 69. https://doi.org/10.3389/fmicb.2011.00069

Peters, J. W., Lanzilotta, W. N., Lemon, B. J., & Seefeldt, L. C. (1998). X-ray crystal structure of the Fe-only hydrogenase (Cpl) from Clostridium pasteurianum to 1.8 angstrom resolution. *Science*, *282*(5395), 1853–1858.

Peters, J. W., Schut, G. J., Boyd, E. S., Mulder, D. W., Shepard, E. M., Broderick, J. B., … Adams, M. W. W. (2015). [FeFe]- and [NiFe]-hydrogenase diversity, mechanism, and maturation. *Biochimica et Biophysica Acta*, *1853*(6), 1350–1369. https://doi.org/10.1016/j.bbamcr.2014.11.021

Plumeré, N., Rüdiger, O., Oughli, A. A., Williams, R., Vivekananthan, J., Pöller, S., … Lubitz, W. (2014). A redox hydrogel protects hydrogenase from high-potential deactivation and oxygen damage. *Nature Chemistry*, *6*(September). https://doi.org/10.1038/nchem.2022

Preissler, J., Wahlefeld, S., Lorent, C., Teutloff, C., Horch, M., Lauterbach, L., … Lenz, O. (2018). Enzymatic and spectroscopic properties of a thermostable [NiFe]‑hydrogenase performing H2-driven NAD+-reduction in the presence of O2. *Biochimica et Biophysica Acta - Bioenergetics*, *1859*(1), 8–18.

https://doi.org/10.1016/j.bbabio.2017.09.006

Rand, D. A. J., & Dell, R. M. (2008). *Hydrogen Energy. Challenges ans Prospects*. RSC Publishing: Cambridge, UK.

Reddie, K. G., & Carroll, K. S. (2008). Expanding the functional diversity of proteins through cysteine oxidation. *Current Opinion in Chemical Biology*, *12*(6), 746–754. https://doi.org/10.1016/j.cbpa.2008.07.028

Reich, H. J., & Hondal, R. J. (2016). Why Nature Chose Selenium. *ACS Chemical Biology*, (11 (4)), 821–841. https://doi.org/10.1021/acschembio.6b00031

Riethausen, J., Rüdiger, O., Gärtner, W., Lubitz, W., & Shafaat, H. S. (2013). Spectroscopic and electrochemical characterization of the [NiFeSe] hydrogenase from Desulfovibrio vulgaris Miyazaki F: reversible redox behavior and interactions between electron transfer centers. *Chembiochem : A European Journal of Chemical Biology*, *14*(14), 1714–1719. https://doi.org/10.1002/cbic.201300120

Roessler, M. M., Evans, R. M., Davies, R. A., Harmer, J., & Armstrong, F. A. (2012). EPR Spectroscopic Studies of the Fe−S Clusters in the O2 Tolerant [NiFe]-Hydrogenase Hyd-1 from Escherichia coli and Characterization of the Unique [4Fe−3S] Cluster by HYSCORE. *J Am Chem Soc*, *134*(37), 15581–15594. https://doi.org/10.1021/ja307117y

Rousset, M., Montet, Y., Guigliarelli, B., Forget, N., Asso, M., Bertrand, P., … Hatchikian, E. C. (1998). [3Fe-4S] to [4Fe-4S] cluster conversion in Desulfovibrio fructosovorans [NiFe] hydrogenase by site-directed mutagenesis. *Proceedings of the National Academy of Sciences of the United States of America*, *95*(20), 11625–11630. Retrieved from http://www.pubmedcentral.nih.gov/articlerender.fcgi?artid=21691&tool=pmcentrez&rendertype=abstract

Saggu, M., Zebger, I., Ludwig, M., Lenz, O., Friedrich, B., Hildebrandt, P., & Lendzian, F. (2009). Spectroscopic insights into the oxygen-tolerant membrane-associated [NiFe] hydrogenase of Ralstonia eutropha H16. *Journal of Biological Chemistry*, *284*(24), 16264–16276. https://doi.org/10.1074/jbc.M805690200

Sakai, T., Mersch, D., & Reisner, E. (2013). Photocatalytic Hydrogen Evolution with a Hydrogenase in a Mediator-Free System under High Levels of Oxygen. *Angewandte Chemie (International Ed. in English)*, *52*(47), 12313–12316. https://doi.org/10.1002/anie.201306214

Schäfer, C., Bommer, M., Hennig, S. E., Jeoung, J. H., Dobbek, H., & Lenz, O. (2016). Structure of an Actinobacterial-Type [NiFe]-Hydrogenase Reveals Insight into O2-Tolerant H2 Oxidation. *Structure*, *24*(2), 285–292. https://doi.org/10.1016/j.str.2015.11.010

Schäfer, C., Friedrich, B., & Lenz, O. (2013). Novel, oxygen-insensitive group 5 [NiFe]-hydrogenase in Ralstonia eutropha. *Applied and Environmental Microbiology*, *79*(17), 5137–5145. https://doi.org/10.1128/AEM.01576-13

Schneider, K., & Schlegel, H. G. (1981). Production of superoxide radicals by soluble hydrogenase from Alcaligenes eutrophus H16. *The Biochemical Journal*, *193*(1), 99–107. https://doi.org/10.1042/bj1930099

Schwartz, E., & Barbel, F. (2006). The H2-Metabolizing Prokaryotes. In *Prokaryotes* (pp. 496–563). https://doi.org/10.1007/0-387-30742-7_17

Shomura, Y., Yoon, K.-S., Nishihara, H., & Higuchi, Y. (2011). Structural basis for a [4Fe-3S] cluster in the oxygen-tolerant membrane-bound [NiFe]-hydrogenase. *Nature*, *479*(7372), 253–256. https://doi.org/10.1038/nature10504

Sorgenfrei, O., Klein, A., & Albracht, S. P. J. (1993). Influence of illumination on the electronic interaction between 77Se and nickel in active F420-non-reducing hydrogenase from Methanococcus voltae. *FEBS Letters*, *332*(3), 291–297. https://doi.org/10.1016/0014-5793(93)80652-B

Sousa, F. L., Preiner, M., & Martin, W. F. (2018). Native metals, electron bifurcation, and CO2 reduction in early biochemical evolution. *Current Opinion in Microbiology*, *43*(January), 77–83. https://doi.org/10.1016/j.mib.2017.12.010

Stephenson, M., & Stickland, L. H. (1931). Hydrogenase: a bacterial enzyme activating molecular hydrogen: The properties of the enzyme. *The Biochemical Journal*, *25*, 205–214.

Stiebritz, M. T., & Reiher, M. (2009). Theoretical Study of Dioxygen Induced Inhibition of [FeFe]-Hydrogenase. *Inorganic Chemistry*, *48*(15), 7127–7140. https://doi.org/10.1021/ic9002127

Stripp, S. T., Goldet, G., Brandmayr, C., Sanganas, O., Vincent, K. A., Haumann, M., … Happe, T. (2009). How oxygen attacks [FeFe] hydrogenases from photosynthetic organisms. *Proceedings of the National Academy of Sciences*, *106*(41), 17331–17336. https://doi.org/10.1073/pnas.0905343106

Stripp, S. T., & Happe, T. (2009). How algae produce hydrogen - news from the photosynthetic

hydrogenase. *Dalton Transactions (Cambridge, England : 2003)*, (45), 9952–9959. https://doi.org/10.1039/b911129h

Swanson, K. D., Ratzloff, M. W., Mulder, D. W., Artz, J. H., Ghose, S., Hoffman, A., … Peters, J. W. (2015). [FeFe]-hydrogenase oxygen inactivation is initiated at the H cluster 2Fe subcluster. *Journal of the American Chemical Society*, *137*(5), 1809–1816. https://doi.org/10.1021/ja510169s

Teixeira, M., Fauque, G., Moura, I., Lespinat, P. A., Berlier, Y., Prickril, B., … Moura, J. J. G. (1987). Nickel-[iron-sulfur]-selenium-containing hydrogenases from Desulfovibrio baculatus (DSM 1743). *European Journal of Biochemistry / FEBS*, *58*, 47–58. https://doi.org/10.1111/j.1432-1033.1987.tb13302

Teixeira, M., Moura, I., Fauque, G., DerVartanian, D. V, Le Gall, J., Peck, H. D., … Huynh, B. H. (1990). The iron-sulfur centers of the soluble [NiFeSe] hydrogenase, from. *Eur J Biochem*, *386*, 381–386.

Thauer, R., Kaster, A.-K., Goenrich, M., Schick, M., Hiromoto, T., & Shima, S. (2010). Hydrogenases from Methanogenic Archaea, Nickel, a Novel Cofactor, and H 2 Storage. *Annual Review of Biochemistry*, *79*(1), 507–536. https://doi.org/10.1146/annurev.biochem.030508.152103

Uchida, H. and, & Harada, M. (2018). Hydrogen Storage and Transport Technologies. In P. Miranda (Ed.), *Science and Engineering of Hydrogen-Based Energy Technologies* (pp. 221–228). Elsevier Inc. https://doi.org/10.1016/B978-0-12-814251-6.00010-1

US Department of Energy. (2013). Report of the Hydrogen Production Expert Panel : A Subcommittee of the Hydrogen & Fuel Cell Technical Advisory Committee. *DoE Fuel Cell Technologies Office*, (October 2012).

Valente, F., Oliveira, S., Gnadt, N., Pacheco, I., Coelho, A., Xavier, A. V, … Pereira, I. A. C. (2005). Hydrogenases in Desulfovibrio vulgaris Hildenborough: structural and physiologic characterisation of the membrane-bound [NiFeSe] hydrogenase. *Journal of Biological Inorganic Chemistry*, *10*(6), 667–682. https://doi.org/10.1007/s00775-005-0022-4

van Gastel, M., Fichtner, C., Neese, F., & Lubitz, W. (2005). EPR experiments to elucidate the structure of the ready and unready states of the [NiFe] hydrogenase of Desulfovibrio vulgaris Miyazaki F. *Biochemical Society Transactions*, *33*(Pt 1), 7–11. https://doi.org/10.1042/BST0330007

Veziroglu, T. N., Sherif, S. A., & Barbir, F. (2005). Hydrogen Energy Solutions. In F. J. Agardy & N. L. Nemerow (Eds.), *Environmental Solutions*. Elsevier Inc. https://doi.org/10.1016/B978-0-12-088441-4.50008-3

Vignais, P. M., & Billoud, B. (2007). Occurrence, classification, and biological function of hydrogenases: an overview. *Chemical Reviews*, *107*(10), 4206–4272. https://doi.org/10.1021/cr050196r

Vignais, P. M., Billoud, B., & Meyer, J. (2001). Classification and phylogeny of hydrogenases 1. *FEMS Microbiology Reviews*, *25*.

Vignais, P. M., Willison, J., & Colbeau, A. (2004). H2 Respiration. In *Respiration in Archae and Bacteria* (pp. 233–254).

Vincent, K. A., Parkin, A., Lenz, O., Albracht, S. P. J., Fontecilla-Camps, J. C., Cammack, R., … Armstrong, F. A. (2005). Electrochemical definitions of O2 sensitivity and oxidative inactivation in hydrogenases. *Journal of the American Chemical Society*, *127*(51), 18179–18189. https://doi.org/10.1021/ja055160v

Vincent, K. a, Cracknell, J. a, Lenz, O., Zebger, I., Friedrich, B., & Armstrong, F. a. (2005). Electrocatalytic hydrogen oxidation by an enzyme at high carbon monoxide or oxygen levels. *Proceedings of the National Academy of Sciences of the United States of America*, *102*(47), 16951–16954. https://doi.org/10.1073/pnas.0504499102

Volbeda, A., Amara, P., Darnault, C., Mouesca, J.-M., Parkin, A., Roessler, M. M., … Fontecilla-Camps, J. C. (2012). X-ray crystallographic and computational studies of the O2-tolerant [NiFe]-hydrogenase 1 from Escherichia coli. *Proceedings of the National Academy of Sciences of the United States of America*, *109*(14), 5305–5310. https://doi.org/10.1073/pnas.1119806109

Volbeda, A., Amara, P., Iannello, M., De Lacey, A. L., Cavazza, C., & Fontecilla-Camps, J. C. (2013). Structural foundations for the O2 resistance of Desulfomicrobium baculatum [NiFeSe]-hydrogenase. *Chemical Communications (Cambridge, England)*, *49*(63), 7061–7063. https://doi.org/10.1039/c3cc43619e

Volbeda, A., Charon, M.-H., Piras, C., Hatchikian, E. C., Frey, M., & Fontecilla-Camps, J. C. (1995). Crystal structure of the nickel–iron hydrogenase from Desulfovibrio gigas.pdf. *Nature*.

Volbeda, A., Garcin, E., Piras, C., De Lacey, A. L., Fernández, V. M., Hatchikian, E. C., … Fontecilla-Camps, J. C. (1996). Structure of the [NiFe] hydrogenase active site: Evidence for biologically uncommon Fe ligands. *Journal of the American Chemical Society*, *118*(51), 12989–12996. https://doi.org/10.1021/ja962270g

Volbeda, A., Martin, L., Cavazza, C., Matho, M., Faber, B. W., Roseboom, W., … Fontecilla-Camps, J. C. (2005). Structural differences between the ready and unready oxidized states of [NiFe] hydrogenases. *Journal of Biological Inorganic Chemistry*, *10*(3), 239–249. https://doi.org/10.1007/s00775-005-0632-x

Volbeda, A., Montet, Y., Vernâ, X., Hatchikian, E. C., & Fontecilla-camps, J. C. (2002). High-resolution crystallographic analysis of Desulfovibrio fructosovorans [NiFe] hydrogenase. *International Journal of Hydrogen Energy*, *27*, 1449–1461.

Wakerley, D. W., & Reisner, E. (2015). Oxygen-tolerant proton reduction catalysis: much O2 about nothing? *Energy & Environmental Science*, *8*(8), 2283–2295. https://doi.org/10.1039/C5EE01167A

Weaver, P. F., Lien, S., & Seibert, M. (1980). Photobiological production of hydrogen. *Solar Energy*. https://doi.org/10.1016/0038-092X(80)90018-3

Wombwell, C., Caputo, C. A., & Reisner, E. (2015). [NiFeSe]-Hydrogenase Chemistry. *Accounts of Chemical Research*, *48*, 2858–2865. https://doi.org/10.1021/acs.accounts.5b00326

Yagy, T., Tsuda M, & H Inokuchi. (1973). Kinetic Studies on Hydrogenase Parahydrogen - Orthohydrogen Conversion and Hydrogen-Deuterium Exchange Reactions Tatsuhiko. *J. Biochem*, *1081*, 1069–1081.

Zacarias, S., Temporão, A., del Barrio, M., Fourmond, V., Leger, C., Matias, P. M., & Pereira, I. A. C. (2019). A hydrophilic channel is involved in oxidative inactivation of a [NiFeSe] hydrogenase. *ACS Catalysis*. https://doi.org/10.1021/acscatal.9b02347

Zacarias, S., Vélez, M., Pita, M., De Lacey, A. L., Matias, P. M., & Pereira, I. A. C. (2018). Characterization of the [NiFeSe] hydrogenase from Desulfovibrio vulgaris Hildenborough. In *Methods in Enzymology* (Vol. 613, pp. 169–201). https://doi.org/10.1016/bs.mie.2018.10.003

Zhang, Y., Romero, H., Salinas, G., & Gladyshev, V. N. (2006). Dynamic evolution of selenocysteine utilization in bacteria: A balance between selenoprotein loss and evolution of selenocysteine from redox active cysteine residues. *Genome Biology*, *7*(10). https://doi.org/10.1186/gb-2006-7-10-r94

Züttel, A., Remhof, A., Borgschulte, A., & Friedrichs, O. (2010). Hydrogen: The future energy carrier. *Philosophical Transactions of the Royal Society A: Mathematical, Physical and Engineering Sciences*, *368*(1923), 3329–3342. https://doi.org/10.1098/rsta.2010.0113

CHAPTER II

CHARACTERIZATION OF THE [NiFeSe] HYDROGENASE FROM *Desulfovibrio vulgaris* HILDENBOROUGH

This chapter is published in:

Zacarias, S., Vélez, M., Pita, M., De Lacey, A. L., Matias, P. M., & Pereira, I. A. C. (**2018**). Characterization of the [NiFeSe] hydrogenase from *Desulfovibrio vulgaris* Hildenborough. *Methods in Enzymology* (Vol. 613, pp. 169–201). https://doi.org/10.1016/bs.mie.2018.10.003

S.Z. was the major contributor in writing this article

Abstract

The [NiFeSe] hydrogenases are a subgroup of the well-characterized family of [NiFe]-hydrogenases, in which a selenocysteine is a ligand to the nickel atom in the binuclear NiFe active site instead of cysteine. These enzymes display very interesting catalytic properties for biological hydrogen production and bioelectrochemical applications: high H_2-production activity, bias for H_2 evolution, low H_2 inhibition, and some degree of O_2 tolerance. Here we describe the methodologies employed to study the [NiFeSe] hydrogenase isolated from the sulfate-reducing bacteria *D. vulgaris* Hildenborough and the creation of a homologous expression system for production of variant forms of the enzyme.

1. Introduction

[NiFe] hydrogenases are the most abundant and well-characterized group of hydrogenases. Their active site contains a NiFe binuclear center bound to the protein chain by four cysteine residues, two of which bridge the two metals while the other two are only bound to Ni. [NiFeSe] hydrogenases are a subclass of the [NiFe] hydrogenases in which a selenocysteine (Sec) replaces cysteine as one of the nickel ligands. Sec is codified by the same codon as “stop” (UGA), and a dedicated cellular machinery is needed to recode this codon as “selenocysteine” instead of “stop” and to insert Sec correctly into the protein. This means that the use of Sec instead of Cys is obviously very costly to the cell (Papp et al. 2007). The evolutionary advantage of using Sec over Cys is associated not only with a higher catalytic efficiency, but most importantly with the ability of Sec to react with O_2 in a readily reversible manner and thus resist oxidative inactivation (Reich et al. 2016; Maroney et al. 2018). This concept was recently confirmed also for the *D. vulgaris* Hildenborough [NiFeSe] hydrogenase, through production of a variant where the Sec residue was replaced by a Cys. This variant exhibited reduced catalytic activity and a higher sensitivity to O_2 inactivation, confirming the role of selenium in the protection against oxidative damage (Marques et al. 2017).

The Sec/Cys hydrogenase variant also displayed a much reduced Ni incorporation, suggesting the direct involvement of Sec in the maturation of the active site.

[NiFeSe] hydrogenases present interesting catalytic properties in comparison with other hydrogenases: *i)* high catalytic activities and a bias for H_2 evolution (Baltazar, et al. 2012); *ii)* lower inhibition by H_2 (Parkin et al. 2008); *iii)* some degree of tolerance to O_2, as they do not form inactive Ni(III) states (Teixeira et al. 1987), and can be rapidly reactivated under reducing conditions (Parkin et al. 2008). These properties have been exploited in biocatalytic applications of [NiFeSe] hydrogenases for photo- and electro-chemical H_2 production (Reisner et al. 2009; Reisner, et al., 2009; Rüdiger et al. 2010; Sakai et al., 2013; Caputo et al. 2014, 2015; Mersch et al. 2015; Lee et al. 2016; Tapia et al. 2016; Dong et al. 2018) and also for electrochemical ATP synthesis (Gutiérrez-Sanz et al. 2016).

To date [NiFeSe] hydrogenases have been reported only in sulfate-reducing bacteria and methanogenic archaea (Baltazar et al. 2011). From these groups only a few [NiFeSe] hydrogenases have been isolated, namely those from the sulfate reducing bacteria *Desulfovibrio salexigens* (Teixeira et al. 1986), *Dm. baculatum* (Teixeira et al. 1987), *D. vulgaris* Hildenborough (Valente et al. 2005) and *D. vulgaris* Miyazaki (Nonaka et al. 2013), and from the methanogens *Methanococcus vannielii* (Yamazaki 1982) and *Methanococcus voltae* (Muth et al. 1987).

In this paper, we describe the methods employed to express, purify and characterize the [NiFeSe] hydrogenase from *D. vulgaris* Hildenborough, which is an anaerobic sulfate reducing organism that can use H_2 as energy source or produce H_2 fermentatively or during syntrophic growth. The *D. vulgaris* Hildenborough genome encodes seven hydrogenases of the [FeFe] and [NiFe] families (Pereira et al. 2011). Four of these are periplasmic: the [FeFe]-hydrogenase (Hyd), two [NiFe]-hydrogenases (HynAB-1 and HynAB-2), and a [NiFeSe]-hydrogenase (HysAB), whereas three are in or facing the cytoplasm, namely the two membrane-associated energy-conserving hydrogenases, Ech and Coo and a soluble [FeFe]-hydrogenase (Pereira et al. 2011).

The *D. vulgaris* Hildenborough [NiFeSe] hydrogenase (HysAB) is membrane-associated periplasmic-facing protein, formed by two subunits, the large subunit (HysA) with 63 kDa and the small subunit (HysB) with 35 kDa (Valente et al. 2005). The membrane association is achieved through a lipidic group linked to Cys4 at the N-

terminus of the large subunit. HysA was the first example reported of a bacterial lipoprotein where the signal peptide is limited to a conserved four-residue lipobox (**Figure 1**), since the other regions present in typical lipoprotein signal peptides, involved in recognition and transport by the general secretory pathway (Sec pathway), are absent (Valente et al. 2007). The reason behind this difference is that HysA is translocated by the Tat pathway in complex with HysB (Rodrigue et al. 1999), which contains a standard Tat signal peptide. Thus, HysA was the first example of a bacterial lipoprotein translocated through the Tat and not the Sec pathway (Valente et al. 2007).

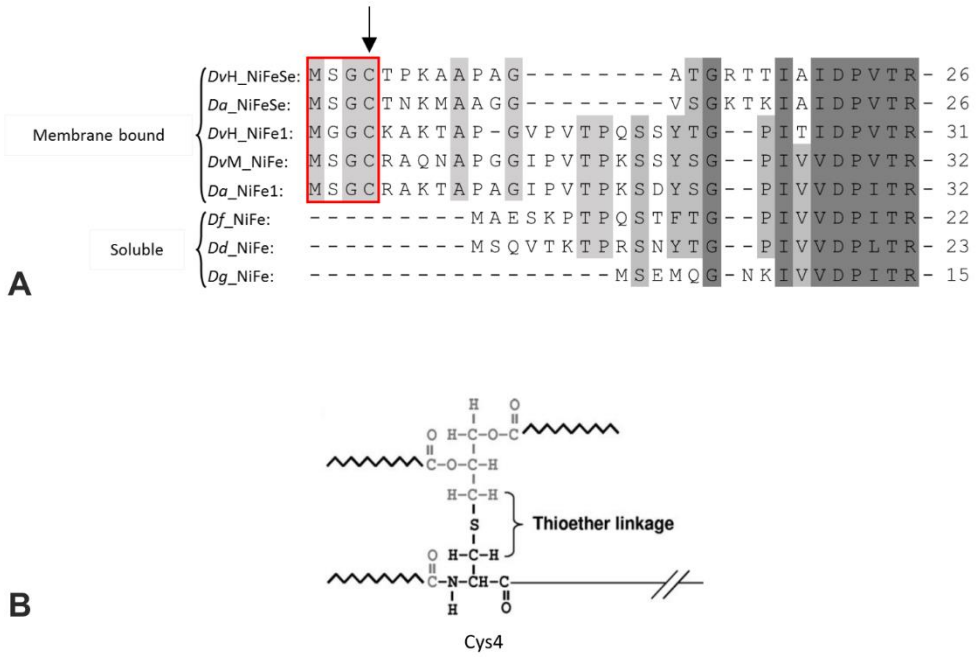

Figure 1: (A) Sequence alignment of the large subunit N-terminus of several *Desulfovibrionacae* hydrogenases. The conserved four-residue lipobox is highlighted by the red box, and the cysteine where the lipid group will bind by an arrow. Membrane-associated hydrogenases: *D. vulgaris* Hildenborough [NiFeSe] (*Dv*H_NiFeSe); *D. alaskensis* [NiFeSe] (*Da*_NiFeSe); *D. vulgaris* Hildenborough [NiFe]1 (*Dv*H_NiFe1); *D. vulgaris* Miyazaki [NiFe] (*Dv*M_NiFe); *D. alaskensis* [NiFe]1 (*Da*_NiFe1). Soluble hydrogenases: *D. fructosovorans* [NiFe] (*Df*_NiFe); *D. desulfuricans* ATTC 27774 [NiFe] (*Db*_NiFe); *D. gigas* [NiFe] (*Dg*_NiFe). (B) Representation of the N-acyl-S-diacylglyceryl group bound to Cys4.

The main physiological role of HysAB is in H_2 oxidation, with the periplasmic type-I cytochrome c_3 (TpIc_3) as the physiological electron acceptor (Pereira et al. 1998; Valente et al. 2005). In solution assays this enzyme is biased towards H_2 production, presenting

very high activities: 4787 U mg^{-1} (7008 s^{-1}) and 6908 U mg^{-1} (10132 s^{-1}) (**Table 1**) in the presence of detergent or phospholipids, respectively.

Table 1 Catalytic activities for D. *vulgaris* Hildenborough [NiFeSe] hydrogenase

	$[NiFeSe]_m$ hydrogenase	**$[NiFeSe]_s$ hydrogenase**	**$[NiFeSe]_r$ hydrogenase**
H_2 evolution	4787 U mg^{-1} (7008 s^{-1}) [a] 6908 U mg^{-1} (10132 s^{-1}) [b]	460 U mg^{-1} (675 s^{-1})	5640 U mg^{-1} (8272s^{-1})
H_2 uptake	900 U mg^{-1} (1320 s^{-1})	N.D.	3037 U mg^{-1} (4454 s^{-1})
H_2 photoproduction	N.D.	N.D.	672 U mg^{-1} (986 s^{-1})
	Isotopic D_2–H^+exchange activity		
HD+H_2 evolution	140 U mg^{-1} (205 s^{-1})	N.D.	1300 U mg^{-1} (2000 s^{-1})

H_2 evolution and uptake activities for $[NiFeSe]_m$ hydrogenase in presence of detergent [a] and phospholipids [b] (Valente et al. 2005). H_2 evolution activity for $[NiFeSe]_s$ hydrogenase (Valente *et al.*, 2005). H_2 evolution activity for $[NiFeSe]_r$ hydrogenase (Marques et al. 2017) and H_2 photoproduction activity (Tapia et al. 2016). Isotopic exchange activities for $[NiFeSe]_m$ hydrogenase in presence of detergent (Gutiérrez-Sanz et al., 2013a) and $[NiFeSe]_r$ hydrogenase (Marques et al. 2017). N.D. – not determined.

Besides the membrane-associated form of the [NiFeSe] hydrogenase (herein named $[NiFeSe]_m$ hydrogenase), a soluble form ($[NiFeSe]_s$ hydrogenase) also exists in the cell, which lacks the first 11 residues of the large subunit and the hydrophobic group. This soluble form may be produced by cleavage of the lipidic group in $[NiFeSe]_m$ hydrogenase by a lipase encoded in the same locus (**Figure 2**) as the [NiFeSe] hydrogenase genes (Valente et al. 2007), or by auto-proteolytic degradation, since its presence increases in aged preparations of the $[NiFeSe]_m$ hydrogenase (Valente et al. 2005). The reported catalytic activities for native $[NiFeSe]_s$ hydrogenase (460 U mg^{-1} for H_2 production) (Valente et al. 2005) were always much lower than those of $[NiFeSe]_m$ hydrogenase.

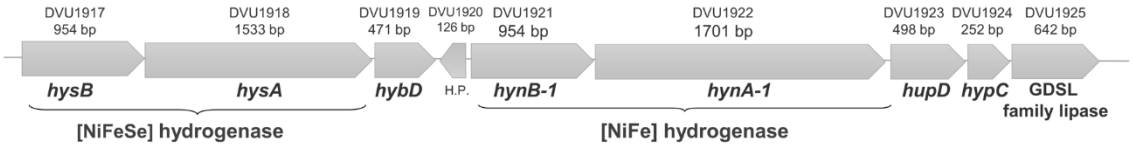

Figure 2 The *D. vulgaris* Hildenborough gene locus containing the [NiFeSe] hydrogenase genes is approximately 8 Kb long. It comprises the genes for the small and large subunit of [NiFeSe] hydrogenase (*hysB* and *hysA*) and [NiFe]1 hydrogenase (*hynB* and *hynA*), a set of maturation genes (*hybD, hupD, hypC*), a hypothetical protein (H.P.) and a gene coding for a GPLS family lipase.

Recently, a recombinant version of the soluble [NiFeSe] hydrogenase ($[NiFeSe]_r$ hydrogenase) was created (Marques et al. 2017). It contains a strep-tag in the N-terminus of the large subunit to facilitate purification and is homologously expressed in *D. vulgaris* Hildenborough, given the known specificity of the maturation proteins and selenocysteine insertion machinery. The $[NiFeSe]_r$ hydrogenase displays a high H_2 production activity of 5640 ± 260 U mg^{-1} (8272 ± 381 s^{-1}) (Table 1) which is comparable with the activities reported for the native membrane form (Valente et al. 2005). This result suggests that the low activities obtained for the native soluble form of the enzyme were mainly caused by the long purification protocol, rather than by the loss of the lipidic N-terminal tail of enzyme.

The structure of *D. vulgaris* Hildenborough [NiFeSe] hydrogenase was solved in 2010 (**Figure 3A**) (Marques et al. 2010) and, as observed for the *D. baculatum* enzyme (Garcin et al. 1999), revealed an overall structure very similar to the standard [NiFe]-hydrogenases, with major differences restricted to the active site and the presence of a medial [4Fe4S] cluster in the small subunit, rather than a [3Fe4S] cluster. The structure of the *D. vulgaris* Hildenborough [NiFeSe] hydrogenase was the first structure reported for an oxidized hydrogenase of the [NiFe] family that did not contain an oxide species bridging the metals in the active site (Marques et al. 2010). However, evidence of O_2 damage was present in the terminal Cys75 ligand of Ni, which was oxidized to a sulfenate/sulfinate. Also, the proximal FeS cluster was partially oxidized to $Fe_4S_3O_2$ (**Figure 3B**) but this oxidative modification is reversed upon reduction (Marques et al. 2013) and has also been observed in the structure of [NiFe] hydrogenase of D.

desulfuricans ATCC (Matias et al. 2001). The active site of the oxidized *D. vulgaris* Hildenborough [NiFeSe] hydrogenase is found in three different conformations. (**Figure 3C**) In two of them, the Se atom is bound to an exogenous sulfur atom (conformers I and II), while the third has a direct Ni−Se bond (conformer III) and corresponds to the conformation of the reduced enzyme. The extra sulfur atom in conformers I and II induces a Sec conformation that shields the NiFe site from contact with oxygen, preventing inactivation associated with bridging oxide ligands (Marques et al. 2013, 2017).

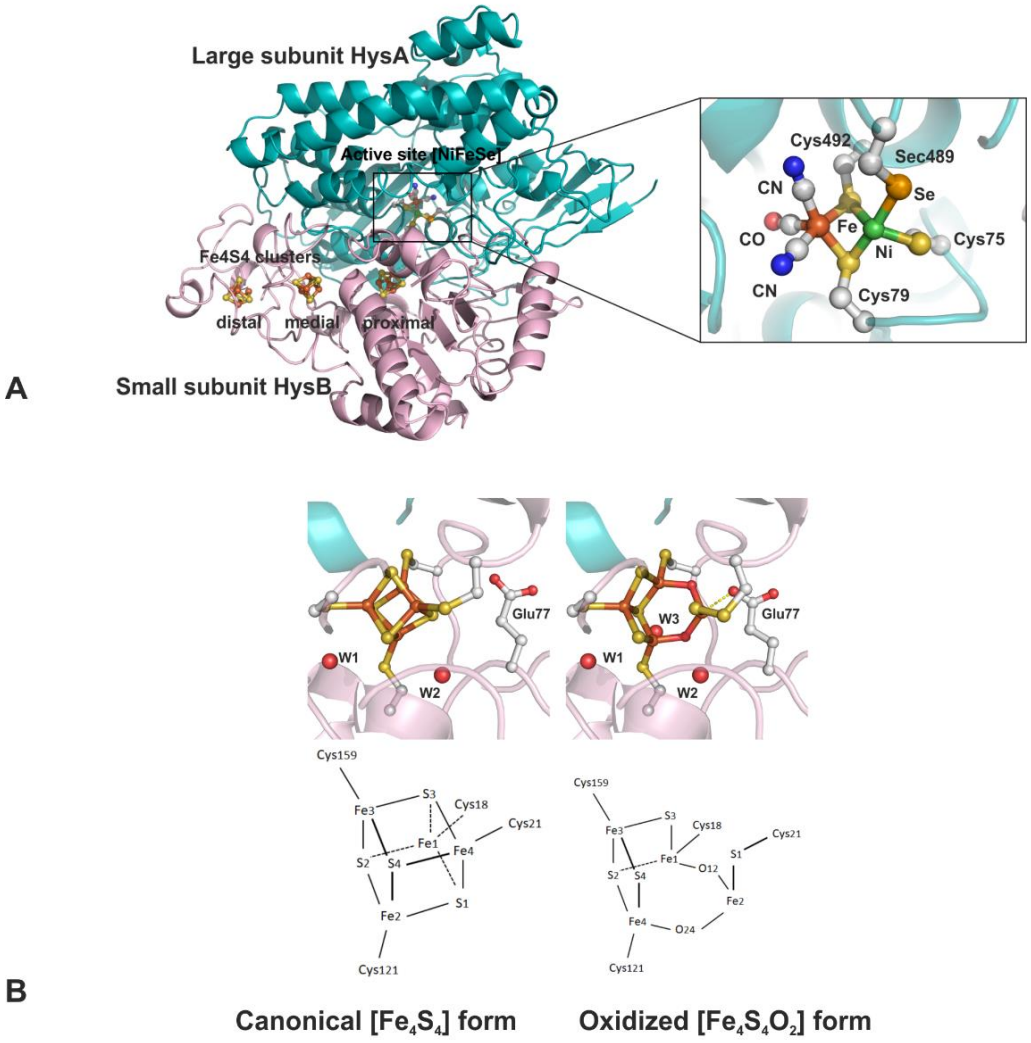

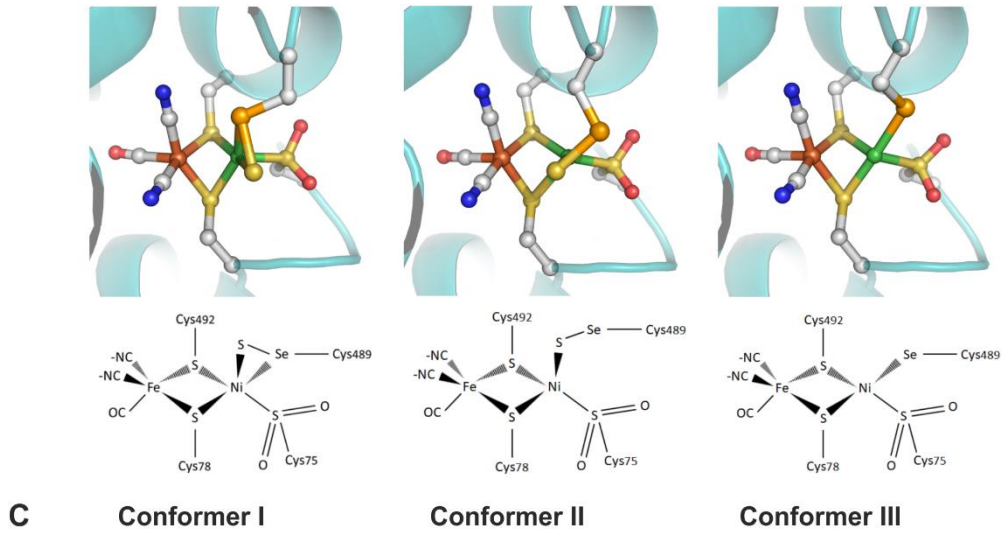

Figure 3: (A) The 3D structure of the *D. vulgaris* Hildenborough [NiFeSe] hydrogenase (taken from PDB 5JSK). **Left**: overall view. The two protein chains are displayed as cartoons; the [NiFeSe] active site, its coordinating ligands and the three [4Fe4S] clusters are drawn in ball-and-stick. **Right**: Close-up view of the active site. The [NiFe] binuclear center and the side-chains of the coordinating protein ligands are shown in ball-and-stick representation. Atom colors are brown for iron, green for nickel, gold for sulfur, red for oxygen, light gray for carbon, blue for nitrogen and orange for selenium. The HysA protein chain is represented as a semitransparent cartoon. **(B)** The canonical and the oxidized forms of the proximal [4Fe4S] cluster in the structure of *D. vulgaris* [NiFeSe] hydrogenase. The proximal cluster becomes partially oxidized under aerobic crystallization conditions. This oxidized form is not observed after reducing with H_2/dithionite or anaerobic crystallization. In the oxidized form, Glu77 approaches atom Fe2 within coordinating bond distance. The three water molecules represented surround the proximal cluster and are conserved in all known structures of [NiFe] and [NiFeSe] hydrogenases with a [4Fe4S] proximal cluster coordinated by 4 cysteine residues. **(C)** The three Sec conformers in the active site of *D. vulgaris* [NiFeSe] hydrogenase. **Conformer I** (taken from PDB 3ZE6) contains an exogenous sulfur atom (presumably as HS^-) bound to both the Ni and Se atoms, and is predominant in crystals obtained aerobically; **Conformer II** (taken from PDB 3ZE8) also contains an exogenous sulfur atom (presumably as HS^-) bound to both the Ni and Se atoms and is predominant in crystals reoxidized under air after reduction with H_2/dithionite or anaerobic crystallization; **Conformer III** (taken from PDB 3ZE7) represents the active form of the enzyme and is predominant after crystal reduction with H_2/dithionite or anaerobic crystallization. The three crystal structures were obtained from an aerobically purified enzyme sample, hence the oxidative damage at Cys75.

Recently, it was proposed that the sulfur atom at the active site results from the sulfide produced from the bacterial metabolism, which may be involved in repair of oxidative damage at the active site (Maroney et al. 2018). This is supported by the fact that in the reduced form of the enzyme the sulfide group can occupy a cavity in the enzyme (Garcin *et al.*, 1999; Marques *et al.*, 2017).

2. Preparation of the native [NiFeSe] hydrogenase from *D. vulgaris* Hildenborough:

2.1 Growth of *D. vulgaris* Hildenborough for expression of the [NiFeSe] hydrogenase

The strain used is *D. vulgaris* Hildenborough (DSM 644). In this organism, the expression of the periplasmic hydrogenases is regulated by the growth substrate, H_2 concentration and by Ni and Se (Valente et al. 2006; Caffrey et al. 2007). Although a higher protein yield can be obtained from cells grown with H_2, the *D. vulgaris* Hildenborough is routinely purified from cells grown in standard lactate-sulfate conditions. To induce the expression of the [NiFeSe] hydrogenase and down-regulate the expression of the Hyd and HynAB-1/2 enzymes, selenium must be present in the medium. In this case the [NiFeSe] hydrogenase becomes the dominant hydrogenase, irrespective of the electron donor used (Valente et al. 2006).

The medium used is the modified Postgate C medium (Postgate 1984), with the following composition: 40 mM sodium lactate, 18 mM Na_2SO_4, 18.5 mM NH_4Cl, 1 g/L yeast extract, 3.7 mM KH_2PO_4, 1 mM sodium citrate tribasic dihydrate, 0.9 mM sodium thioglycolate, 0.6 mM ascorbic acid, 0.4 mM $CaCl_2.2H_2O$, 0.2 mM $MgSO_4.7H_2O$, 26 µM $FeSO_4.7H_2O$, 1 µM $NiCl_2.6H_2O$, 1 µM $NaSeO_3.5H_2O$ and 0.001% (w/v) resazurin (giving a pink color when oxygen is present). The pH is adjusted to 7.2 ± 0.1 with HCl. Cells grow at 37 °C, always in anaerobic conditions, achieved by degassing the medium solution and replacing the atmosphere with N_2.

To grow *D. vulgaris* Hildenborough, 1mL of a cell suspension freezer stock (stored in vials at -80 °C in 10% (v/v) glycerol) are added to 10 mL medium and grown overnight. A 10% (v/v) inoculum is used for all growth transfers. Depending on the amount of protein required, the growth volume can vary from 30 L to 300 L. The 30 L growth volume is performed using three 10 L size Schott flasks with a small headspace filled with N_2. The 300 L growth is performed in a bioreactor with N_2 in the headspace.

The initial downstream processes are usually performed under air, with no major impact on the [NiFeSe] hydrogenase activity, given the presence of sulfide in the crude cell extract. Cells are transferred to centrifuge bottles inside the fume hood to avoid inhalation of hydrogen sulfide and collected by centrifuging them at 11000 *g*, 4°C. Cells can be stored at -80 °C up to several years without affecting the enzyme activity.

2.2 Purification of the membrane form of the [NiFeSe]-hydrogenase:

Cells are suspended in 20 mM Tris-HCl pH 7.6 with DNase and disrupted by three passages through a French press at 6.9 MPa. The resulting extract is centrifuged at 12000 *g*, 10 minutes, 4 °C to remove cell debris. The supernatant is then centrifuged at 180000 *g*, 90 minutes, 4 °C to collect the cell membranes, which can be processed immediately or stored at -80 °C. Membranes are first washed and homogenized by suspending them in 20mM Tris-HCl pH 7.6 with 1mM EDTA and DNase followed by ultracentrifugation at 180000 *g*, 90 minutes, 4 °C. The washed membranes are solubilized in 20 mM Tris-HCl at pH 7.6 with 2% (w/v) Zwittergent SB3-12 (SB3-12) in the presence of protease inhibitors. Solubilization is carried out overnight in an ice bath with gentle stirring, with the headspace of the glass vial filled with N_2 to avoid prolonged contact with O_2. The solubilized proteins are separated by ultracentrifugation at 180000 *g*, 90 minutes, 4°C, and the pellet can be used for a second solubilization using the same conditions. The extract with solubilized membrane proteins is loaded on a Q-Sepharose HP column (XK 26/10 – GE Healthcare) equilibrated with buffer A (20 mM Tris-HCl at pH 7.6 plus 0.2% (w/v) SB3-12). Flow-rate is 4 ml/min and a stepwise gradient of NaCl concentration is performed (0-350 mM, with 50 mM steps). Fractions eluted at different NaCl

concentrations are concentrated in an Amicon stirred ultrafiltration cell with a 30 kDa cutoff membrane, where the ionic strength is also adjusted, if necessary. The total protein concentration is determined by the Bradford assay and an activity-stained native gel is run to identify which fractions have hydrogenase activity. The $[NiFeSe]_m$ hydrogenase elutes around 300 mM NaCl.

The membrane-bound Ech and Coo hydrogenases of *D. vulgaris* Hildenborough are not detected during purification of the membrane extract. This can be due to intrinsic instability of these hydrogenases, a characteristic of the family of multi-subunit membrane [NiFe] hydrogenases related to Complex I (Hedderich 2004), or to a low expression level (Valente et al. 2005).

One step of ionic exchange chromatography is not enough to obtain pure protein, so the fraction of interest from the first chromatographic step is again loaded in a second Q-Sepharose HP column (XK 16/10 – GE Healthcare) and the procedures described above are repeated. For the final polishing step, the fraction with activity for $[NiFeSe]_m$ hydrogenase is loaded in a Q-resource column equilibrated with 20 mM Tris-HCl at pH 7.6 and 0.1 % (w/v) n-Dodecyl β-D-maltoside (DDM) or 0.2% SB3-12, and a stepwise NaCl gradient is performed (0-350 mM, with 50 mM steps). This column yields pure $[NiFeSe]_m$ hydrogenase as judged by the sodium dodecyl sulfate-polyacrylamide gel electrophoresis (SDS-PAGE) and activity-stained native gels. The fraction with pure enzyme is concentrated and the ionic strength is adjusted. It is stored in 20 mM Tris-HCl buffer pH 7.6 with 0.1% (w/v) DDM or 0.2% SB3-12.

2.3 Purification of the soluble form of the [NiFeSe] hydrogenase:

The $[NiFeSe]_s$ hydrogenase can be purified either from the soluble extract obtained by washing the crude membranes (Valente et al. 2005) or from the solubilized membranes (Marques et al. 2009). The purification of the soluble form follows the steps described above for the membrane form, with the exception that no detergent is used after the first column.

Another way to obtain the $[NiFeSe]_s$ hydrogenase is by incubating the membrane form with a commercial lipase (Valente et al. 2007). This procedure allows circumventing the low and non-reproducible yield when the $[NiFeSe]_s$ hydrogenase is isolated directly from the membranes. The procedure consists in mixing 50 mM $[NiFeSe]_m$ hydrogenase with 5 mg of lipase, in a 20 mM Tris-HCl pH 8.0 buffer, at 37 °C for 12 h. After that, a yield of almost 99% soluble $[NiFeSe]_s$ hydrogenase was obtained (Marques et al. 2013). It should be noted that the lipase acts here as a protease, similarly to what happens *in vivo*, cleaving off the first 11 residues from the large subunit (Valente et al. 2007).

3. Production of the recombinant *D. vulgaris* Hildenborough [NiFeSe] hydrogenase

3.1 Creation of the deletion mutant for the [NiFeSe] hydrogenase

The growth medium used when genetically manipulating *D. vulgaris* is the MOYLS4 rich medium (Zane et al. 2010) with the following composition: 60 mM sodium lactate, 30mM Na_2SO_4, 8 mM $MgCl_2$, 20 mM NH_4Cl, 0.6 mM $CaCl_2$, 2 mM phosphate (K_2HPO_4/NaH_2PO_4), 60 µM $FeCl_2$, 120 µM EDTA, 30 mM Tris (pH 7.4), 1 g/L yeast extract, 1 mL/L Thauers vitamin (Brandis et al. 1981) and 6 mL/L trace elements solution with pH adjusted to 7.2, plus 0.001% (w/v) resazurin (as oxygen indicator). The trace elements solution contains 2.5 mM $MnCl_2.4H_2O$, 1.26 mM $CoCl_2.6H_2O$, 1.47 mM $ZnCl_2$, 210 µM $Na_2MoO_4.2H_2O$, 320 µM H_3BO_3, 380 µM $NiSO_4.2H_2O$, 11.7 µM $CuCl_2.2H_2O$, 35 µM $Na_2SeO_3.5H_2O$ and 24 µM $Na_2WO_4.2H_2O$.

A mutant strain for *hys*A and *hys*B genes, (coding for the large and small subunit of [NiFeSe] hydrogenase, respectively) was produced by double homologous recombination in *D. vulgaris* Hildenborough, based on the marker exchange approach as previously described (Keller, Wall, et al 2011). For the *hys*AB deletion, the plasmid pMOIP01 was produced by sequence ligation independent cloning (SLIC) (Li et al.2007), using the following PCR amplified segments: 1,055 bp upstream of *hys*AB (hysAB Up Fw – GCCTTTTGCTGGCCTTTTGCTCACATGGACAAGGATGAGCCCGTTGTGAA and hysAB Up

Rev – AAGACTGTAGCCGTACCTCGAATCTATGC AGTGCCAGCCAATAGAGTGAA), 885 bp downstream of hysAB (hysAB Dwn Fw – AATCCGCTCACTAAGTTCATAGACCGGACGCCCA TGATGTTAGGGTTCCAA and *hys*AB Dwn Rev – CGAGGCATTTCTGTCCTGGCTGGGCGTACG CATTACGCACGTATCAT); the kanamycin resistance gene, taken from the pSC27 plasmid (Keller et al. 2009) (Kan Fw – TAGATTCGAGGTACGGCTACAGTCTTACGGTCACAAACAGGT ACGCCCCCAGAGTC and Kan Rev –CGGTCTATGAACTTAGTGAGCGGATTTCTCGTGTAGCCG ATGCAGTGAGGTAGCTTGCAG); spectinomycin resistance gene and the pUC ori portion taken from pMO719 background (Keller et al. 2009). The products from the amplifications were transformed into *E. coli* α-select Silver Efficiency (Bioline), and successful transformants were isolated on LB-agar medium containing 50 µg/mL kanamycin and 100 µg/mL spectinomycin. Correct isolates were identified by the expected polymerase chain reaction (PCR) amplicons from the plasmid constructs and also by sequencing. The pMOIP01 plasmid was electroporated into *D. vulgaris* Hildenborough with the following parameters: 1500 V, 250 Ω, and 25 µF, from which the deletion strain for *hys*AB, IPAR01 (Δ*hys*AB) was obtained, by selection with MOYLS4 medium containing 400 µg/mL geneticin, according to (Keller, Wall et al. 2011). The deletion of *hys*AB was confirmed by Southern blot using as probe an upstream fragment of the *hys*AB gene.

3.2 Expression vector and complemented strain for [NiFeSe] hydrogenase expression

To produce the recombinant soluble form of [NiFeSe]-Hydrogenase an expression vector was constructed encoding *hys*B followed by a Strep-tag and *hys*A, lacking the codons for the first 11 amino acid residues. To create this vector, two segments were amplified by PCR: the *hys*B gene (HysB Fw – AGGTTGGGAAGCCCTGCAATGCAGTCCCAGG AGGTACCATATGAGTCTCACAAGGCGTGATTTCGTC and HysB Rev – TTTTTCGAACTGCGGG TGGCTCCACATGATAT CCTCCTGAAGCGACTGACGG) and the Strep-tag in the N-terminal of *hys*A gene (HysA Fw – TGGAGCCACCCGCAGTTCGAAAAAGGGGCCACCGGCAGGACGAC CATC and HysA Rev – GATCGTGATCCCCTGCGCCATCAGATCCTTGGCTCGCGGCCCCTCCCC

TTCATGAT); and then added into pMO9075 background shuttle plasmid (Keller *et al*.,2009) via SLIC, creating the pMOIP03 plasmid. For that, the amplification products were transformed into *E. coli* α-select Silver Efficiency, and cells were plated on LB-agar with 100 µg/mL spectinomycin. The correct plasmid construct was screened by colony PCR and later confirmed by sequencing. In the pMO9075 vector plasmid, the *hysA*B gene stays under the control of the Km^R gene-*aph(3')-II* promoter, which is known to be constitutively expressed in *D. vulgaris* (Keller et al., 2009). The pMOIP03 vector was successfully introduced in the deletion strain IPAR01 by electroporation, with the following parameters: 1250 V, 250 Ω, 25 µF. The complemented strain for HysAB, was grown in MOYLS4 medium containing 400 µg/mL geneticin and 100 µg/mL spectinomycin. The plasmid was confirmed by PCR amplification of the insert and also by sequencing. Western-Blot against the Strep-Tactin AP (IBA) antibody was performed to confirm expression.

3.3 Site-directed mutagenesis of the [NiFeSe] hydrogenase:

For site-directed mutagenesis, the plasmid pMOIP03 carrying a *hys*A_{Strep}*hys*B fragment is used as a template. The amino acid exchange is done with the NZYMutagenesis kit (Nzytech), with mutagenic primers designed considering the codon usage in *D. vulgaris* Hildenborough. For propagation, the mutagenic plasmid is transformed into *E. coli* Nzy5α (Nzytech), which is transferred to 1 mL LB medium for growth for 1h at 37 °C, 180 rpm, in aerobic conditions. Cells are plated in LB-agar medium containing 100 µg/mL spectinomycin, and isolated colonies grown on LB medium. The plasmid is extracted by Miniprep and sequenced to check for the correct aminoacid exchange. The plasmid pMOIP03 carrying the correct mutation is then electroporated aerobically into the deletion IPAR01 strain using the Gene Pulser XCell (Biorad), with the following parameters: 1250 V, 250 Ω, 25 µF. Electroporated cells are transferred to 1 mL of MOYLS4 medium and left to recover anaerobically overnight at 37 °C. About 50 – 100 µL of these cells are plated, with molten MOYLS4 medium containing 400 µg/mL geneticin and 100 µg/mL spectinomycin poured over the cells and swirled. Once solidified, plates are inverted and placed in an airtight rectangular jar

(Mitsubishi Gas Chemical Co., Inc., Japan) with an oxygen indicator stripe (Biomérieux) and GenBox Anaer (Biomérieux) to absorb traces of O_2. The plates are incubated in a growth chamber at 37 °C, between 2 to 5 days until *D. vulgaris* Hildenborough colonies appear (**Figure 4**). The colonies are selected with a sterile toothpick and inserted into MOYLS4 liquid medium with 100 µg/mL spectinomycin. The first *D. vulgaris* Hildenborough [NiFeSe] hydrogenase variant was recently reported, where the Sec489 residue was exchanged for a Cys, transforming the active site of the [NiFeSe] hydrogenase into that of a [NiFe] hydrogenase (Marques et al. 2017).

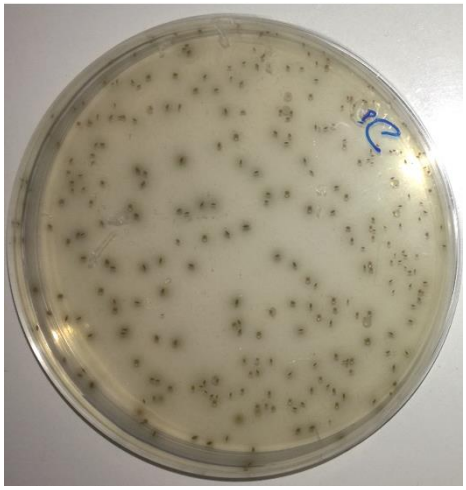

Figure 4: Colonies of *D. vulgaris* Hildenborough plated in MOYLS4 medium.

3.4 Purification of the recombinant [NiFeSe] hydrogenase

Cells are suspended in 20 mM Tris-HCl pH 7.6 with DNase and disrupted by three passages through a French press at 6.9 MPa. The resulting extract is centrifuged at 12000 *g*, 10 minutes, 4°C to remove cell debris. The supernatant is then centrifuged at 180000 *g*, 90 minutes, 4 °C to separate membranes from the soluble fraction. The soluble fraction is loaded on a Q-Sepharose HP column (XK 26/10 – GE Healthcare) equilibrated with 20mM Tris-HCl pH 7.6. A stepwise NaCl gradient is performed (0-350 mM, with 50 mM steps). The fractions with $[NiFeSe]_r$ hydrogenase activity usually elute between 250 and 300 mM NaCl. This fraction is applied in an Amicon stirred ultrafiltration cell with a 30 kDa cutoff membrane, to concentrate and adjust the ionic strength. Then affinity

chromatography is performed by loading the fraction onto a gravity column containing Strep-Tactin resin (IBA Lifesciences) equilibrated with 100 mM Tris-HCl pH 8.0, 150 mM NaCl (Buffer W). After five washing steps with buffer W, the recombinant protein was eluted with buffer W plus 2.5 mM desthiobiotin. This column yields pure [NiFeSe] hydrogenase as judged by the SDS-PAGE. Protein concentration is determined based on ε_{410}= 48 000 M^{-1} cm^{-1}, using the protein molecular weight of 88000 g/mol.

4. Hydrogenase Activities:

The steady-state activity of the [NiFeSe] hydrogenase is routinely quantified by measuring the rates of hydrogen oxidation and proton reduction with artificial redox dyes. We use methyl viologen (MV) (E=-449 mV at all pH values) both as electron donor for H_2 production and as electron acceptor for H_2 oxidation. The natural physiological partner, TpIc_3, can also be used as electron acceptor or donor to assay hydrogenase activity *in vitro* (Valente et al. 2005). The H_2 oxidation activity can also be assessed qualitatively by activity-stained native gels.

The H/D isotope exchange activity measured by membrane-inlet mass spectrometry shows the reversibility of the [NiFeSe] hydrogenase catalytic function (**Figure 5**). It is performed in the absence of a redox partner. Thus, no intermolecular electron transfer takes place; only H_2 cleavage/formation and proton exchange with the solution is involved during this catalytic process. (Vignais 2005)

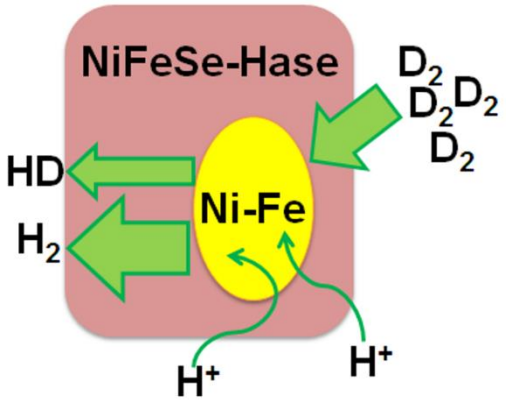

Figure 5: Scheme of the H/D isotope exchange activity of NiFeSe hydrogenase in D_2/H_2O.

Oriented immobilization of the [NiFeSe] hydrogenase on electrodes allows measuring its H_2 oxidation/production activities by electrochemical methods. Correct immobilization of the enzyme allows direct electron transfer with the electrode, thus avoiding the use of redox dyes as electron donors or acceptors (Rüdiger et al. 2010). The redox potential applied on the electrode drives the electrocatalytic process towards either proton reduction or H_2 oxidation, while the current is proportional to the enzymatic activity (Vincent et al. 2007). Benchmark H_2 oxidizing currents of 1.7 mA cm^{-2} with bioanodes based on the *D. vulgaris* Hildenborough [NiFeSe] hydrogenase immobilized in a viologen-modified hydrogel, were recently achieved (Ruff et al. 2017).

4.1 H_2 Evolution and Uptake with artificial mediators:

4.1.1 H_2 Evolution assay:

H_2 evolution is measured by gas chromatography (GC) in a Trace GC Ultra (Thermo Scientific) equipped with a thermal conductivity detector (TCD), with a MolSieve 5A 80/100 column (Althech) and N_2 as a carrier gas. The assay is performed in a gas-tight screw cap vial containing 1 mL of 50mM Tris-HCl buffer at pH 7 plus 1 mM MV, 15 mM sodium dithionite, 0.5 mg/mL bovine serum albumin (BSA) and 9 ml volume headspace filled with N_2. The reaction is initiated by adding to the vial 10 µL of approximately 9 nM enzyme with a gas-tight syringe. Dithionite-reduced MV is the electron donor for the [NiFeSe] hydrogenase. This reaction mixture is incubated in a shaker at 37 °C, for 10 minutes and a headspace sample injected in the GC every 5-10 mins. The GC measurements are calibrated by controlled injections of H_2 under identical liquid and gas volume headspaces. One unit of enzyme is defined as the amount of hydrogenase evolving 1 µmol of H_2/min. The purified $[NiFeSe]_r$ Hydrogenase presents a H_2 production activity of around 5646 ± 260 U/mg (8280 ± 382 s^{-1}).

4.1.2 H_2 Uptake assay:

H_2 uptake is measured spectrophotometrically in a Coy anaerobic chamber (95% N_2, 5% H_2), using a UV-1800 Shimadzu. The enzyme is first activated with 0.5 bar H_2 at room-temperature for approximately 30 minutes in an anaerobic vial containing 1 mL of 50 mM Tris-HCl buffer at pH 8 and 1 mM MV. Inside the anaerobic chamber, the reaction is started by adding 10 µL of approximately 25 nM enzyme to a cuvette in the spectrophotometer, containing 1ml of H_2-saturated 50 mM Tris-HCl buffer at pH 8 and 2 mM MV, with constant stirring. The H_2 oxidation activity is measured from the reduction of MV, following the MV color change rate at 604 nm (ε=13.6 mM^{-1} cm^{-1}) at 30 °C, according to the reaction: $H_2 + 2MV^{+2} \rightarrow 2H^+ + 2MV^+$. One unit of enzyme is defined as the amount of hydrogenase reducing 2 µmol of MV per minute, which is equivalent to 1 µmol H_2 oxidized per minute. The $[NiFeSe]_r$ hydrogenase presents an H_2 uptake activity of around 3037 ± 151 U/mg (4454 ± 221 s^{-1}).

4.1.3 Activity-stained Native Gels:

For a qualitative assessment of the hydrogenase activity, either in crude cell extracts or in the purification fractions, activity staining is performed using native polyacrylamide gel electrophoresis (**Figure 6**). The band intensity is related to the H_2 uptake activity, since the enzyme will oxidize H_2 and transfer the electrons to MV, giving rise to a blue band on the gel. Activity stained gels are routinely used throughout the protein purification process, to identify fractions with hydrogenase activity as well as to rapidly screen for [NiFeSe] hydrogenase variants with significant differences in H_2 oxidation activity, based on the intensity of the bands.

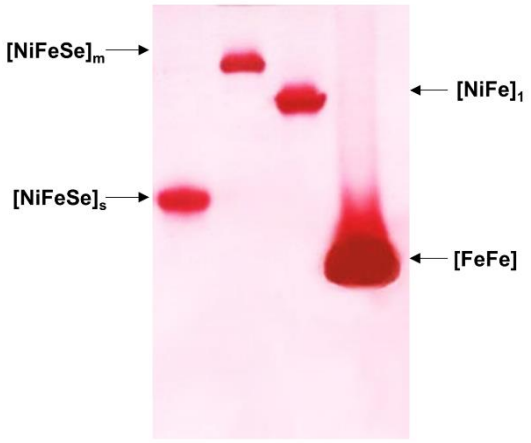

Figure 6: Activity-stained native gel for hydrogenase activity of pure protein samples isolated from *D. vulgaris* Hildenborough. The $[NiFeSe]_r$ hydrogenase, not represented here, migrates on the gel with the same profile as the $[NiFeSe]_s$ hydrogenase.

Samples of 50-200 µg total protein from either soluble fractions or fraction coming from the ionic exchange chromatography are run in a 7.5% (v/v) polyacrylamide gel containing 0.1% (v/v) Triton X-100. Detergent is important for the membrane-associated hydrogenases to run properly since without it only band streaking is observed. The gel is transferred to a 50 mL N_2 saturated solution of 50 mM Tris-HCl pH 7.6 with 0.5 mM MV and then incubated under 0.5 bar H_2. Once blue bands are well developed, they are fixed by adding 10 mM 2,3,5-tri-phenyltetrazolium chloride solution, that will be reduced by MV to produce a permanent oxygen-insensitive red stain for the enzyme band.

4.2 H/D Isotope Exchange Activity:

The H/D isotope exchange activity of the hydrogenase is measured in a thermostated 37 °C reactor with magnetic stirring that is connected via a 14 µm Teflon membrane to a mass spectrometer (Pfeiffer Prisma) (Gutiérrez-Sanz, Marques et al. 2013). The output signal of the spectrometer for mass values 2 and 4 is calibrated by saturating a buffered solution with 100% H_2 and by 20% D_2 in 80% Ar respectively, which are flushed through

an oxygen filter (Varian) before entering the reactor. The output signal is proportional to the partial pressure of the corresponding gas in the reaction vessel (Vignais 2005). Calibration for the single exchange product of the enzymatic reaction (HD) is determined from the average values measured for H_2 and D_2.

Generally, the exchange activity is measured in 10 mL of buffered H_2O solution purged with 20% D_2 in Ar. After reaching a plateau value for mass 4, the reactor lid is closed while excluding the gas phase in the reactor. The enzymatic reaction is started by adding in succession, through a rubber septum with gas-tight syringes, 100 µL of 1 % DDM, 1 µL of 1 M sodium dithionite to eliminate residual oxygen, and typically 25 µL of 0.1 µM hydrogenase. During the measurement, masses 2, 3 and 4 are scanned at a rate of 1 atomic mass unit/s. The initial rates of H_2 and HD production are calculated from the difference in the slopes after and before enzyme addition (Gutiérrez-Sanz, Marques et al. 2013). Alternatively, the isotope exchange activity can be measured by saturating with H_2 a buffered D_2O solution. In this case HD and D_2 production rates are measured by monitoring the evolution of masses 3 and 4 respectively. In this case the hydrogenase sample has to be previously incubated overnight in the D_2O buffered solution for exchanging the enzyme's protons to deuterons (Gutiérrez-Sanz, Marques et al. 2013).

4.3 Electrocatalytic H_2 production and oxidation:

Covalent immobilization of the [NiFeSe] hydrogenase on a gold electrode modified with a 4-aminothiophenol (4-ATP) self-assembled monolayer (SAM) allows measuring its electrocatalytic H_2 oxidation/production activity by direct electron transfer. The 4-ATP SAM is formed by immersing a clean Au electrode on a 5 mM ethanol solution of 4-ATP during 18 hours at room temperature. After rinsing, the Au electrode is covered by 6 µL of 27 µM hydrogenase in 10 mM MES, pH 6.5 for 30 minutes and in a second step 5.5 µl of 14 mM N-(3-dimethylaminopropyl)-N'-ethylcarbodiimide hydrochloride and 4.5 µl of 21 mM N-hydroxysuccinimide, in the same buffer solution, is added for formation of amide bonds between enzyme and the 4-ATP SAM on the electrode. The mixture is left to react for 90 minutes, then the modified Au surface is washed for 5 minutes in 0.1 M phosphate, pH 7.0, 0.25 M KCl buffer solution with stirring to remove non-covalently

bound hydrogenase (Rüdiger et al. 2010). Electrocatalytic experiments are controlled by an Autolab potentiostat and measured in a three-electrode glass cell with a saturated calomel reference electrode (SCE) separated from the main compartment in a sidearm connected by a Luggin capillary and a platinum wire counter-electrode. The electrochemical cell is surrounded by a water jacket for controlling the temperature at 40 °C. The gold working electrode is connected to a MSR electrode rotator (Pine Instruments). The electrocatalytic activity of H_2 oxidation is measured by chronamperometry at -0.25 V *vs.* SHE under 1 atm H_2 at 2500 rpm electrode rotation, whereas the H_2 production is measured at -0.45 V *vs.* SHE under 1 atm N_2 (Rüdiger et al. 2010). The membrane form of the [NiFeSe] hydrogenase can be immobilised on Au gold electrodes modified with a phospholipid bilayer by using the enzyme´s hydrophobic tail as anchor to the supported biomimetic membrane. Two different orientations of the membrane-bound hydrogenase on the electrode are possible: *i)* the enzyme is inserted via its hydrophobic tail onto a phospholipid bilayer supported on a 4-ATP modified Au electrode with its [4Fe4S] distal cluster facing the bulk solution; *ii)* the enzyme is covalently bound to the 4-ATP-Au with its [4Fe4S] distal cluster facing the electrode and a phospholipid bilayer is formed on top of the hydrogenase monolayer using the hydrophobic tail as scaffold (Gutiérrez-Sánchez, Olea et al. 2011). The first configuration is obtained by incubating the 4-ATP-Au electrode in a 0.6 mg/mL liposome suspension (300 nm diameter) from *E. coli* polar extract in 10 mM MES buffer at pH 5 for 45 minutes at room temperature. After rinsing carefully with MES buffer 10 mM at pH 7, the electrode was incubated in 27 µM $[NiFeSe]_m$ hydrogenase in pH 6.0 MES buffer and 48 mg of dry CALBIOSORB adsorbent were added to the solution for 1.5 hours to remove the detergent present in the hydrogenase solution (Gutiérrez-Sánchez et al. 2011). The second configuration is obtained in two steps by first immobilizing covalently on the 4-ATP-Au the $[NiFeSe]_m$ hydrogenase as described above but in presence of 0.1% DDM. The second step involves incubating the hydrogenase-modified electrode in the liposomes suspension in presence of CALBIOSORB adsorbent for 90 minutes (Gutiérrez-Sanz, Marques, et al. 2013; Rüdiger et al. 2010). It has been shown that the hydrogenase immobilized on electrodes in the latter configuration is able to create a proton gradient across the biomimetic membrane upon electrocatalytic H_2 oxidation (Gutiérrez-Sanz et

al. 2015) and to induce ATP synthesis when a ATP-synthase is incorporated in the phospholipid bilayer (Gutiérrez-Sanz et al. 2016).

4.4 Photocatalytic H_2 production:

The [NiFeSe] hydrogenase can produce H_2 when combined with appropriate visible light-absorbing semiconductors such as In_2S_3 (Tapia et al. 2016). In_2S_3 should be synthesized as a polycrystalline powder with a controlled pore size around 15-20 nm in diameter, suitable to host the enzyme and allow electron transfer. A successful In_2S_3 can be synthesized following a hydrothermal procedure: a Teflon-lined steel high-pressure reactor containing a Pyrex beaker is filled with 50 mL aqueous solution containing 148 mM $InCl_3$, 178 mM thiourea and 80 µL HCl 37%, and left to react at 435 K for 2 days (Lucena et al. 2008). Afterwards, the material is cleaned by three centrifugation-resuspension cycles in distilled water and another one in ethanol. Finally, the material is dried during 12 h at 333 K.

The [NiFeSe] hydrogenase is incubated during 6 hours with the In_2S_3 to physically adsorb the enzyme on the chalcogenide surface. This process is performed at 4 °C by mixing 0.26 pmol of hydrogenase with 22.1 µmol of In_2S_3 in 10 mL of a pH 7.0 solution containing 50 mM Tris-HCl and 0.2 M Na_2SO_3 (Tapia et al. 2016). The sample is then taken into a glass-made reactor vessel connected to a mass spectrometer through a gas-permeable Teflon membrane, taking care to avoid a gas phase inside the reaction chamber. The [NiFeSe] hydrogenase was previously activated by bubbling a 1:4 H_2/Ar mixture during 10 min followed by pure Ar bubbling to remove all the H_2 from the reactor. H_2 was produced by irradiating the activated sample with light coming from a 450 W Xe lamp solar simulator. The H_2 production rate was measured with the mass-spectrometer monitoring mass = 2.

5. Structure Determination of D. vulgaris Hildenborough [NiFeSe] hydrogenase by X-Ray Crystallography:

5.1 Crystallization

The soluble form of the [NiFeSe] hydrogenase (either native or recombinant version), are crystallized aerobically at 20 °C by sitting drop vapor diffusion method, using microbridges in 24-well plates (Hampton Research). Crystallization drops are prepared by mixing 1 µL or 2 µL of pure protein with a concentration varying from 80 µM to 114 µM with an equal volume of reservoir solution, containing *ca.* 20% PEG 1500 (w/v), 0.1 mM Tris-HCl pH 7. The exact percentage of PEG 1500 varies somewhat depending on the protein batch, and some optimization is usually required to obtain the best quality crystals. Drops are equilibrated against 500 µL reservoir solution. Brown monoclinic blocks, with dimensions varying from 100 µm to 500 µm, grow over 4–6 days (**Figure 7A**). Crystals are prepared for data collection with the reservoir solution adjusted to include 10% (v/v) glycerol and flash-cooled in liquid nitrogen or under a nitrogen gas stream at 100K. Recombinant [NiFeSe] hydrogenase and variants usually crystallize in the monoclinic space group *C*2 with one molecule in the asymmetric unit, but the as-isolated native soluble enzyme was crystallized in monoclinic space group $P2_1$ and occasionally crystallization occurs in other space groups.

For anaerobic crystallization, the procedure is the same as described above but done in a Coy anaerobic chamber (95% N_2, 5% H_2). All the plastic material and solutions are degassed and introduced in the chamber one day in advance. A 24-well crystallization plate with the crystallization drops is kept in an airtight rectangular jar (Mitsubishi Gas Chemical Co., Inc., Japan) with an oxygen indicator stripe (Biomérieux) and GenBox Anaer (Biomérieux), outside the anaerobic chamber in a 20 °C room (**Figure 7B**). Harvesting crystals under anaerobic conditions is achieved by filling a container with argon, and the crystal plate and the stereoscopic microscope are placed in this container.

The $[NiFeSe]_m$ hydrogenase could never be crystalized to date, despite screening of multiple crystallization conditions at the 100 nL scale using a robot.

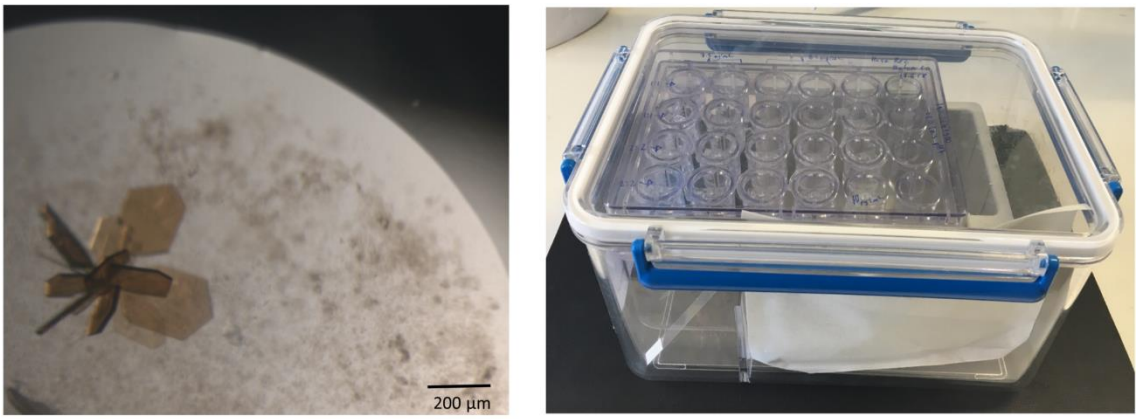

Figure 7: (A) Crystals of the [NiFeSe]$_r$ hydrogenase. (B) Crystallization plate inside an airtight jar to allow crystal growth under anaerobic conditions. An oxygen indicator stripe and GenBox Anaer are placed inside the jar.

5.2 Data Collection and Structure Determination

The crystals of [NiFeSe]$_r$ hydrogenase usually display good diffraction quality on a home X-ray source (either a rotating anode X-ray generator or a microsource) coupled to a mirror system and a CCD detector, yielding diffraction data to a resolution of *ca.* 1.5 Å. The use of a 4-circle diffractometer allows obtaining very complete diffraction data with high multiplicity, obviating the cusp that can result from measuring a monoclinic crystal on a 1-circle goniometer. Nevertheless, modern detectors and data collection software at synchrotron sources allow obtaining nearly 100% complete diffraction data to a resolution approaching 1 Å, with the added benefit of wavelength selection at some beamlines, which is very important to validate the structure of the active site, in particular the bimetallic NiFe and the position of the Se atom in the selenocysteine ligand.

However, the diffraction quality displayed by the first crystals of the as-isolated soluble form of [NiFeSe] hydrogenase was not as good. The first data set was obtained *in-house* to a resolution of 2.4 Å, and although a homologous structure from *Dm. baculatum* [NiFeSe] hydrogenase was already known [PDB 1CC1; (Garcin et al. 1999)] and a clear solution could be obtained by the molecular replacement method, the electron density maps were not of sufficiently good quality to rebuild several regions in

the structure (Marques et al. 2009). Therefore, the crystal structure of $[NiFeSe]_s$ hydrogenase from *D. vulgaris* Hildenborough was determined at 2 Å resolution from a crystal of the as-isolated soluble form, using the Multiple Wavelength Anomalous Dispersion Method at the Fe K-edge (Marques et al. 2010) from data measured at Diamond Light Source beamline I04 (Didcot, U.K.) (**Figure 8**). The peak and inflection point wavelengths were chosen to maximize the anomalous and dispersive signals with CHOOCH (Evans et al. 2001) from an X-ray fluorescence scan near the Fe K-edge, and the remote wavelength was chosen around 1 Å to minimize absorption effects and maximize dispersive differences during phasing. The diffraction images for the three data sets were processed with XDS (Kabsch 1993).

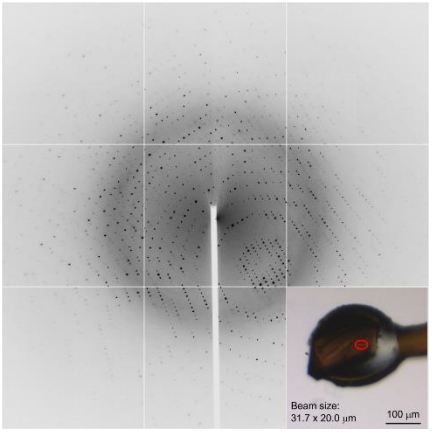

Figure 8: Diffraction image from the data set measured at the Fe peak wavelength (1.7244 Å) used in the structure determination of *D. vulgaris* [NiFeSe] hydrogenase. The inset shows a typical cryocooled crystal used for diffraction data measurements at the Diamond Light Source.

The as-isolated soluble form of $[NiFeSe]_s$ hydrogenase from *D. vulgaris* Hildenborough crystallized in space group $P2_1$ with one heterodimer in the asymmetric unit, therefore 14 Fe sites were expected (one in the NiFe active site, 12 in the three [4Fe4S] clusters, and one bound to the C-terminal of the large subunit). Using the HKL2MAP graphical interface (Pape et al. 2004) and the SHELXC/D/E program suite (Schneider et al. 2002; Sheldrick 2002, 2010) the data set was scaled and analyzed with SHELXC, the iron substructure was determined with SHELXD and the phase problem solved with SHELXE. However, although a good solution for the Fe-atom substructure was obtained with SHELXD, a clear and unequivocal discrimination between the correct

and inverted substructures could not be obtained with SHELXE and the electron density maps could not be interpreted. Improved phases were obtained using the maximum-likelihood heavy-atom parameter refinement in SHARP (Bricogne et al. 2003) and a subsequent optimizing density modification procedure using SOLOMON (Abrahams et al. 1996) and DM (Cowtan 1994). Automated model building with ARP/wARP (Perrakis et al. 1999) produced a near complete model for the protein chains of both subunits (except for a few disordered N-terminal residues). Prior to structure refinement, the [4Fe4S] clusters and the NiFe co-factors were modelled with COOT (Emsley et al. 2010).

Subsequent crystal structures of the as-isolated soluble or recombinant forms of [NiFeSe] hydrogenase from *D. vulgaris* Hildenborough were determined by the Molecular Replacement Method with PHASER (McCoy 2007) using an earlier crystal structure as phasing model, with separate rotation/translation calculations for each subunit, and usually omitting the metal cofactors. High-resolution diffraction data for these structural studies have been measured at several European synchrotron sources: ESRF (Grenoble, France), SLS (Villigen, Switzerland), ALBA (Cerdanyola del Vallès, Spain) and DLS (Didcot, UK).

5.3 Structure Refinement

The first crystal structure of the as-isolated soluble form of [NiFeSe] hydrogenase from *D. vulgaris* Hildenborough was refined against the 2.04 Å peak data measured at the DLS using a maximum-likelihood procedure with REFMAC (Murshudov et al. 2011) as implemented in the CCP4i graphics user interface (Potterton et al. 2003). Prior to refinement, a random 5% sample of the reflection data were flagged for cross-validation using R-free. (Brünger 1992) Improved atomic displacement parameters at this resolution were obtained by using a simple TLS (translation-libration-screw) rigid body model (Winn et al. 2001) where each of the two subunits (including its respective co-factors) was treated as a rigid body. During refinement, the structure was regularly inspected and corrected against σ_A-weighted $2|F_o|-|F_c|$ and $|F_o|-|F_c|$ electron density maps using COOT. The map coefficients were calculated by REFMAC at the end of each refinement procedure. In this crystal structure, electron density for the aliphatic chains

of four sulfobetaine 3-12 detergent molecules used in the purification was observed in two hydrophobic pockets open to the solvent and the visible atoms were included in the refinement. Solvent molecules were located with ARP/wARP and by inspection of σ_A-weighted $2|F_o|-|F_c|$ and $|F_o|-|F_c|$ electron density maps and included in the refinement.

Refinements of subsequent crystal structures of both as-isolated soluble and recombinant forms of [NiFeSe] hydrogenase from *D. vulgaris* Hildenborough were carried out using PHENIX (Adams et al. 2010). Although considerably slower than REFMAC, PHENIX allows for the refinement of occupation factors, which in the case of these structures is very important to elucidate the fine structural details of the active site. Since most datasets have been measured just above the K-absorption edge of selenium, the Se atom in selenocysteine displays significant anomalous dispersion properties ($\Delta f' \sim -4\ e^-$ and $\Delta f'' \sim 3.5\ e^-$) and anomalous refinement is used, increasing the number of experimental data and allowing the direct calculation of anomalous difference maps, very useful to validate structural changes in the active site and the proximal 4Fe4S cluster. In all refinements, hydrogen atoms are included at calculated positions with REFMAC or the READYSET tool in PHENIX. At intermediate resolutions (up to *ca.* 1.5 Å) a TLS refinement of the atomic displacement parameters is followed by refinement of individual isotropic atomic displacement parameters for all non-hydrogen atoms. The TLS rigid bodies are chosen by submitting a previously refined structure with isotropic atomic displacement parameters to the TLS Motion Determination (TLSMD) server (Painter et al. 2006) or by using the internal PHENIX tool. At higher resolutions, anisotropic refinement of atomic displacement parameters for all non-hydrogen atoms is undertaken. Solvent molecules can be added automatically during the refinement process in PHENIX or by inspection of the σ_A-weighted $2|F_o|-|F_c|$ and $|F_o|-|F_c|$ electron density maps produced at the end of each refinement calculation.

6. *D. vulgaris* Hildenborough [NiFeSe] hydrogenase Biophysical characterization

6.1 Infrared spectroscopy

The different redox states of the bimetallic active site of the hydrogenase can be studied by Fourier-transform infrared spectroscopy (FTIR) because its CO and CN^- ligands can absorb infrared radiation and the vibrational frequencies of their bands are sensitive to changes in the electron density at the active site (De Lacey et al. 2007). FTIR-spectroelectrochemical experiments of the [NiFeSe] hydrogenase are performed in a cell with 8 μm path length described by (Moss et al. 1990). For these measurements 10 μL of hydrogenase solution with a concentration of at least 0.8 mM in buffered solution with 0.2 M KCl is required. The sample must contain in addition a mixture of redox mediators, 0.05 mM each, whose redox potentials span from 0 to -450 mV vs SHE in order to reach redox equilibrium for the sample. The redox potential of the cell is controlled with a BAS CV-27 potentiostat and measured with a Fluke 77 multimeter. The temperature of the cell is controlled at 25 °C with a thermostat. Spectra are recorded in a FTIR spectrometer with a Mercury Cadmium Telluride (MCT) detector and purged with a CO_2- and H_2O-free atmosphere (**Figure 9**). The FTIR spectra are averaged from 1024 scans and the spectral resolution is 2 cm^{-1} (De Lacey, et al. 2008).

Surface enhanced infrared absorption spectroscopy (SEIRAS) is a non-conventional infrared spectroscopy technique that is based in the surface enhancement effect of infrared absorption in rough (at the nanoscale) metals. It can be used for studying the [NiFeSe] hydrogenase immobilized on 4-AP-Au electrodes. For this type of measurements, a trapezium-shaped silicon ATR-IR element covered with a nanostructured SEIRA Au film formed by electroless deposition is used. All spectra are recorded in a spectral window of 4000 to 1000 cm^{-1} and with a resolution of 2 cm^{-1} using a FTIR spectrometer with a MCT detector. For each spectrum, 620 scans are accumulated (Gutiérrez-Sanz, Marques et al. 2013).

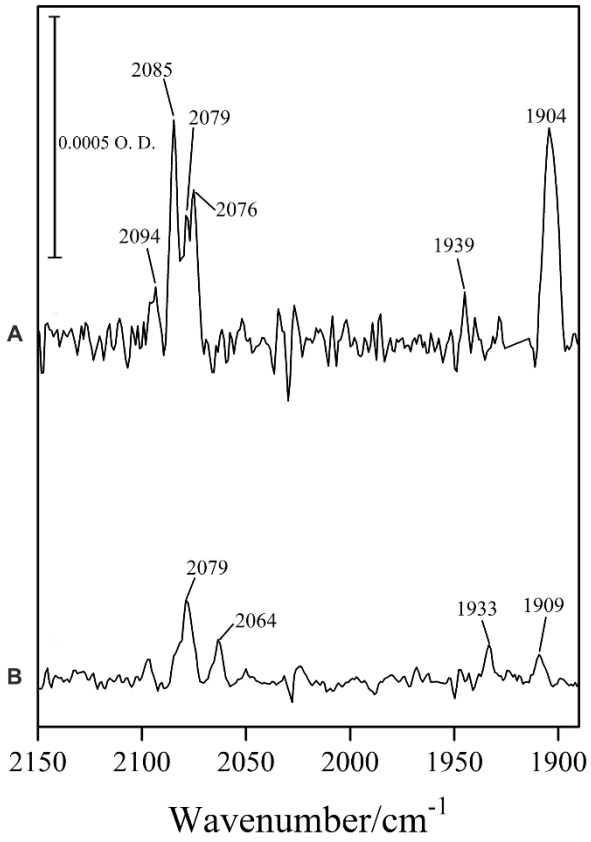

Figure 9 FTIR spectra of *D. vulgaris* Hildenborough NiFeSe-Hydrogenase active site as isolated aerobically **(A)** and after reduction with 1 atm of H_2 **(B)**.

6.2 Atomic Force Microscopy

The Atomic Force Microscope (AFM) images the topography of modified surfaces describing the height and density of the proteins on the surface as well as the integrity and smoothness of a lipid bilayer. AFM is performed on flat substrates consisting of 200 nm gold evaporated over 1 – 4 nm chromium prepared on borosilicate glass (Metallhandel Schröder GMBH). Substrates are cleaned with “piranha” solution followed by exhaustive rinsing with Milli Q water and a final rinse with ethanol/water (2:1). They are then annealed to an orange glow for a few seconds in a propane flame (this operation was repeated 5 times). This treatment is known to produce Au (111) grains of a few mm radius with atomically flat surfaces, suitable for AFM characterization. This atomically flat gold surface was then treated as described above (section 4.3) to form the 4-ATP self-assembled monolayer and to covalently attach the

enzyme for direct electron transfer. The protocol to form the bilayer on the gold substrate is also the same as the one mentioned in section 4.3. Imaging is done either on a Nanotec microscope operating in jumping mode, or with an Agilent Technologies (Santa Clara, CA) 5500 microscope used in tapping mode. Measurements were always made under liquid conditions in PBS buffer at room temperature using Olympus rectangular silicon nitride cantilevers (RC800PSA, 200 x 20 µm) with a spring constant of 0.05-0.10 N/m, an estimated tip radius of 20 nm, and a resonance frequency in the liquid cell of approximately 27 kHz. Scanning rates were kept close to 1 Hz. Images contain 512 x 512 pixels and are first-order flattened using Picoimage software from Agilent or WSxM software from Nanotec Electronica (Rüdiger et al., 2010; Gutiérrez-Sánchez et al., 2011).

6.3 Quartz Crystal Microbalance

Quartz Crystal Microbalance (QCM) measures in real time the amount of material adsorbed on a surface. It is a useful technique to aid in the sequential modification of electrodes described in section 4.3 to measure electrocatalytic H_2 production and oxidation coupled to the creation of a proton gradient across a lipid membrane used to synthesize ATP. QCM measurements are used to verify the formation of a lipid bilayer containing ATPase synthase. Experiments are performed with 5 MHz SiO_2 quartz crystals from Q-Sense. Before each measurement SiO_2-coated crystals were cleaned in a 2% (w/v) sodium dodecyl sulfate (SDS) solution for 15 min, rinsed extensively with distilled water, dried under a stream of nitrogen gas and exposed to a UV/ozone cleaner (Bioforce Nanoscience, model UV.TC:220) for at least 30 min. The UV light cleans the SiO_2 by eliminating organic contaminants and oxidizing the silicon surface, rendering it hydrophilic. After cleaning, crystals were immediately mounted in the QCM chamber. All buffers solutions used for QCM measurements were degassed for 1 hour using a 2510 Branson Sonicator with degas function (Branson Ultrasonic) immediately before use. QCM measurements were performed using a QCM-Z500 resonator from KSV (Finland) with dissipation monitoring, equipped with a flow module. The sample was continuously delivered to the measurement chamber by a syringe pump (KD Scientific, model

KDS120) at a flow rate of 50 µL/min. All measurements were performed at 23 ± 0.5 °C. Temperature was internally controlled by a Peltier and externally by a refrigerated thermoblock (Nahita model 603/20). After obtaining a stable baseline, a temperature-equilibrated 0.1 mg/mL proteoliposome solution was injected into the QCM chamber. The excess of nonadsorbed proteoliposomes were removed from the chamber by rinsing with buffer (Gutiérrez-Sanz et al. 2016).

Acknowledgments:

This work was financially supported by Fundação para a Ciência e Tecnologia (Portugal) through fellowship SFRH/BD/100314/2014 (to SZ), grant PTDC/BBB-BEP/2885/2014 (to PM and IACP), and R&D units UID/Multi/04551/2013 (Green-IT) and LISBOA-01-0145-FEDER-007660 (MostMicro) cofunded by FCT/MCTES and FEDER funds through COMPETE2020/POCI. Funding from the European Union's Horizon 2020 research and innovation programme under grant agreement No 810856 and from MINECO/FEDER (projects CTQ2015-71290-R and FIS2015-70339-C2-2-R) are also acknowledged

Bibliography

Abrahams, J. P., & Leslie, A. G. W. (1996). Methods used in the structure determination of bovine mitochondrial F1 ATPase. *Acta Crystallographica Section D: Biological Crystallography*, *52*(1), 30–42. https://doi.org/10.1107/S0907444995008754

Adams, P. D., Afonine, P. V., Bunkóczi, G., Chen, V. B., Davis, I. W., Echols, N., … Zwart, P. H. (2010). PHENIX: A comprehensive Python-based system for macromolecular structure solution. *Acta Crystallographica Section D: Biological Crystallography*, *66*(2), 213–221. https://doi.org/10.1107/S0907444909052925

Baltazar, C. S. A., Marques, M., Soares, C. M., De Lacey, A. L., Pereira, I. A. C., & Matias, P. M. (2011). Nickel-Iron-Selenium Hydrogenases - An Overview. *European Journal of Inorganic Chemistry*, *2011*(7), 948–962. https://doi.org/10.1002/ejic.201001127

Baltazar, C. S. A., Teixeira, V. H., & Soares, C. M. (2012). Structural features of [NiFeSe] and [NiFe] hydrogenases determining their different properties: a computational approach. *Journal of Biological Inorganic Chemistry*, *17*(4), 543–555. https://doi.org/10.1007/s00775-012-0875-2

Brandis, A., & Thauer, R. (1981). Growth of Desulfovibrio species on Hydrogen and Sulphate as Sole Energy Source. *Microbiology*, *126*(1), 249–252. https://doi.org/10.1099/00221287-126-1-249

Bricogne, G., Vonrhein, C., Flensburg, C., Schiltz, M., & Paciorek, W. (2003). Generation, representation and flow of phase information in structure determination: recent developments in and around SHARP 2.0. *Acta Crystallographica Section D*, *59*, 2023–2030.

https://doi.org/10.1107/S0907444903017694

Brünger, A. T. (1992). Free R Value: A Novel Statistical Quantity for Assessing the Accuracy of Crystal-Structures. *Nature*, *355*(6359), 472–475. https://doi.org/10.1038/355242a0

Caffrey, S. M., Park, H.-S., Voordouw, J. K., He, Z., Zhou, J., & Voordouw, G. (2007). Function of periplasmic hydrogenases in the sulfate-reducing bacterium Desulfovibrio vulgaris Hildenborough. *Journal of Bacteriology*, *189*(17), 6159–6167. https://doi.org/10.1128/JB.00747-07

Caputo, C. A., Gross, M. A., Lau, V. W., Cavazza, C., Lotsch, B. V., & Reisner, E. (2014). Photocatalytic Hydrogen Production using Polymeric Carbon Nitride with a Hydrogenase and a Bioinspired Synthetic Ni Catalyst. *Angewandte Chemie International Edition*, *126*(43), n/a-n/a. https://doi.org/10.1002/anie.201406811

Caputo, C. A., Wang, L., Beranek, R., & Reisner, E. (2015). Carbon Nitride-TiO2 Hybrid Modified with Hydrogenase for Visible Light Driven Hydrogen Production. *Chemical Science*, (10), 5690–5694. https://doi.org/10.1039/C5SC02017D

Cowtan, K. (1994). 'Dm': an Automated Procedure for Phase Improvement By Density Modification. *Joint CCP4 and ESF-EACBM Newsletter on Protein Crystallography*, *31*, 34–38.

De Lacey, A. L., Fernández, V. M., Rousset, M., & Cammack, R. (2007). Activation and inactivation of hydrogenase function and the catalytic cycle: spectroelectrochemical studies. *Chemical Reviews*, *107*(10), 4304–4330. https://doi.org/10.1021/cr0501947

De Lacey, A. L., Gutiérrez-Sánchez, C., Fernández, V. M., Pacheco, I., & Pereira, I. A. C. (2008). FTIR spectroelectrochemical characterization of the Ni-Fe-Se hydrogenase from Desulfovibrio vulgaris Hildenborough. *Journal of Biological Inorganic Chemistry : JBIC : A Publication of the Society of Biological Inorganic Chemistry*, *13*(8), 1315–1320. https://doi.org/10.1007/s00775-008-0412-5

Dong, A., Nam, H., Zhang, J., Andrei, V., Heidary, N., Wagner, A., … Reisner, E. (2018). Solar Water Splitting with a Hydrogenase Integrated in Photoelectrochemical Tandem Cells. *Angewandte Chemie (International Edition)*. https://doi.org/10.1002/anie.201805027

Emsley, P., Lohkamp, B., Scott, W. G., & Cowtan, K. (2010). Features and development of Coot. *Acta Crystallographica Section D: Biological Crystallography*, *66*(4), 486–501. https://doi.org/10.1107/S0907444910007493

Evans, G., & Pettifer, R. F. (2001). CHOOCH: a program for deriving anomalous- scattering factors from X-ray fluorescence spectra. *Journal of Applied Crystallography*, *34*, 82–86.

Garcin, E., Vernede, X., Hatchikian, E. C., Volbeda, A., Frey, M., & Fontecilla-Camps, J. C. (1999). The crystal structure of a reduced [NiFeSe] hydrogenase provides an image of the activated catalytic center. *Structure*, *7*(5), 557–566. Retrieved from http://www.ncbi.nlm.nih.gov/pubmed/10378275

Gutiérrez-Sánchez, C., Olea, D., Marques, M., Fernández, V. M., Pereira, I. A. C., Vélez, M., & De Lacey, A. L. (2011). Oriented immobilization of a membrane-bound hydrogenase onto an electrode for direct electron transfer. *Langmuir : The ACS Journal of Surfaces and Colloids*, *27*(10), 6449–6457. https://doi.org/10.1021/la200141t

Gutiérrez-Sanz, Ó., Marques, M., Baltazar, C. S. A., Fernández, V. M., Soares, C. M., Pereira, I. A. C., & De Lacey, A. L. (2013). Influence of the protein structure surrounding the active site on the catalytic activity of [NiFeSe] hydrogenases. *Journal of Biological Inorganic Chemistry : JBIC : A Publication of the Society of Biological Inorganic Chemistry*, *18*(4), 419–427. https://doi.org/10.1007/s00775-013-0986-4

Gutiérrez-Sanz, Ó., Marques, M., Pereira, I. A. C., De Lacey, A. L., Lubitz, W., & Rüdiger, O. (2013). Orientation and function of a membrane-bound enzyme monitored by electrochemical surface-enhanced infrared absorption spectroscopy. *Journal of Physical Chemistry Letters*, *4*(17), 2794–2798. https://doi.org/10.1021/jz4013678

Gutiérrez-Sanz, Ó., Natale, P., Márquez, I., Marques, M., Zacarias, S., Pita, M., … Vélez, M. (2016). H2-fueled ATP synthesis on an electrode: Mimicking cellular respiration. *Angewandte Chemie - International Edition*, *55*(21), 6216–6220. https://doi.org/10.1002/anie.201600752

Gutiérrez-Sanz, Ó., Tapia, C., Marques, M., Zacarias, S., Vélez, M., Pereira, I. A. C., & De Lacey, A. L. (2015). Induction of a Proton Gradient across a Gold-Supported Biomimetic Membrane by Electroenzymatic H2 Oxidation. *Angewandte Chemie International Edition*, *54*, 2684–2687. https://doi.org/10.1002/anie.201411182

Hedderich, R. (2004). Energy-Converting [NiFe] Hydrogenases from Archaea and Extremophiles: Ancestors of Complex I. *Journal of Bioenergetics and Biomembranes*, *36*(1), 65–75. https://doi.org/10.1023/B:JOBB.0000019599.43969.33

Kabsch, W. (1993). Automatic processing of rotation diffraction data from crystals of initially unknown

symmetry land cell constants. *Journal of Applied Crystallography*, *26*(pt 6), 795–800. https://doi.org/10.1107/S0021889893005588

Keller, K. L., Bender, K. S., & Wall, J. D. (2009). Development of a markerless genetic exchange system for Desulfovibrio vulgaris Hildenborough and its use in generating a strain with increased transformation efficiency. *Applied and Environmental Microbiology*, *75*(24), 7682–7691. https://doi.org/10.1128/AEM.01839-09

Keller, K. L., Wall, J. D., & Chhabra, S. (2011). *Methods for engineering sulfate reducing bacteria of the genus Desulfovibrio. Methods in enzymology* (1st ed., Vol. 497). Elsevier Inc. https://doi.org/10.1016/B978-0-12-385075-1.00022-6

Lee, C. Y., Park, H. S., Fontecilla-Camps, J. C., & Reisner, E. (2016). Photoelectrochemical H2 Evolution with a Hydrogenase Immobilized on a TiO2-Protected Silicon Electrode. *Angewandte Chemie - International Edition*, *55*(20), 5971–5974. https://doi.org/10.1002/anie.201511822

Li, M. Z., & Elledge, S. J. (2007). Harnessing homologous recombination in vitro to generate recombinant DNA via SLIC, *4*(3), 251–256. https://doi.org/10.1038/NMETH1010

Lucena, R., Aguilera, I., Palacios, P., Wahnón, P., & Conesa, J. C. (2008). Synthesis and Spectral Properties of Nanocrystalline V-Substituted In2S3, a Novel Material for More Efficient Use of Solar Radiation. *Chemistry of Materials*, *20*(16), 5125–5127. https://doi.org/10.1021/cm801128b

Maroney, M. J., & Hondal, R. J. (2018). Selenium versus sulfur: Reversibility of chemical reactions and resistance to permanent oxidation in proteins and nucleic acids. *Free Radical Biology and Medicine*, *127*, 228–237. https://doi.org/10.1016/j.freeradbiomed.2018.03.035

Marques, M., Coelho, R., De Lacey, A. L., Pereira, I. A. C., & Matias, P. M. (2010). The three-dimensional structure of [NiFeSe] hydrogenase from Desulfovibrio vulgaris Hildenborough: a hydrogenase without a bridging ligand in the active site in its oxidised, "as-isolated" state. *Journal of Molecular Biology*, *396*(4), 893–907. https://doi.org/10.1016/j.jmb.2009.12.013

Marques, M., Coelho, R., Pereira, I. A. C., & Matias, P. M. (2009). Purification, crystallization and preliminary crystallographic analysis of the [NiFeSe] hydrogenase from Desulfovibrio vulgaris Hildenborough. *Acta Crystallographica. Section F, Structural Biology and Crystallization Communications*, *65*(Pt 9), 920–922. https://doi.org/10.1107/S1744309109031261

Marques, M., Coelho, R., Pereira, I. A. C., & Matias, P. M. (2013). Redox state-dependent changes in the crystal structure of [NiFeSe] hydrogenase from Desulfovibrio vulgaris Hildenborough. *International Journal of Hydrogen Energy*, *38*(21), 8664–8682. https://doi.org/10.1016/j.ijhydene.2013.04.132

Marques, M., Tapia, C., Gutiérrez-Sanz, Ó., Ramos, A. R., Keller, K. L., Wall, J. D., … Pereira, I. A. C. (2017). The direct role of selenocysteine in [NiFeSe] hydrogenase maturation and catalysis. *Nature Chemical Biology*, *13*(5), 554–550. https://doi.org/10.1038/nchembio.2335

Matias, P. M., Soares, C. M., Saraiva, L. M., Coelho, R., Morais, J., Le Gall, J., & Carrondo, M. A. (2001). [NiFe] hydrogenase from Desulfovibrio desulfuricans ATCC 27774: gene sequencing, three-dimensional structure determination and refinement at 1.8 Å and modelling studies of its interaction with the tetrahaem cytochrome c 3. *Journal of Biological Inorganic Chemistry*, *6*(1), 63–81. https://doi.org/10.1007/s007750000167

McCoy, A. J. (2007). Solving structures of protein complexes by molecular replacement with Phaser. *Acta Crystallographica. Section D, Biological Crystallography*, *63*(Pt 1), 32–41. https://doi.org/10.1107/S0907444906045975

Mersch, D., Lee, C. Y., Zhang, J. Z., Brinkert, K., Fontecilla-Camps, J. C., Rutherford, A. W., & Reisner, E. (2015). Wiring of Photosystem II to Hydrogenase for Photoelectrochemical Water Splitting. *Journal of the American Chemical Society*, *137*(26), 8541–8549. https://doi.org/10.1021/jacs.5b03737

Moss, D., Nabedryk, E., Breton, J., & Mantele, W. (1990). Redox-linked conformational changes in proteins detected by a combination of infrared spectroscopy and protein electrochemistry: Evaluation of the technique with cytochrome c. *European Journal of Biochemistry*, *187*(3), 565–572. https://doi.org/10.1111/j.1432-1033.1990.tb15338.x

Murshudov, G. N., Skubák, P., Lebedev, A. A., Pannu, N. S., Steiner, R. A., Nicholls, R. A., … Vagin, A. A. (2011). REFMAC5 for the refinement of macromolecular crystal structures. *Acta Crystallographica Section D: Biological Crystallography*, *67*(4), 355–367. https://doi.org/10.1107/S0907444911001314

Muth, E., Morschel, E., & Klein, A. (1987). Purification and characterization of an 8-hydroxy-5-deazaflavin-reducing hydrogenase from the archaebacterium Methanococcus voltae. *European Journal of Biochemistry*, *169*(3), 571–577. https://doi.org/10.1111/j.1432-1033.1987.tb13647.x

Nonaka, K., Nguyen, N. T., Yoon, K.-S., & Ogo, S. (2013). Novel H2-oxidizing [NiFeSe]hydrogenase from

Desulfovibrio vulgaris Miyazaki F. *Journal of Bioscience and Bioengineering*, *115*(4), 366–371. https://doi.org/10.1016/j.jbiosc.2012.10.011

Painter, J., & Merritt, E. A. (2006). Optimal description of a protein structure in terms of multiple groups undergoing TLS motion. *Acta Crystallographica Section D: Biological Crystallography*, *62*(4), 439–450. https://doi.org/10.1107/S0907444906005270

Pape, T., & Schneider, T. R. (2004). HKL2MAP: a graphical user interface for macromolecular phasing with SHELX programs. *Journal of Applied Crystallography*, *37*(5), 843–844. https://doi.org/10.1107/S0021889804018047

Papp, L. V., Lu, J., Holmgren, A., & Khanna, K. K. (2007). From Selenium to Selenoproteins: Synthesis, Identity, and Their Role in Human Health. *Antioxidants & Redox Signaling*, *9*(7), 775–806. https://doi.org/10.1089/ars.2007.1528

Parkin, A., Goldet, G., Cavazza, C., Fontecilla-Camps, J. C., & Armstrong, F. a. (2008). The difference a Se makes? Oxygen-tolerant hydrogen production by the [NiFeSe]-hydrogenase from Desulfomicrobium baculatum. *Journal of the American Chemical Society*, *130*(40), 13410–13416. https://doi.org/10.1021/ja803657d

Pereira, I. A. C., Ramos, A. R., Grein, F., Marques, M., da Silva, S. M., & Venceslau, S. S. (2011). A comparative genomic analysis of energy metabolism in sulfate reducing bacteria and archaea. *Frontiers in Microbiology*, *2*(April), 69. https://doi.org/10.3389/fmicb.2011.00069

Pereira, I. A. C., Romão, C. V, Xavier, A. V, Le Gall, J., & Teixeira, M. (1998). Electron transfer between hydrogenases and mono- and multiheme cytochromes in Desulfovibrio ssp. *Journal of Biological Inorganic Chemistry*, 494–498.

Perrakis, a, Morris, R., & Lamzin, V. S. (1999). Automated protein model building combined with iterative structure refinement. *Nature Structural Biology*, *6*(5), 458–463. https://doi.org/10.1038/8263

Postgate, J. R. (1984). *Sulphate-Reducing Bacteria*. Cambridge University Press, London, UK. https://doi.org/10.1017/CBO9780511541490

Potterton, E., Briggs, P., Turkenburg, M., & Dodson, E. (2003). A graphical user interface to the CCP4 program suite research papers A graphical user interface to the CCP 4 program suite. *Acta Crystallographica Section D Biological Crystallography*, 1131–1137.

Reich, H. J., & Hondal, R. J. (2016). Why Nature Chose Selenium. *ACS Chemical Biology*, (11 (4)), 821–841. https://doi.org/10.1021/acschembio.6b00031

Reisner, E., Fontecilla-camps, J. C., & Armstrong, F. A. (2009). Catalytic electrochemistry of a [NiFeSe]-hydrogenase on TiO2 and demonstration of its suitability for visible-light driven H2 production. *Chem. Commun.*, (5), 550–552. https://doi.org/10.1039/b817371k

Reisner, E., Powell, D. J., Cavazza, C., Fontecilla-Camps, J. C., & Armstrong, F. a. (2009). Visible light-driven H(2) production by hydrogenases attached to dye-sensitized TiO(2) nanoparticles. *Journal of the American Chemical Society*, *131*(51), 18457–18466. https://doi.org/10.1021/ja907923r

Rodrigue, A., Chanal, A., Beck, K., Müller, M., Wu, L., & Mu, M. (1999). Co-translocation of a Periplasmic Enzyme Complex by a Hitchhiker Mechanism through the Bacterial Tat Pathway. *The Journal of Biological Chemistry*, *274*(19), 13223–13228. https://doi.org/10.1074/jbc.274.19.13223

Rüdiger, O., Gutiérrez-Sánchez, C., Olea, D., Pereira, I. A. C., Vélez, M., Fernández, V. M., & De Lacey, A. L. (2010). Enzymatic anodes for hydrogen fuel cells based on covalent attachment of Ni-Fe hydrogenases and direct electron transfer to SAM-modified gold electrodes. *Electroanalysis*, *22*(7–8), 776–783. https://doi.org/10.1002/elan.200880002

Ruff, A., Szczesny, J., Zacarias, S., Pereira, I. A. C., Plumeré, N., & Schuhmann, W. (2017). Protection and Reactivation of the [NiFeSe] Hydrogenase from Desulfovibrio vulgaris Hildenborough under Oxidative Conditions. *ACS Energy Letters*, 964–968. https://doi.org/10.1021/acsenergylett.7b00167

Sakai, T., Mersch, D., & Reisner, E. (2013). Photocatalytic Hydrogen Evolution with a Hydrogenase in a Mediator-Free System under High Levels of Oxygen. *Angewandte Chemie (International Ed. in English)*, *52*(47), 12313–12316. https://doi.org/10.1002/anie.201306214

Schneider, T. R., & Sheldrick, G. M. (2002). Substructure solution with SHELXD. *Acta Crystallographica Section D: Biological Crystallography*, *58*(10 I), 1772–1779. https://doi.org/10.1107/S0907444902011678

Sheldrick, G. M. (2002). Macromolecular Phasing with SHELXE. *Zeitschrift Für Kristallographie*, *217*(June), 644–650.

Sheldrick, G. M. (2010). Experimental phasing with SHELXC/D/E: Combining chain tracing with density modification. *Acta Crystallographica Section D: Biological Crystallography*, *66*(4), 479–485. https://doi.org/10.1107/S0907444909038360

Tapia, C., Zacarias, S., Pereira, I. A. C., Conesa, J. C., Pita, M., & De Lacey, A. L. (2016). In Situ Determination of Photobioproduction of H2 by In2S3 -[NiFeSe] Hydrogenase from Desulfovibrio vulgaris Hildenborough Using Only Visible Light. *ACS Catalysis*, *6*(9), 5691–5698. https://doi.org/10.1021/acscatal.6b01512

Teixeira, M., Fauque, G., Moura, I., Lespinat, P. A., Berlier, Y., Prickril, B., … Moura, J. J. G. (1987). Nickel-[iron-sulfur]-selenium-containing hydrogenases from Desulfovibrio baculatus (DSM 1743). *European Journal of Biochemistry / FEBS*, *58*, 47–58. https://doi.org/10.1111/j.1432-1033.1987.tb13302

Teixeira, M., Moura, I., Fauque, G., Czechowski, M., Berlier, Y., Lespinat, P. A., … Moura, J. J. G. (1986). Redox properties and activity studies on a nickel-containing hydrogenase isolated from a halophilic sulfate reducer Desulfovibrio salexigens. *Biochimie*, *68*(0300-9084 (Print)), 75–84. https://doi.org/10.1016/S0300-9084(86)81071-9

Valente, F., Almeida, C., Pacheco, I., Saraiva, M., & Pereira, I. A. C. (2006). Selenium Is Involved in Regulation of Periplasmic Hydrogenase Gene Expression in Desulfovibrio vulgaris Hildenborough. *Journal of Bacteriology*, *188*(9), 3228–3235. https://doi.org/10.1128/JB.188.9.3228

Valente, F., Oliveira, S., Gnadt, N., Pacheco, I., Coelho, A., Xavier, A. V, … Pereira, I. A. C. (2005). Hydrogenases in Desulfovibrio vulgaris Hildenborough: structural and physiologic characterisation of the membrane-bound [NiFeSe] hydrogenase. *Journal of Biological Inorganic Chemistry*, *10*(6), 667–682. https://doi.org/10.1007/s00775-005-0022-4

Valente, F., Pereira, P. M., Venceslau, S. S., Regalla, M., Coelho, A. V, & Pereira, I. A. C. (2007). The [NiFeSe] hydrogenase from Desulfovibrio vulgaris Hildenborough is a bacterial lipoprotein lacking a typical lipoprotein signal peptide. *FEBS Letters*, *581*(18), 3341–3344. https://doi.org/10.1016/j.febslet.2007.06.020

Vignais, P. M. (2005). H/D exchange reactions and mechanistic aspects of the hydrogenases. *Coordination Chemistry Reviews*, *249*(15-16 SPEC. ISS.), 1677–1690. https://doi.org/10.1016/j.ccr.2005.01.026

Vincent, K. A., Parkin, A., & Armstrong, F. a. (2007). Investigating and exploiting the electrocatalytic properties of hydrogenases. *Chemical Reviews*, *107*(10), 4366–4413. https://doi.org/10.1021/cr050191u

Winn, M. D., Isupov, M. N., & Murshudov, G. N. (2001). Use of TLS parameters to model anisotropic displacements in macromolecular refinement research papers Use of TLS parameters to model anisotropic displacements in macromolecular refinement. *Acta Crystallographica Section D Biological Crystallography*, 122–133.

Yamazaki, S. (1982). A selenium-containing hydrogenase from Methanococcus vannielii. *The Journal of Biological Chemistry*, 7926–7929.

Zane, G. M., Yen, H. B., & Wall, J. D. (2010). Effect of the deletion of qmoABC and the promoter-distal gene encoding a hypothetical protein on sulfate reduction in Desulfovibrio vulgaris Hildenborough. *Applied and Environmental Microbiology*, *76*(16), 5500–5509. https://doi.org/10.1128/AEM.00691-10

CHAPTER III

A HYDROPHILIC CHANNEL IS INVOLVED IN OXIDATIVE INACTIVATION OF A [NiFeSe] HYDROGENASE

This chapter is published in:

Zacarias, S., Temporão, A., del Barrio, M., Fourmond, V., Leger, C., Matias, P. M.*, & Pereira, I. A. C.* (2019). A hydrophilic channel is involved in oxidative inactivation of a [NiFeSe] hydrogenase. *ACS Catalysis*. https://doi.org/10.1021/acscatal.9b02347

S.Z, I.A.C.P. and P.M. conceived and S.Z. performed the biochemistry and X-ray crystallography experiments. The electrochemistry experiments were performed by S.Z. and french co-authors in a period spent in the lab of Dr. Léger in Marseille. S.Z was involved in analyzing the data and writing the article together with the other co-authors.

Abstract

Hydrogenases are metalloenzymes that catalyze the redox conversion between H_2 and protons. The so-called [NiFeSe] hydrogenases are highly active for both H_2 production and oxidation, but like all hydrogenases, they are inhibited by O_2. In the [NiFeSe] enzyme from *Desulfovibrio vulgaris* Hildenborough this results from the oxidation of an active site cysteine ligand. We designed mutations that constrict a hydrophilic channel that connects the protein surface to this active site cysteine. Two of the variants show markedly increased tolerance to O_2 inactivation, while retaining high catalytic activities in both directions of the reaction, and structural studies confirm that these mutations prevent the oxidation of the cysteine. Our results indicate that the diffusion of O_2 or ROS to the active site can occur through a hydrophilic water channel, in contrast to the widely held assumption that only hydrophobic channels are involved in active site inactivation. This provides an original strategy for optimizing the enzyme by protein engineering.

1. Introduction

Hydrogenases are extremely efficient biocatalysts for H_2 production and oxidation, which use only earth-abundant transition metals as cofactors. The study of these enzymes and their catalytic mechanism may lead to important insights in the efforts to develop an H_2-based economy (Lubitz et al. 2014). However, most hydrogenases are sensitive to O_2, which hampers their use in large-scale applications. Thus, understanding and preventing the inhibition of hydrogenases by O_2 is of major interest, as it could crucially influence the applicability of these enzymes as efficient catalysts in an H_2-fueled economy.

The most common hydrogenases are the [NiFe] and the [FeFe] hydrogenases, so named on the basis of the active site metal content (Lubitz et al. 2014). In both classes, this active site is deeply buried inside the protein and a network of hydrophobic

channels guides the diffusion of substrate H_2 and inhibitors, such as O_2 and CO, between the solvent and the active site (Montet et al. 1997; Volbeda et al. 2002; Teixeira et al. 2006; Leroux et al. 2008; Fontecilla-Camps et al. 2009; Liebgott et al. 2010; Kalms et al. 2016, 2018). Most [FeFe] hydrogenases are slowly but irreversibly damaged by O_2 (Kubas et al. 2017). The inactivation of the so-called "standard" [NiFe] hydrogenases involves the formation of a mixture of two EPR-detectable inactive states where an oxygen species bridges the active site metal ions; the two inactive states can be reactivated by reduction, albeit at very different rates (Fernández et al. 1985; Lamle et al. 2004; Abou Hamdan et al. 2013). The [NiFeSe] hydrogenases are a subclass of the [NiFe] hydrogenases, where a selenocysteine (Sec) replaces cysteine as one of the nickel terminal ligands (**Figure S1**) (Baltazar et al. 2011; Wombwell et al. 2015).

Two [NiFeSe] hydrogenases have been studied in detail, from *Dm. baculatum* (Teixeira et al. 1987) and *D. vulgaris* Hildenborough (Valente et al. 2005). Both exhibit very high catalytic activities, (Valente et al. 2005; Marques et al. 2017; Parkin et al. 2008) and the *Dm. baculatum* enzyme was shown to be less inhibited by H_2 and O_2 than the [NiFe] counterparts, which results in the ability to produce H_2 under low levels of O_2 (Parkin et al. 2008; Reisner et al. 2009; Wakerley et al. 2015). The active site Sec ligand of the *D. vulgaris* Hildenborough [NiFeSe] hydrogenase was observed to play a key role in its high activity and oxygen tolerance, (Marques et al. 2017) but other features are also relevant. These include a ''cage effect'' observed through experimental data and predicted by theoretical calculations, enabling a high H_2 density near the active site, (Baltazar et al. 2012; Gutiérrez-Sanz et al. 2013; Tamura et al. 2016) and differences in the proton transfer pathways and H_2 channels (Baltazar et al. 2012). [NiFeSe] hydrogenases are inactivated in the presence of high O_2 concentrations, but they can be quickly reactivated by reduction, (Parkin et al. 2008; Ceccaldi et al. 2015) probably because of the reversible reactivity of Sec with O_2 (Maroney et al. 2018). An exogenous sulfur atom bound to Ni, observed in the structure of *D. vulgaris* Hildenborough [NiFeSe] hydrogenase (**Figure S1**), may also play a role by preventing the formation of inactive species where an oxide bridges the two metal ions (Marques et al. 2013, 2017). Nevertheless, oxygen damage has been observed in the crystal structures of both [NiFeSe] hydrogenases. In the aerobically isolated enzyme from *D. vulgaris* Hildenborough the proximal iron-sulfur cluster is reversibly modified by the binding of

two oxygen atoms, and the terminal Ni ligand, Cys 75 (large subunit), is irreversibly oxidized to sulfinate (Marques et al. 2013). In addition, the sulfur species at the active site causes the side-chain of Sec489 to be present in three possible conformations, named I, II and III (**Figure S1**), where conformer III corresponds to that found in the active reduced form of the [NiFe] and [NiFeSe] hydrogenases (Marques et al. 2010, 2013). In the [NiFeSe] hydrogenase from *Dm. baculatum*, the crystal structure of the enzyme purified aerobically displayed a complex mixture of oxidized states (Volbeda et al. 2013). Some of these could be resolved only when the enzyme was purified anaerobically, showing a mixture of three oxidized states, including seleninate and selenate species and an additional oxygen or sulfur atom bridging the Ni and Fe ions. Despite the structural similarity between the two [NiFeSe] hydrogenases, (Garcin et al. 1999; Marques et al. 2010) the available data indicates that the effects of O_2 inactivation are quite enzyme specific (Volbeda et al. 2013; Marques et al. 2013). Nevertheless, it should be noted that the experimental conditions used to expose both enzymes to O_2 were different.

Recently, we developed a system for recombinant expression of a soluble form of the [NiFeSe] hydrogenase from *D. vulgaris* Hildenborough, (Marques et al. 2017) allowing the production of stable and abundant protein with high H_2 production and oxidation activities (Marques et al. 2017; Zacarias et al. 2018). The recombinant enzyme has been applied in optimized biofuel cells, which show benchmark open circuit voltages and current densities for H_2 oxidation (Ruff et al. 2017, 2018; Szczesny et al. 2018). Its high H_2 production activity makes this enzyme attractive for photochemical H_2 production, (Tapia et al. 2016) and other applications such as electrochemical ATP synthesis (Gutiérrez-Sanz et al. 2016).

The engineering of a [NiFeSe] hydrogenase to improve its O_2 tolerance has not been reported before. Here, we used rational design to prevent the irreversible oxidation of Cys75. The mechanism of Cys75 oxidation probably involves reaction with ROS, (Paulsen et al. 2013) which may be formed close to the active site by reduction of O_2. However, Cys75 is not directly accessible via the hydrophobic channel through which O_2 molecules are proposed to diffuse (Montet et al. 1997; Volbeda et al. 2002; Teixeira et al. 2006; Leroux et al. 2008; Fontecilla-Camps et al. 2009; Liebgott et al. 2010; Kalms et al. 2016, 2018). It is possible that the oxidation of Cys75 may arise due to its location at the end

of a water channel leading to the protein surface, which is only found in the crystal structures of [NiFeSe] hydrogenases (**Figure 1**). However, this channel is hydrophilic and, as a non-polar molecule, O_2 is expected to diffuse instead through the hydrophobic channels, (Montet et al. 1997) so evidence for O_2 diffusion through this water channel would be unprecedented for hydrogenases. We examined the effects of replacing two residues that line this hydrophilic channel, Gly50, located near the protein surface, and Gly491, which is near Cys75. We observed that mutations G491A and G491S prevent, or considerably slow, the oxidation of Cys75, resulting in more oxygen-tolerant variants and demonstrating the role of this solvent channel in providing access of O_2 or ROS to the active site in the *D. vulgaris* Hildenborough [NiFeSe] hydrogenase.

2. Results

2.1 Rational design of [NiFeSe] hydrogenase variants

Based on a structural alignment between the *D. vulgaris* Hildenborough [NiFeSe] hydrogenase and other members of the [NiFe] hydrogenase family (**Figure S2**) we selected two residues in the large subunit of the [NiFeSe] enzyme, which are in a solvent channel linking Cys75 to the protein surface (**Figure 1**). Gly50 is near the protein surface at *ca.* 15 Å from the Ni atom in the active site, whereas Gly491 is very close to the active site at distance of *ca.* 6 Å from the same atom. In [NiFe] hydrogenases, Gly50 and Gly491 are replaced with threonine or glutamine, and alanine or serine, respectively, so a similar channel does not exist. With the aim to block the solvent channel leading directly to Cys75 and try to prevent its oxidation, we generated the G50T and G491A variants, which reproduce the sequence of standard [NiFe] hydrogenases. We also produced the G491S, G491T and G491V variants, to test the effects of side chain polarity and size at position 491.

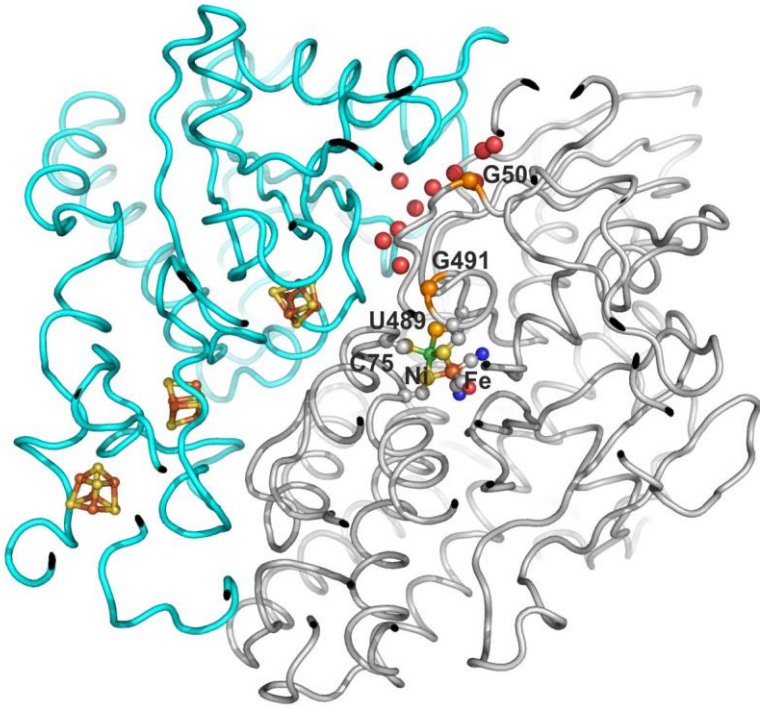

Figure 1. The solvent channel in the 0.95 Å resolution structure of the anaerobically crystallized wild-type [NiFeSe] hydrogenase from *D. vulgaris* Hildenborough (PDB 5JSH). The protein Cα backbone is colored light cyan for the small subunit and grey for the large subunit; the water molecules in the solvent channel, are shown as red spheres; the active site and the iron-sulfur clusters are depicted in ball-and-stick representation with atom colors grey for carbon, blue for nitrogen, red for oxygen, gold for sulfur and brown for iron; the G50 and G491 residues are highlighted in orange.

2.2 Kinetic and structural characterization of the [NiFeSe] hydrogenase variants

Variants G50T, G491A and G491S were successfully purified and characterized. However, no stable protein could be obtained for the G491T and G491V variants. Although threonine and valine are not bulky residues, the additional carbon atom at position 491 may induce a steric disruption. The G50T, G491A and G491S mutations moderately decreased the H_2 production and oxidation activities of enzyme (**Table 1**),

but the turnover frequencies remained near or above 3000 s^{-1}, which is high in the context of [NiFe] hydrogenases. All variants retain a catalytic bias towards H_2 production in the solution assays.

Table 1 - Turnover rate (s^{-1}) for *D. vulgaris* Hildenborough [NiFeSe] hydrogenase and variants

	WT	G491A	G491S	G50T
H_2 evolution	8270 ± 380[a]	6020 ± 100	3510 ± 140	3820 ± 210
H_2 uptake	4850 ± 260	4080 ± 80	2810 ± 150	n.d

[a] **from** (Marques et al. 2017)/ n.d. not determined

Turnover rate for H_2 production at 37 °C in 50mM Tris-HCl buffer at pH 7 with 1 mM MV reduced with 15 mM sodium dithionite. Turnover rate for H_2 oxidation under 0.5 bar H_2, at 30 °C, in 50 mM Tris/HCl pH 8 containing 2 mM of MV.

Crystal structures of the G50T, G491A and G491S variants were obtained in aerobic conditions at resolutions of 1.10, 1.36 and 1.20 Å, respectively (**Table S1** and **S2**). The previously reported 1.30 Å structure of the recombinant WT [NiFeSe] hydrogenase in the as-isolated, oxidized form (PDB 5JSH) is used for comparison (Marques et al. 2017). No changes are observed in the overall protein structures, relative to the WT. The structural analysis of the variants will focus on the oxidative modification of the active site (**Table S3**), namely the relative abundance of the three different Sec conformations (**Figure S1**) and degree of oxidation of Cys75 to sulfenate and sulfinate.

In the G50T crystal structure, Sec489 displays conformers I, II and III with occupancies of 46%, 20% and 34% (**Figure S3 A,B**), similar to those previously reported for the WT structure (52%, 20% and 29% respectively). In the G491A structure only Sec489 conformers II and III are observed with occupancies of 23% and 77%, respectively, indicating that this residue is mainly in the active, reduced conformation (**Figure 2**). Finally in the G491S structure, conformers I, II and III are present with occupancies of 29%, 18% and 53%, respectively, with Sec489 still predominantly in the active conformation (**Figure S3 C,D**). In the G50T structure, the terminal Cys75 Ni ligand is extensively oxidized to the sulfenate (20%) and sulfinate (54%) states, similarly to the WT (38% and 62%, respectively). Thus, the G50T mutation has no significant effect on the oxidized state of the active site. In contrast, in the G491A structure, Cys75 is not oxidized at all (**Figure 2**), and in the G491S structure it is only slightly oxidized to the sulfinate state (*ca.* 20%) (**Figure S3 C,D**). These results are a clear indication that the

G491 mutations protect Cys75 from oxidative modification. Furthermore, the G491S variant shows reduced oxygenation of the proximal cluster (**Table S3**), raising the possibility that this mutation may also reduce access of ROS/O_2 to this cluster.

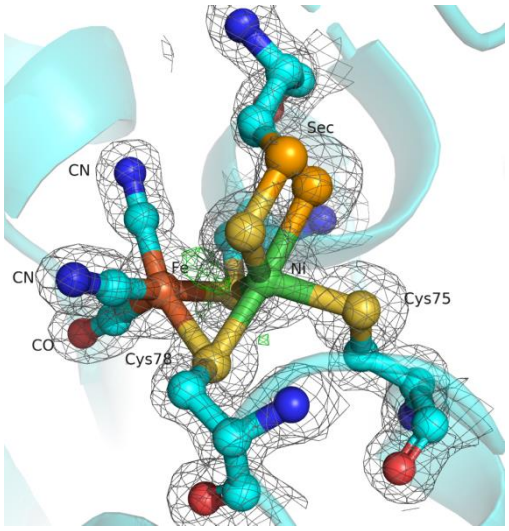

Figure 2: The active site surroundings in the crystal structure of the aerobically purified and crystallized G491A [NiFeSe] hydrogenase variant and its corresponding $2|F_o| - |F_c|$ (gray mesh, 1.5 map r.m.s.) and $|F_o| - |F_c|$ (green mesh, 3.5 map r.m.s.) maps. No negative peaks are visible at –3.5 r.m.s. in the $|F_o| - |F_c|$ map. Atoms are colour coded as follows: brown, Fe; green, Ni; gold, S; red, O; light blue, C; blue, N; orange, Se. H atoms omitted for clarity.

2.3 Electrochemical studies of O_2 and CO inhibition

The (in)activation of NiFeSe hydrogenase in response to changes in O_2 concentration or redox conditions has been studied by electrochemistry,(Parkin et al. 2008; Ceccaldi et al. 2015) in experiments where electron transfer between the enzyme and the electrode is direct and the turnover frequency is measured as a current (Sensi et al. 2017; del Barrio et al. 2018). In particular, we have shown that *D. vulgaris* Hildenborough [NiFeSe] hydrogenase inactivates either in the presence of O_2 or at high electrode potential, to inactive states that can be reduced when the electrode potential is swept down. The potential where reactivation occurs in voltammetric experiments strongly

depends on the scan rate because the rate of reactivation increases as the electrode potential decreases, (Ceccaldi et al. 2015) as occurs with all [NiFe] and [FeFe] hydrogenases characterized so far. Here we focus on the kinetics of inactivation by O_2. The experiment consists in measuring the hydrogen oxidation current (which is proportional to turnover rate) and examining the effect of injecting a small volume of air-saturated buffer solution (containing 240 µM O_2) into the electrochemical cell, to reach 0.5 µM O_2. The O_2 concentration increases instantly at the time of injection and then decreases exponentially over time, as the dissolved O_2 is flushed out of the cell by the stream of H_2. We perform these experiments at high electrode potential to prevent the direct reduction of O_2 on the electrode, which would contribute to the current, decrease the concentration of O_2 that the enzyme experiences, and produce reactive oxygen species (Léger et al. 2004). The changes in H_2 oxidation current obtained for the WT enzyme and variants are shown in **Figure 3.** When O_2 is introduced (at 175 s in the figure), the activity of the WT and G50T variant quickly vanishes, whereas, all things being equal, the G491S and G491A variants are slowly and only partially inactivated. The initial decrease in current, before O_2 addition, is due to enzyme desorption and anaerobic oxidative inactivation (Fourmond et al. 2009) and was corrected by assuming that the loss of current follows 1st order kinetics. The inactivation rate constants were determined by fitting to the data a model that assumes that the enzyme inactivates in an oxygen-dependent reaction (second order rate constant k_{in}^{O2}), followed by either reactivation (1st order rate constant k_a) or irreversible inactivation (k_3) (del Barrio et al. 2019):

$$\mathrm{A} \underset{k_a}{\overset{k_{in}^{O_2}[\mathrm{O_2}]}{\rightleftharpoons}} \mathrm{I} \xrightarrow{k_3} \mathrm{D} \qquad \textbf{[1]}$$

In this scheme, “A” represents the active species, “I” the inactive species, and “D” the dead-end species formed by irreversible inactivation.

The best values of the inactivation and reactivation rate constants are listed in **Table 2.** At the potential used, we observed a very slow reactivation ($k_a \approx 10^{-4}$ s^{-1}) for all four enzymes. The k_3 rate constants were small (possibly zero) and could not be determined accurately. However, the values of k_{in}^{O2} in Table 2 demonstrate that the two G491 mutations decrease the rate of inactivation by O_2 by about 7-fold.

In [NiFe] hydrogenases, it is believed that both CO and O_2 access the active site through the same gate at the end of a hydrophobic gas channel, and it was found that the rate of CO inhibition is a good proxy to the rate of intramolecular diffusion of other gases to the active site (Liebgott et al. 2010). We evaluated the rates of inhibition by CO (k_{in}^{CO}) and the rate of CO release (k_{out}^{CO}) for the WT and the variants by monitoring the H_2 oxidation current after exposure to CO at -60mV, 40°C (**Figure S6**). In all cases, the current decreases upon CO injection and then recovers its initial value as CO is flushed away from the solution, showing that the enzymes are reversibly inhibited by CO. To determine the constants of CO inhibition we fitted to the data a model that assumes bimolecular CO binding to the active and first-order kinetics for CO release (Leroux et al. 2008):

$$E \underset{k_{out}}{\overset{k_{in}\times[CO]}{\rightleftharpoons}} ECO \quad \textbf{[2]}$$

Since CO inhibition of [NiFe] hydrogenases is competitive (Léger et al. 2004) the measured rate constant of CO binding is not the true rate, but is multiplied by $(K_m)/(K_m+[H_2])$ (Almeida et al. 2007; Liebgott et al. 2010). This does not matter here for comparison of the rates, since we have not observed any effect of the mutations on the Michaelis constant for H_2. In contrast to what we observed with O_2, all four enzymes react with CO at about the same rate.

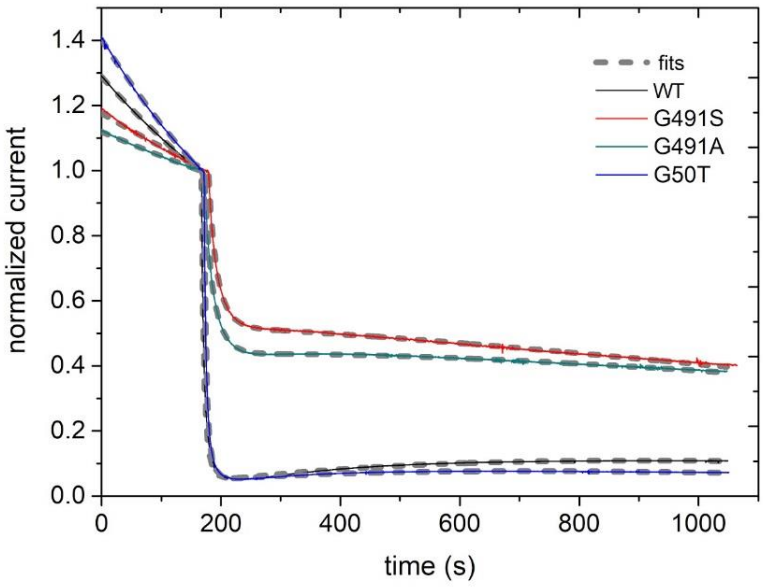

Figure 3: Effect of O_2 on the H_2 oxidation current of WT [NiFeSe] hydrogenase and variants adsorbed onto a graphite rotating electrode. The grey dashed lines are the best fits of the kinetic model in equation [1]. Experimental conditions: [O_2] = 0.5 µM, E= 0.14 V *vs.* SHE, 1 bar H_2, pH 7, T= 40°C, electrode rotation rate = 3000 rpm.

Table 2 | Kinetic properties of the *D. vulgaris* Hildenborough [NiFeSe] hydrogenase WT and variants

	k_{in}^{O2} ($mM^{-1}s^{-1}$)[a]	k_{out}^{O2} (s^{-1})[a]	$^{app}k_{in}^{CO}$ ($mM^{-1}s^{-1}$)[b]	k_{out}^{CO} (s^{-1})[b]
WT	527±10	(3±1) x 10^{-4}	290±50	0.3±0.1
G50T	629±260	(3±0.1) x 10^{-4}	410±220	0.8±0.5
G491A	77±15	(6±2) x 10^{-4}	380±80	0.9±0.4
G491S	86±15	(8±3) x 10^{-4}	400±170	1.0±0.1

[a] Conditions: E=+0.14 V *vs.* SHE, 1 bar H_2, pH 7, T=40°C, [O_2] = 0.5 µM

[b] Conditions: E=-0.06 V *vs.* SHE, 1 bar H_2, pH 7, T=40°C, [CO] = 1, 2, 4 µM

2.4 Effect of O_2 exposure on H_2 uptake activity in solution

To study the effect of prolonged air exposure and the reversibility of oxidative damage, we first activated each enzyme with H_2 and then exposed them to air for either 1 hour, 4 hours or overnight (*ca.* 16 hours) at room temperature. After exposure to air, no activity was detected either in the WT or variants, consistent with previous evidence that reactivation requires that the enzyme be reduced (Parkin et al. 2008; Ceccaldi et al. 2015). The inactive samples were then incubated under H_2 for 10, 30 or 90 minutes, before measuring how much activity remained or was irreversibly lost. The G50T variant was not tested in this experiment since the structural and electrochemical data indicated no significant difference from the WT.

For the WT enzyme we observed that after 1 hour exposure to air and reactivation with H_2, the enzyme loses 30% of the initial activity. The loss in activity increases with exposure time, reaching 50% after overnight exposure to air (**Figure 4**). In contrast, the G491S variant is more tolerant to O_2, since even after overnight air exposure (followed by reduction), the activity was not significantly affected. The G491A variant is less sensitive than the WT during the first hours, but overnight air exposure results in a similar loss of activity, by about 50%. The duration of the incubation under H_2 made no difference (**Figure S4**), with 10 minutes being enough to reactivate all the proteins. The different behaviour between the G491S and G491A variants and the WT suggests that this mutation prevents, or at least considerably delays, the formation of inactive species that do not reactivate. This experiment also emphasizes the robust catalytic behavior of the [NiFeSe] hydrogenase, since the turnovers for WT and variants are all above 1000 s^{-1} even after overnight air exposure and reactivation, which is a very high activity compared to most [NiFe] hydrogenases.

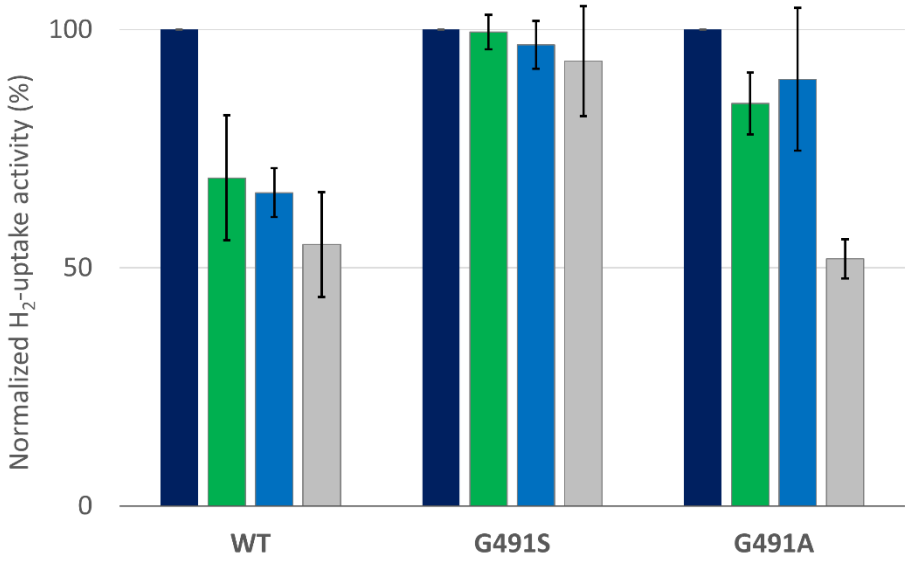

Figure 4: H_2 uptake activity of WT and variants after 1 hour (green), 4 hours (blue) and 16 hours (grey) exposure to air, followed by a 30 minute reactivation under 0.5 atmosphere of H_2. The activities were normalized by the corresponding maximum activity of each protein (dark blue), reported in Table 1. Each experiment was performed three times (technical replicates) and the error bars show the corresponding standard deviations.

2.5 Structural analysis of the [NiFeSe] hydrogenase channels

We used the software CAVER (Chovancova et al. 2012) to analyze and compare the shapes of the channels in the WT *D. vulgaris* Hildenborough [NiFeSe] hydrogenase, (Marques et al. 2017) in the variants obtained in this work, in the *Dm. baculatum* [NiFeSe] hydrogenase (Volbeda et al. 2013) and in the standard [NiFe] hydrogenases listed in **Figure S2**. Hydrogen atoms were added to the analyzed structures, whenever necessary, using the PHENIX *phenix.ready_set* tool (Adams et al. 2010). The *D. vulgaris* Myiazaki F [NiFe] hydrogenase (Ogata et al. 2015) is shown as representative of the results obtained. As illustrated in **Figure 5** and previously described, (Montet et al. 1997) both [NiFe] and [NiFeSe] hydrogenases contain a branched hydrophobic channel system through which H_2 and other small gas molecules diffuse to/from the active site. A second channel system is present in both [NiFeSe] hydrogenases, linking the Ni terminal ligands

Sec489 and Cys75 (*D. vulgaris* Hildenborough numbering) to the protein surface (**Figure 5B** and **5C**). CAVER calculations revealed that this channel is not present in the [NiFe] hydrogenases analyzed (**Figure 5** and **Table S4**), here represented by the *D. vulgaris* Myiazaki F [NiFe] hydrogenase (**Figure 5A**). In the *D. vulgaris* Hildenborough [NiFeSe] hydrogenase, this second channel has a hydrophilic character, starting from the active site, and then divides into two branches (**Figures 5B** and **6A**); the first branch continues the initial hydrophilic segment, while the second is lined by hydrophobic residues and is absent in the [NiFeSe] hydrogenase from *Dm. baculatum* (**Figure 5C**).

The G50T mutation is located after the branching point, near the end of the hydrophilic branch closer to the surface, while the G491A and G491S mutations are in the first segment of the hydrophilic channel, before the branching point. **Figure 6** shows that the G50T mutation obstructs the hydrophilic branch (**Figure 6B**), while the G491A and G491S substitutions block channel access to Cys75 (**Figures 6C** and **6D**).

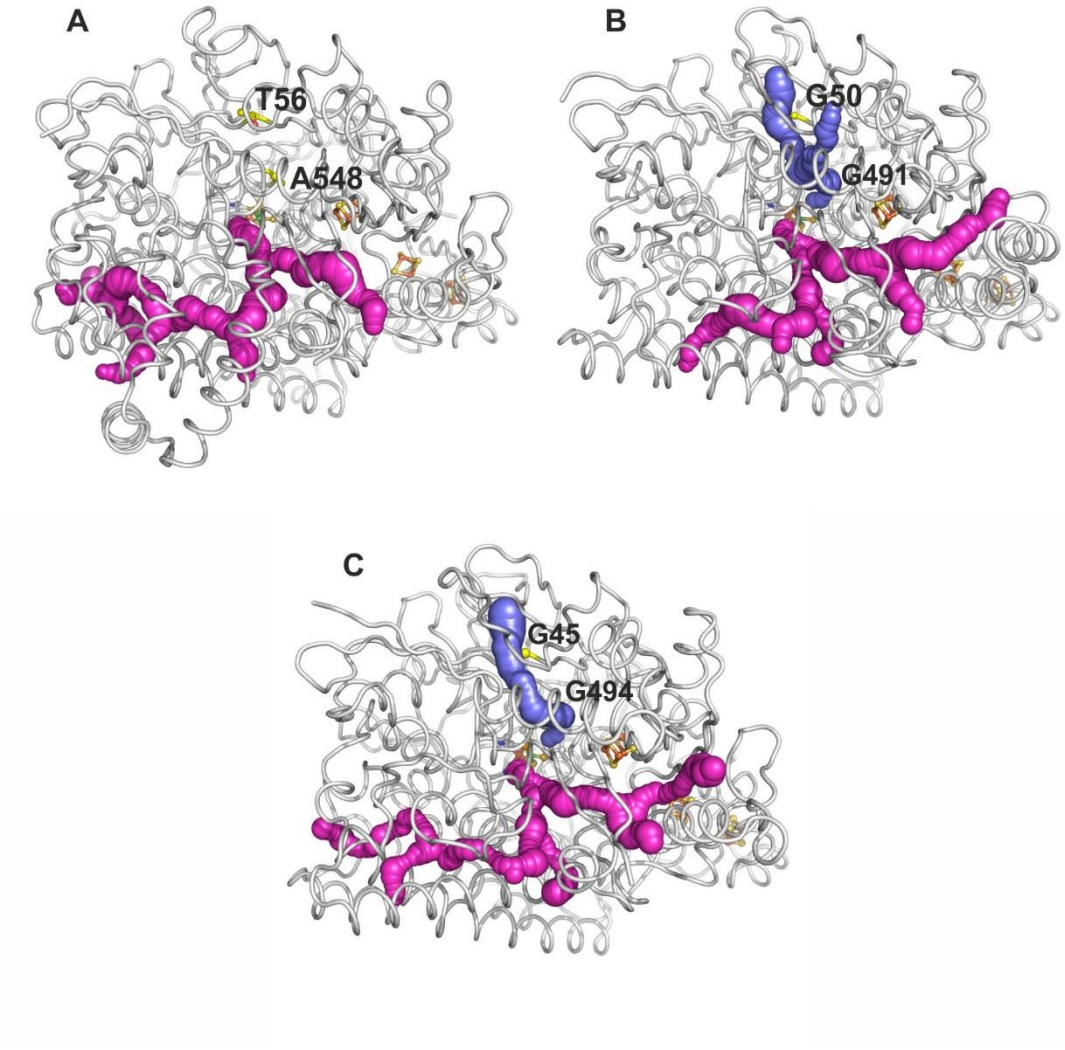

Figure 5. Channels in the high-resolution structures of [NiFe] hydrogenase from *D. vulgaris* Myiazaki F (**A**, 0.86 Å, PDB 489H) and [NiFeSe] hydrogenases from *D. vulgaris* Hildenborough (**B**, 0.95 Å, PDB 5JSK, crystallized anaerobically) and *Dm. baculatum* (**C**, 1.4 Å, PDB 4KN9), calculated with CAVER. The hydrophobic channel system allowing H_2 exchange with the active site is colored light magenta, and the channels connecting Sec and Cys 75 Sγ atoms with the enzyme exterior are displayed in blue. The protein Cα backbones are shown as gray tubes; the active site and the iron-sulfur clusters are shown in ball-and-stick representation with atom colors gray for carbon, blue for nitrogen, red for oxygen, gold for sulfur and brown for iron; the G50 and G491 residues in *D. vulgaris* Hildenborough and their structurally equivalent Thr 56 and Ala 548 residues in *D. vulgaris* Myiazaki F and G45 and G494 in *Dm. baculatum*, are displayed in ball-and-stick representation with carbon atoms colored yellow. For clarity, only the side chains of the protein residues are shown.

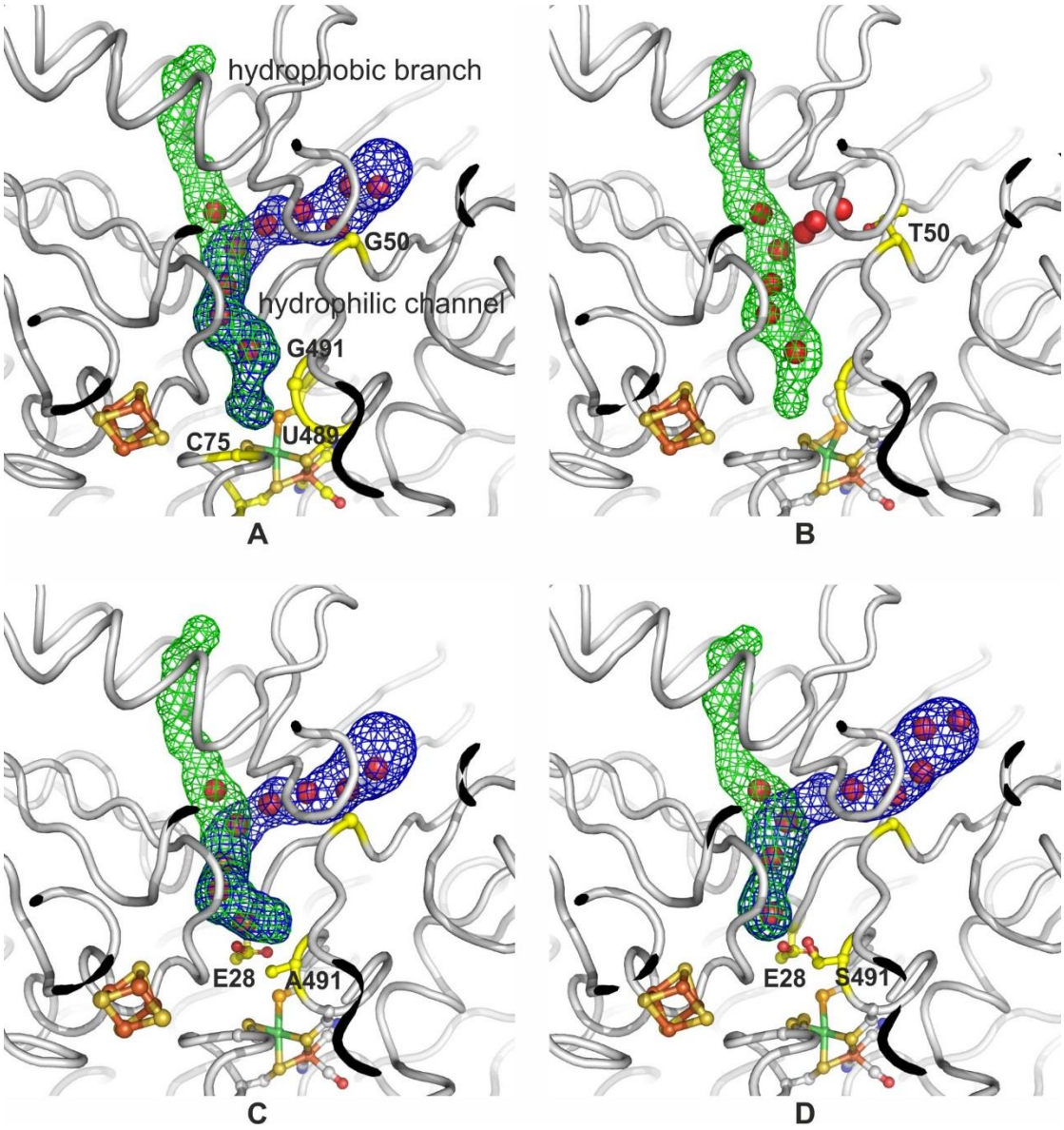

Figure 6. Close-up view of the channels in the structure of the *D. vulgaris* Hildenborough [NiFeSe] hydrogenase and variants, calculated with CAVER. A, wild-type (PDB 5JSK); B, G50T variant; C, G491A variant; D, G491S variant. The channels connecting the enzyme exterior with the Sec and the Cys 75 Sγ atoms are displayed as meshes. The hydrophilic branch of the channel in shown in blue and the hydrophobic branch is green. The water molecules enclosed by the channels are represented as red spheres.

3. Discussion

In [NiFe] hydrogenases, the importance of hydrophobic gas channels was emphasised when experiments on O_2-tolerant Regulatory Hydrogenases (RH) revealed that bulky residues at the end of the hydrophobic channel, narrow the access of gas molecules to the active site. This was initially proposed as the possible reason for the O_2-tolerance of these enzymes (Volbeda et al. 2002; Buhrke et al. 2005; Duché et al. 2005). These observations prompted studies on the standard O_2-sensitive [NiFe] hydrogenase from *D. fructosovorans*, where bulky residues were introduced in the hydrophobic channel to restrict the access of inhibitory gases O_2 and CO. The effect of modifying the gas channel in the *D.fructosovorans* hydrogenase was to slow O_2 access to the active site (Liebgott et al. 2010) and also to increase the reactivation rates (Abou Hamdan et al. 2012). These mutations also resulted in strongly decreased H_2 production rates since H_2 also diffuses through the same channel, in a step that limits the rate of H_2 production in these mutants (Abou Hamdan et al. 2012).

[NiFeSe] hydrogenases are powerful biocatalysts, which we aim to improve further by decreasing their O_2 sensitivity. Here, we tested mutations aiming to prevent the irreversible oxidation of Cys75. This residue is not directly accessible via the hydrophobic channel through which H_2 and O_2 are believed to diffuse; it is positioned at the end of a hydrophilic solvent channel that connects the active site of [NiFeSe] hydrogenases to the surface. This solvent channel seems to be present only in [NiFeSe] hydrogenases, since it is not seen in any of the O_2- resistant or O_2-sensitive [NiFe] hydrogenases that have been crystallized (**Table S4**). We tested the hypothesis that the hydrophilic channel leading to Cys75 also guides O_2 or ROS towards this residue, by examining how replacing amino acids whose side chains line this tunnel affects Cys75 oxidation and oxygen sensitivity. We observed that the G50T mutation has no significant effect, but both the G491A and G491S mutations significantly improve resistance against Cys75 irreversible oxidation. In protein film voltammetry experiments, the G491A and G491S variants are more slowly inactivated by O_2 than the WT, with 7-fold lower rate constants for O_2 inhibition. In addition, the results of solution assays show that the G491S variant is much more tolerant to prolonged air exposure, recovering nearly full activity even after overnight under air. Therefore, our kinetic data reveal that the mutation prevents the

formation of irreversibly oxidised species. From a molecular point of view, the X-Ray structures of the variants show that the G491 mutations prevent the oxidation of Cys75. Channel prediction with CAVER explains why the G50T mutation has no effect on Cys75 oxidation: this residue is positioned at the entrance of the hydrophilic water channel, but a branching point in this channel still allows access of oxygen species to the active site in the G50T variant. In contrast, the G491 residue is close to the active site, and its substitution does prevent (or strongly delay) the access of oxidising species to Cys75. In support of our hypothesis, we note that the oxidation of this terminal Ni ligand has never been observed in any [NiFe] hydrogenase, where this tunnel is absent. Moreover, the rate of inhibition of the WT [NiFeSe] hydrogenase by O_2 (530 $mM^{-1}s^{-1}$ at 40°C) is well above the typical range observed with [NiFe] hydrogenases (5 to 20 $mM^{-1}s^{-1}$, from (del Barrio et al. 2019)), whereas the G491 mutations decrease the rate of inhibition to a less remarkable value of around 80 $mM^{-1}s^{-1}$, which likely corresponds to O_2 diffusion through the hydrophobic channel as observed in standard [NiFe] hydrogenases (del Barrio et al. 2019). This supports the idea that the mutations render ineffective the hydrophilic channel that is not present in [NiFe] hydrogenases.

Interestingly, the G491 mutations slow O_2 inhibition but have no effect on CO inhibition. Carbon monoxide is a competitive inhibitor of [NiFe] hydrogenases, and in the case of *D. fructosovorans* [NiFe] hydrogenase, the rate of inhibition by CO is limited by the rate of CO access to the active site (Leroux et al. 2008; Liebgott et al. 2010). Here we observed no correlation between changes in k_{in}^{O2} and k_{in}^{CO}, suggesting that in *D. vulgaris* Hildenborough [NiFeSe] hydrogenase, the CO molecules diffuse preferentially through the hydrophobic channel system, whereas O_2/ROS diffuse faster through the hydrophilic channel system, as revealed by the inhibition kinetics.

Overall, our structural, biochemical and electrochemical results provide strong support to the hypothesis that O_2 or ROS can reach the active site of *D. vulgaris* Hildenborough [NiFeSe] hydrogenase through a hydrophilic water channel. This argues against the general idea that aerobic inactivation occurs only through O_2 diffusion through hydrophobic channels. A few previous studies have also suggested that O_2 diffusion can occur through hydrophilic channels: in the enzyme nitrogenase it has been observed that a hydrophilic channel is used for transport of the non-polar substrate N_2 (Durrant 2001; Barney et al. 2010). In catalase, MD simulations indicate that the same

channel is used by substrates and products, H_2O_2, H_2O and O_2 (Amara et al. 2001). Interestingly, in O_2-tolerant hydrogenases it has been proposed that hydrophilic channels are involved in removal of the water molecules produced during H_2 oxidation in the presence of O_2 (Fritsch et al. 2011).

All *D. vulgaris* [NiFeSe] hydrogenase variants studied here are slightly less active than the WT, but still more active than any [NiFe] hydrogenase. Residue 491 is close to the highly conserved Glu28 (**Figure 6C** and **6D**), which in [NiFe] hydrogenases is part of the proton transfer pathway (Dementin et al. 2004). A plausible explanation for the mutation-induced decrease in activity is that the bulkier side chains of the G491 variants may place some steric hindrance in the side chain motion of Glu28 and thus interfere with proton transfer. This could be especially relevant in the case of the G491S variant, where in the crystal structure Ser491 forms a hydrogen bond with Glu28 that could further hinder the proton transfer action of Glu28. Indeed, as shown in **Table 1**, the H_2 evolution activities of the variants are more affected than those of H_2 oxidation, and particularly so in the case of G491S. In the G50T variant, the threonine sidechain breaks the chain of water molecules in the hydrophilic channel, possibly creating a barrier to proton transfer and thus lowering the enzyme activity. Proton transfer is proposed to be the rate-limiting step of H_2 production in the WT form of *D. fructosovorans* [NiFe] hydrogenase (Bertrand et al. 2000). If proton transfer also limits the rate of H_2 production by *D. vulgaris* Hildenborough [NiFeSe] hydrogenase, then mutations that interfere with the proton transfer pathway should slow H_2 evolution more than H_2 uptake, as indeed observed in our experiments (Table 1). The oxidation of Cys75 to the sulfinate state is also expected to lower activity of the G491S variant. This modification is apparently formed during prolonged air exposure (long purification and crystallization), since we observe reduced levels of Cys75 sulfinate in aerobically crystalized samples since we started working with recombinant protein (~60% vs 100% previously), for which affinity purification is much faster (Marques et al. 2017). We have previously measured the decrease in activity of the WT enzyme in the crystallization conditions,(Marques 2014) and observed a gradual loss of activity, reaching about 10% after 10 days. This indicates that formation of Cys75 sulfinate leads to activity reduction, but whether the modified form retains any activity or not is difficult to ascertain. The observation that the reduced form (conformer III) could still be obtained by H_2 reduction

of aerobic crystals,(Marques et al. 2013) where Cys75 sulfinate was already present in most molecules, may suggest that some activity is retained. On the other hand, the precision of the crystallographic assignments for the sulfinate state is about ±10%, so we cannot discard that there were some active enzyme molecules left without the sulfinate modification, which were sufficient to generate enough electrons inside the crystal leading to reduction of the sulfinate-modified molecules (also obtained with dithionite(Marques et al. 2013)).

4. Conclusion

In conclusion, we show that a single mutation (G491A or G491S) can improve the O_2-tolerance of a [NiFeSe] hydrogenase, while retaining high activity in both directions of H_2 catalysis. Both variants exhibit a lower rate of inactivation by O_2 and a faster rate of reactivation after O_2 exposure. These results emphasize the fact that the O_2 sensitivity of hydrogenases from different families may be determined by specific structural features. Furthermore, our results also reveal that O_2 and/or ROS can access the active site of [NiFeSe] hydrogenase through a hydrophilic channel, in contrast with the general assumption that O_2 molecules are guided by hydrophobic channels.

5. Methods

5.1 Variant expression and purification

The *D. vulgaris* Hildenborough [NiFeSe] hydrogenase variants were created by site-directed mutagenesis with NZYMutagenesis kit (Nzytech) using the expression vector pMOIP03 carrying a *hys*A$_{Strep}$*hys*B fragment as a template (Marques et al. 2017; Zacarias et al. 2018). The vectors were electroporated into the IPAR01 deletion strain, (Marques et al. 2017) using the Gene Pulser XCell (Biorad), 1250 V, 250 Ω, 25 µF (Keller, Wall et al. 2011). Cells were grown at 37 °C in standard lactate-sulfate medium supplement with 1 µM $NiCl_2.6H_2O$ and 1 µM $NaSeO_3.5H_2O$. Cells were collected and disrupted in the French press at 6.9 MPa. The expression of the protein variants was assessed by Western blot against native *D. vulgaris* Hildenborough [NiFeSe] hydrogenase and against the Strep-

Tactin AP (IBA Lifesciences). For purification the soluble fraction was first applied in a Q-Sepharose HP column (XK 26/10 – GE Healthcare) equilibrated with 20mM Tris-HCl pH 7.6 and a stepwise NaCl gradient of 50 mM step was performed. Fractions with [NiFeSe] hydrogenase activity were affinity-purified using a gravity column containing Strep-Tactin resin (IBA Lifesciences) equilibrated with 100 mM Tris-HCl pH 8.0, 150 mM NaCl (Buffer W); the recombinant protein was eluted with buffer W plus 2.5 mM desthiobiotin. The purity of [NiFeSe] hydrogenase WT and variants was analyzed by SDS-PAGE stained with Comassie Blue.

5.2 Hydrogenase Activities

H_2-oxidation activity was routinely determined spectrophotometrically by following the H_2-dependent reduction of methyl viologen (MV) at 604 nm (ε=13.6 mM^{-1} cm^{-1}) at 30 °C inside a Coy anaerobic chamber (95% N_2, 5% H_2). The assay solution contained 2 mM MV in H_2-saturated 50 mM Tris-HCl buffer at pH 8 and the as-isolated enzyme was previously activated with 0.5 bar H_2 for 30 minutes. One unit of enzyme is defined as the amount of hydrogenase reducing 2 µmol of MV per minute, which is equivalent to 1 µmol H_2 oxidized per minute.

For H_2-production the enzyme was reduced with 1 mM methyl viologen (MV) reduced by 15 mM sodium dithionite and the reaction mixture was incubated in a shaker at 37 °C, for 10 minutes. A headspace sample was measured, every 4 minutes, in a gas chromatographer Trace GC Ultra (Thermo Scientific) equipped with a thermal conductivity detector and a MolSieve 5A 80/100 column (Althech) with N_2 as a carrier gas.

5.3 Electrochemistry

All electrochemical experiments were carried out in a glovebox (Jacomex) filled with N_2, with the electrochemical set-up and equipment as previously described (Léger et al. 2004). We used a pyrolytic graphite edge (PGE) rotating disk working electrode (area ≈ 3 mm^2), a platinum wire as a counter electrode, and a saturated calomel electrode (SCE), located in a Luggin sidearm of the electrochemical cell and immersed in 0.1 M NaCl, as a reference. The enzyme was co-adsorbed with neomycin (Bertrand et al. 2007) on the

working electrode. The electrode surface was first polished with an aqueous alumina slurry (1 µm) and sonicated. Then it was covered with 0.5 µL neomycin (200 mg/mL in water) and 1 µL of the *D. vulgaris* Hildenborough [NiFeSe] hydrogenase (50 µg/mL in pH 7 mixed buffer consisting of 5mM MES, 5mM CHES, 5mM HEPES, 5mM TAPS, 5mM sodium acetate and 100mM NaCl). The protein film was let to dry and then rinsed with water. The electrochemical cell contained pH 7 mixed buffer and was continuously flushed with pure H_2. The temperature was regulated at 40 °C by circulating water in the double jacket of the cell. The data were analysed using QSoas (Fourmond 2016) an open source program available at http://www.qsoas.org.

5.4 O_2 tolerance studies in solution

Samples of the as-isolated enzymes (0.25 µM) were activated for 1h in 0.5 bar H_2, 50 mM Tris-HCl pH 8, 1 mM MV, and were kept under H_2 atmosphere overnight. The H_2 oxidation activity was measured and taken as corresponding to the maximal activity of each protein. Next, the enzyme solutions were put in contact with air and diluted to 0.125 µM in an aerobic buffer of 50 mM Tris-HCl pH 8. Three samples of each enzyme solution were kept in aerobic conditions for 1 hour, 4 hours or overnight (≈ 16 hours) at room temperature, after which no H_2 oxidation activity was detected in any of the samples. Following this air exposure, oxidised MV was added to each sample up to a concentration of 1 mM, and the enzymes were reactivated again under 0.5 bar H_2 for 10, 30 or 90 minutes, following which H_2 oxidation activities were measured.

5.5 Crystallization and X-ray diffraction data collection

Crystals of the three *D. vulgaris* [NiFeSe] hydrogenase variants were obtained at 20 °C by the sitting drop variant of the vapor diffusion method. Drops of 1 or 2µL of pure protein (80 µM – 114 µM), were mixed with an equal volume of reservoir solution containing 20% PEG 1500 (w/v) and 0.1 mM Tris–HCl, pH 7 and equilibrated against 500 µL reservoir solution.

Crystals appeared after about one week and were harvested, briefly dipped in a cryoprotecting solution with the same composition as the reservoir solution and adjusted to include 10% (v/v) glycerol, flash cooled in liquid nitrogen and shipped to a synchrotron beamline for data collection. The G50T and G491S datasets were collected at the European Synchrotron Radiation Facility (ESRF, Grenoble, France) at beamlines ID29 and ID30A-3, respectively, and the G491A dataset was measured at the beamline I03 of the Diamond Light Source (DLS, Didcot, UK). The data collection and processing statistics are listed in **Table S1**.

The G50T and G491A datasets were integrated with XDS (Kabsch 2010) and AutoPROC (Vonrhein et al. 2011), analyzed with POINTLESS (Evans 2006) and scaled and merged with STARANISO (Tickle et al. 2016) and AIMLESS (Evans et al. 2013). The G491A dataset was integrated and scaled with XDS, analyzed with POINTLESS and merged with AIMLESS.

5.6 Structure determination and refinement

The crystal structures were determined by the molecular replacement method with PHASER (McCoy 2007) via the CCP4 Graphics User Interface (Potterton et al. 2003). The coordinates of the protein chains of the large and small subunits of the previously published crystal structure of *D. vulgaris* [NiFeSe] hydrogenase (PDB 5JSH) (Marques et al. 2017) were used as search models, after removal of all non-protein atoms. Following a quick initial refinement with REFMAC, (Murshudov et al. 2011) COOT (Emsley et al. 2010) was used to perform model corrections and addition of the active site metals and Fe-S clusters. Refinement was continued with PHENIX, (Adams et al. 2010) consisting of five macrocycles with refinement of positional coordinates, individual isotropic atomic displacement parameters for all non-hydrogen atoms and anomalous dispersion parameters for the Se atom. Model inspection and editing was done with COOT against σ_A-weighted $2|F_o|-|F_c|$ and $|F_o|-|F_c|$ electron density maps. Water molecules were added with PHENIX and checked with COOT. Hydrogen atoms in calculated positions were added to the structural models and included in the refinement in riding positions. In the final refinement stages, individual anisotropic atomic displacement parameters for all protein non-hydrogen atoms were refined for structures G50T and G491S. For structure G491A, TLS (translation-libration-screw) rigid body refinement of atomic

displacement parameters was carried out instead, followed by refinement of individual isotropic B-factors. Six and 7 TLS groups were used respectively for the small subunit (chain A) and the large subunit (chain B). These groups were adapted from the list determined with the *find_tls_groups* tool in PHENIX from a previous full isotropic refinement to also include the active site and the iron-sulfur clusters.

MOLPROBITY (Chen et al. 2010) was used to investigate model geometry in combination with the validation tools provided in COOT: for all three crystal structures reported here, the number of Ramachandran outliers did not exceed 0.13% of the total number of non-proline and non-glycine residues and the clash score did not exceed 2.5. The refinement statistics are included in **Table S2**.

Structure figures were created using the PyMOL Molecular Graphics System, Version 2.1.0 Open Source (Schrödinger, LLC). CAVER calculations were done using the PyMOL plug-in with default parameters (minimum probe radius of 0.9 Å, shell depth of 4 Å, shell radius of 3 Å, a clustering threshold of 3.5 and a starting point optimization with 3 Å maximum distance and a desired radius of 5 Å) and atomic coordinates including hydrogen atoms in calculated positions. The final atomic coordinates and experimental structure factors were deposited in the Worldwide Protein Data Bank (Berman et al. 2003) with accession codes 6RTP, 6RU9 and 6RUC for the G50T, G491A and G491S structures, respectively.

Acknowledgments:

This work was financially supported by Fundação para a Ciência e Tecnologia (Portugal) through fellowship SFRH/BD/100314/2014 (to SZ), grant PTDC/BBB-BEP/2885/2014 (to PM and IACP), and R&D units UID/Multi/04551/2013 (Green-IT) and LISBOA-01-0145-FEDER-007660 (MostMicro) co-funded by FCT/MCTES and FEDER funds through COMPETE2020/POCI. Support from ESRF and the beamline staff of ID29 and ID30A-3 for the G50T and G491S data collections is acknowledged and we also thank Diamond Light Source for access to beamline I02 under proposal number MX10515 for the G491A data collection. Funding from the European Union's Horizon 2020 research and innovation programme under grant agreement No 810856 is also acknowledged and the French authors are part of the French bioinorganic chemistry research network (www.frenchbic.cnrs.fr).

Supplementary Information

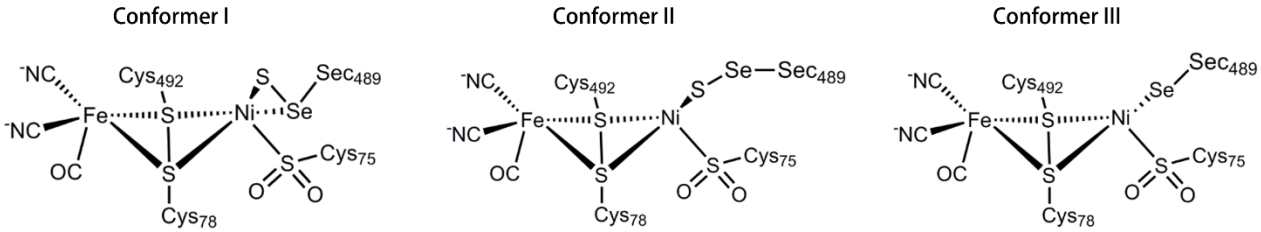

Figure S1. Active site conformations of the as-isolated *D. vulgaris* Hildenborough [NiFeSe] hydrogenase. In conformer I and II an exogenous sulfur is bound to Ni, while in conformer III no exogenous sulfur is present and Se atom is bond directly to Ni. The latter corresponds to the conformer found in the reduced form of the enzyme.

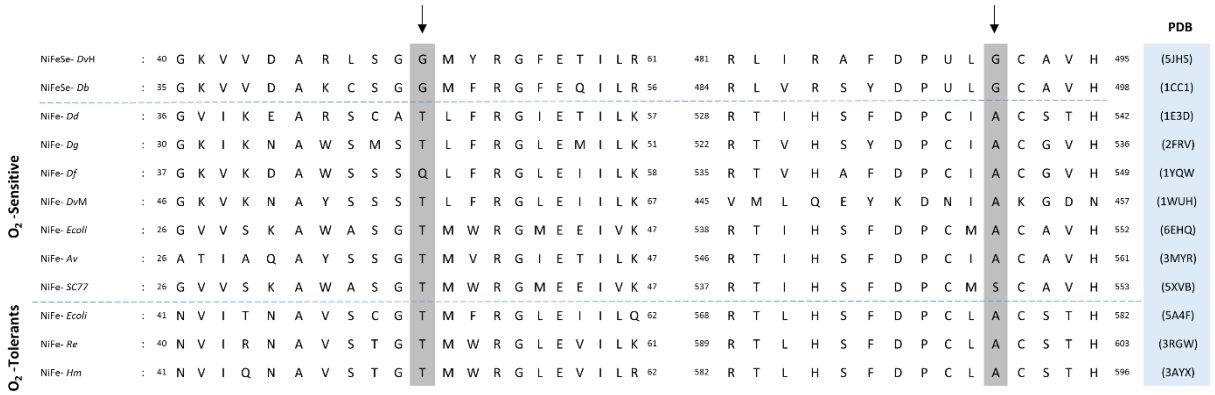

Figure S2. Structure-based sequence alignment of the large subunits of [NiFeSe] hydrogenases from *D. vulgaris* Hildenborough and *D. baculatum* with the standard O_2-sensitive [NiFe] hydrogenases from *D. desulfuricans* ATCC 27774, *D. gigas*, *D. fructosovorans*, *D. vulgaris* Miyazaki, *E. coli*, *Allochromatium vinosum* and *Citrobacter sp.* S-77 with the [NiFe] O_2-tolerant hydrogenases from *E.coli* Hyd-1, *Ralstonia eutropha* and *Hydrogenovibrio marinus.*

Table S1. Data collection and processing statistics

	G50T	***G491A***	***G491S***
Data Collection			
Beamline	ESRF ID29	DLS I02	ESRF ID30A-3
Detector	PILATUS3 6M	PILATUS 6M-F	PILATUS 6M
Wavelength (Å)	0.88560	0.97949	0.88560
Space Group	$C\,2$	$P\,2_1$	$C\,2$
Unit cell parameters:			
a, b, c (Å)	106.18, 62.68, 110.30	60.45, 98.66, 63.88	105.41, 63.59, 110.70
β (°)	105.10	105.36	104.88
Data Processing	AutoPROC/STARANISO	AutoPROC/STARANISO	XDS/CCP4
Resolution limits of ellipsoid fitted to resolution cut-off surface (Å)	1.084, 1.218, 1.223	1.36, 1.56, 1.54	-
Resolution, spherical limits (Å)	53.2-1.084 (1.199-1.084)	61.6-1.36 (1.51-1.36)	45.7-1.20 (1.22-1.20)
Nr. Observations	972918 (45622)	329698 (14355)	1414791 (50213)
Unique reflections	213931 (10698)	112189 (5610)	216144 (9023)
Multiplicity	4.5 (4.3)	2.9 (2.6)	6.5 (5.6)
Completeness, spherical (%)	72.5 (14.0)	71.9 (13.1)	97.9 (83.0)
Completeness, ellipsoidal (%)	90.9 (52.5)	92.7 (52.7)	-
R-merge (%) [b]	11.1 (87.1)	6.2 (58,9)	10.1 (133)
R-p.i.m. (%) [c]	5.9 (46.0)	4.3 (43.7)	4.2 (60.0)
<I/σ (I)>	6.9 (1.6)	10.9 (1.5)	9.4 (1.2)
CC $^{1/2}$	0.992 (0.575)	0.996 (0.613)	0.999 (0.509)
Wilson B (Å²)	10.3	17.6	8.6
Z [d]	1	1	1
Estimated V_M [e]	2.02	2.10	2.05
Estimated Solvent Content (%) [e]	39.2	41.4	40.0

[a] Values in parentheses refer to the highest resolution shell; [b] R-merge = merging R-factor, $(\Sigma_{hkl}\,\Sigma_i\,|I_i(hkl) - \langle I(hkl)\rangle|) / (\Sigma_{hkl}\,\Sigma_i\,I(hkl)) \times 100$ %; [c] R-p.i.m. = precision-independent R-factor, $\Sigma_{hkl}\,[1/(N-1)]^{1/2}\,\Sigma_i\,|I_i(hkl) - \langle I(hkl)\rangle| / (\Sigma_{hkl}\,\Sigma_i\,I_i(hkl)) \times 100$ %.[1] For each unique Bragg reflection with indices (hkl), I_i is the i-th observation of its intensity and N its multiplicity; [d] Nr. molecules in the asymmetric unit; [e] According to Matthews 1968.

Table S2. Refinement statistics

Dataset	G50T	G491A1	G491S1
Resolution limits (Å)[a]	53.2-1.10 (1.11-1.10)	49.3-1.36 (1.37-1.36)	45.7 1.20 (1.21-1.20)
R_{work} [b]	0.139 (0.318)	0.143 (0.272)	0.128 (0.286)
R_{free} [c]	0.158 (0.329)	0.162 (0.310)	0.148 (0.297)
ML coordinate error estimate (Å) [d]	0.12	0.12	0.12
Model composition and completeness			
Regions omitted [e]	--	1A-6A, 12B-13B	12B
Non-hydrogen protein atoms [f]	6099	5853	6018
Ligand/ion atoms	45	45	45
Solvent molecules	826	859	671
Glycerol molecules	3	1	3
Mean B values (Å^2) [g]			
Protein	13.6	18.8	14.0
Ligand/ion	10.2	14.3	10.4
Solvent	27.2	33.1	27.4
Glycerol	35.4	23.9	34.8
Model r.m.s. deviations from ideality			
Bond lengths (Å)	0.008	0.010	0.008
Bond angles (º)	1.328	1.314	1.273
Chiral centers (Å^3)	0.088	0.089	0.089
Planar groups (Å)	0.008	0.008	0.007
Model validation [h]			
% Ramachandran outliers	0.13	0.13	0.13
% Ramachandran favored	97.6	97.6	98.0
% Rotamer outliers	0.61	0.97	0.78
C^β outliers	0	0	0
Clash score	1.7	2.4	2.3
PDB Accession code	6RTP	6RU9	6RUC

[a] Values in parentheses refer to the highest resolution shell; [b] $R_{work} = (\Sigma_{hkl} ||F_{obs}(hkl)| - |F_{calc}(hkl)||) / (\Sigma_{hkl} |F_{obs}(hkl)|) \times 100$ %; [c] R_{free} is calculated as above from a random sample containing 5% of the total number of independent reflections measured; [d] Maximum-likelihood estimate by PHENIX; [e] HysA (large subunit) is chain B, HysB (small subunit is chain A); [f] Including atoms in the alternate conformations of disordered groups of residues; [g] Calculated from isotropic or equivalent isotropic B-values; [h] Calculated with MolProbity (Chen et al. 2010).

Table S3. Structural details

	WT (5JHS)	G50T	G491A1	G491S1
Ni atom[1]				
Occupancy	84%	67%	78%	86%
Sec489				
Conformer I	52%	46%	n.d.	29%
Conformer II	20%	20%	23%	18%
Conformer III	29%	34%	77%	53%
Cys75				
Not oxidized	-	16%	100%	76%
Sulfenate	38%	20%	-	2%
Sulfinate	62%	54%	-	21%
S atom[2]				
Occupancy	96%	81%	71%	83%
Proximal Cluster[3]				
[4Fe-4S]	75%	62%	75%	91%
[4Fe-4S-2O]	25%	38%	25%	9%

Notes:

1. In all crystal structures, the Ni ion was refined with partial occupancy: 67%, 78% and 86% in G50T, G491A and G491S, respectively, compared to 84% for the WT. The incomplete Ni occupancy probably results from a mismatch between the rates of recombinant protein expression and the native nickel incorporation machinery (Marques et al. 2017).
2. The sulfur species bound to the Ni and Se in conformers I and II was refined with occupation levels of 81%, 71% and 83%, in G50T, G491A, and G491S respectively, compared to 96% for the WT.
3. Unlike the oxidation of Cys75 to the sulfinate state, the partial oxidation of the proximal iron-sulfur cluster to [$Fe_4S_4O_2$] is reversible (Marques et al. 2013). In the previously reported WT structure the proximal iron-sulfur cluster was 25% oxidized (Marques et al. 2017) and, except for structure G491S where this oxidation level is only *ca.* 9%, comparable values are observed for the G50T and G491A structures, 38% and 25% respectively.

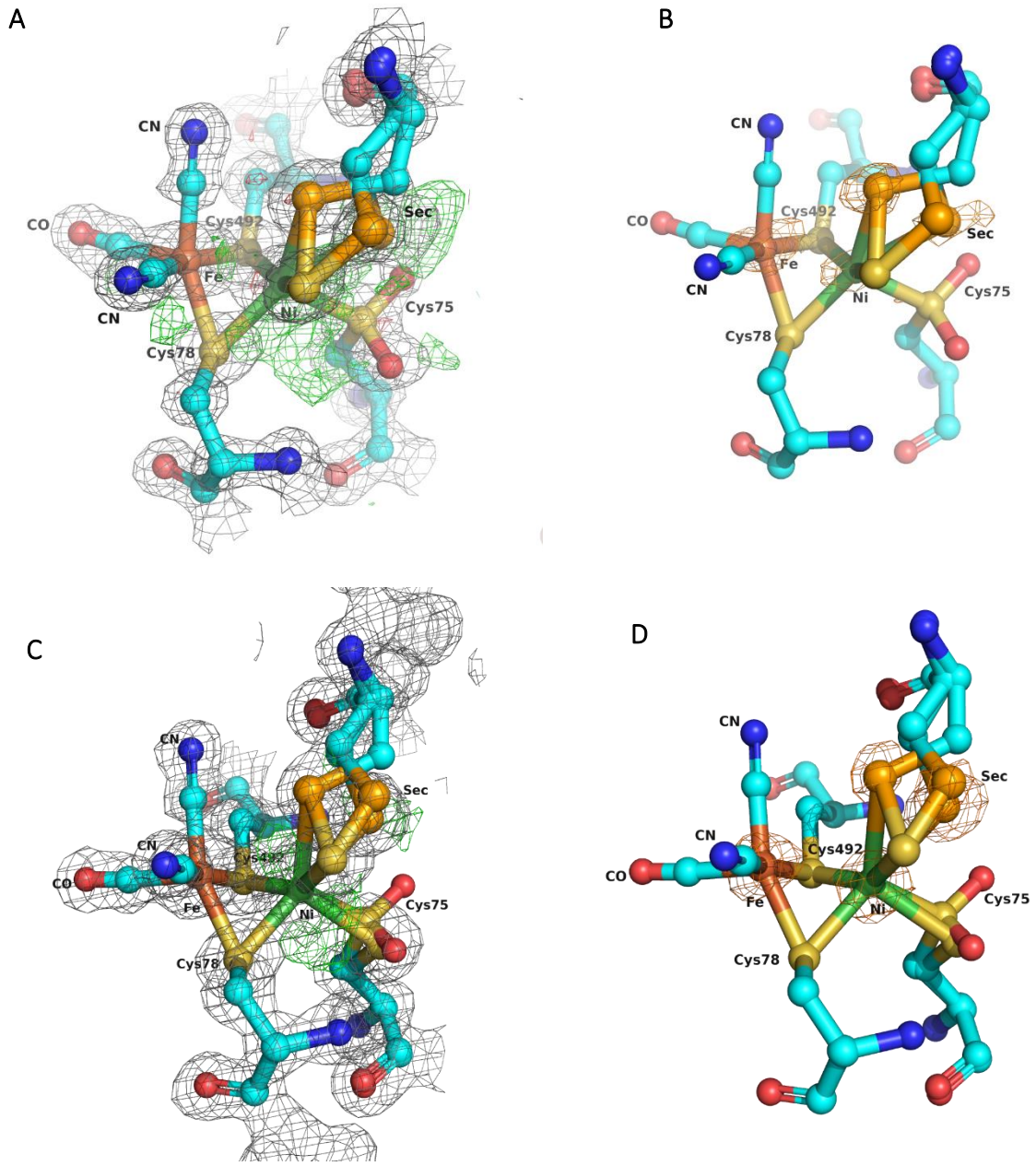

Figure S3. Active site of the aerobically purified and crystallized [NiFeSe] hydrogenase variants. (**A, C**) View of the refined structures of G50T (A) and G491S (C) with their corresponding $2|F_o|-|F_c|$ and $|F_o|-|F_c|$ maps, showing the additional Sec positions. The $2|F_o|-|F_c|$ map (gray mesh) is drawn at the 1.5 map r.m.s. level and the $|F_o|-|F_c|$ map is represented at the 3.5 (green mesh) and -3.5 (red mesh) map r.m.s. levels. (**B, D**) View of the final refined structure of G50T (**B**) and G491S (**D**) superimposed with the anomalous Fourier map (orange mesh) drawn at the 4.5 map r.m.s. level and calculated with phases from the partially refined structure represented in (a and c, respectively). The [NiFe] binuclear center and the sidechains of its protein ligands are represented in ball-and-stick and the protein chain is represented as a semitransparent cartoon.

Atom colors are brown for iron, green for nickel, gold for sulfur, red for oxygen, light blue for carbon, blue for nitrogen and orange for selenium. Hydrogen atoms are omitted for clarity.

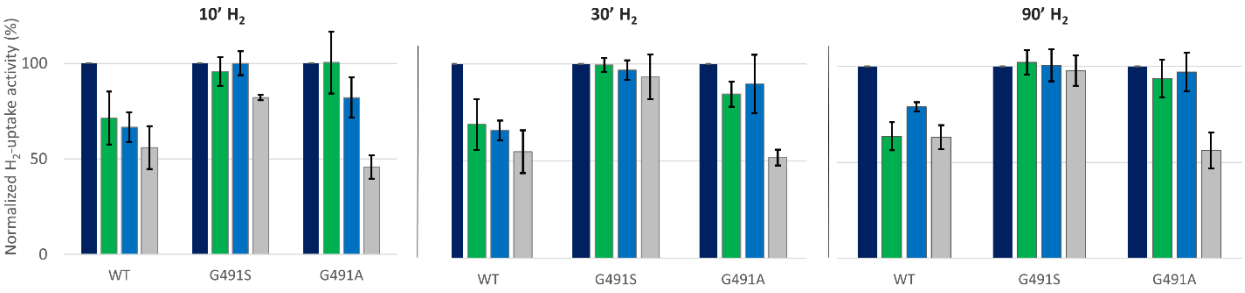

Figure S4. H_2 uptake activity of WT and variants after 1 hour (green), 4 hours (blue) and overnight (grey) exposure to air, followed by 10, 30 and 90 minutes reactivation under 0.5 atmosphere H_2. The activities were normalized by the corresponding maximum activity of each protein (dark blue), reported in Table 1. The data correspond to the average of three individual.

Table S4. Channels predicted by CAVER in [NiFe] and [NiFeSe] hydrogenase structures

Organism	PDB	Starting atom 1[(a)]	C1	C2	Starting atom 2 [(a)]	C1	C2
*Dv*H	5jhs	C75 Sγ	Y	Y	-	-	-
*Dv*H G50T	This work	C75 Sγ	N	Y	-	-	-
*Dv*H G491A	This work	C75 Sγ	N	N	A491 Cβ	Y	Y
*Dv*H G491S	This work	C75 Sγ	N	N	S491 Oγ	Y	Y
Dmb	4kn9	C70 Sγ	Y	N	-	-	-
*Dv*MF	4u9h	C81 Sγ	N	N	A548 Cβ	N	N
Dd	1e3d	C71 Sγ	N	N	A538 Cβ	N	N
Dg	2frv	C65 Sγ	N	N	A532 Cβ	N[b]	N[b]
Df	1yqw	C72 Sγ	N	N	A545 Cβ	N	N
E.coli	6ehq	C61 Sγ	N	N	A548 Cβ	N	N
Av	3myr	C61 Sγ	N	N	A557 Cβ	N	N
Cs77	5xvb	C61 Sγ	N	N	S548 Oγ	Y	N
E.coli	5a4f	C76 Sγ	N	N	A578 Cβ	N	N
Re	3rgw	C75 Sγ	N	N	A599 Cβ	N	N
Hm	3ayx	C76 Sγ	N	N	A592 Cβ	N	N

[a] Both residues are in the large subunit. The second starting atom is explored in instances where the first atom yields a negative result; [b] a tunnel system with 5 branches appears in this calculation, matching the hydrophobic tunnel system.

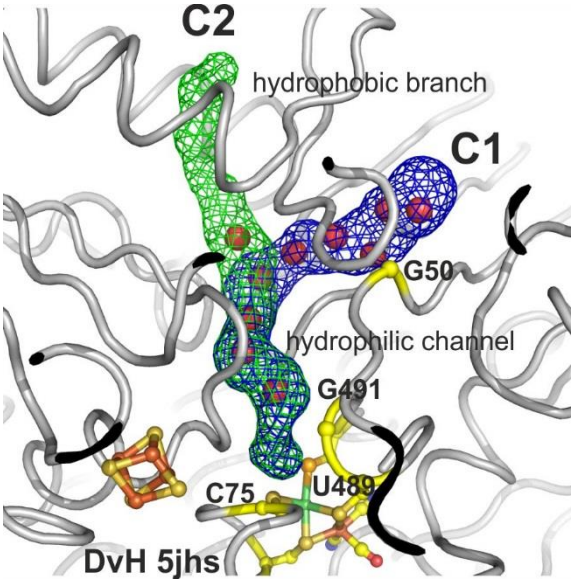

Figure S5. The hydrophilic channel (C1) and hydrophobic side-channel (C2) referenced in Table S4.

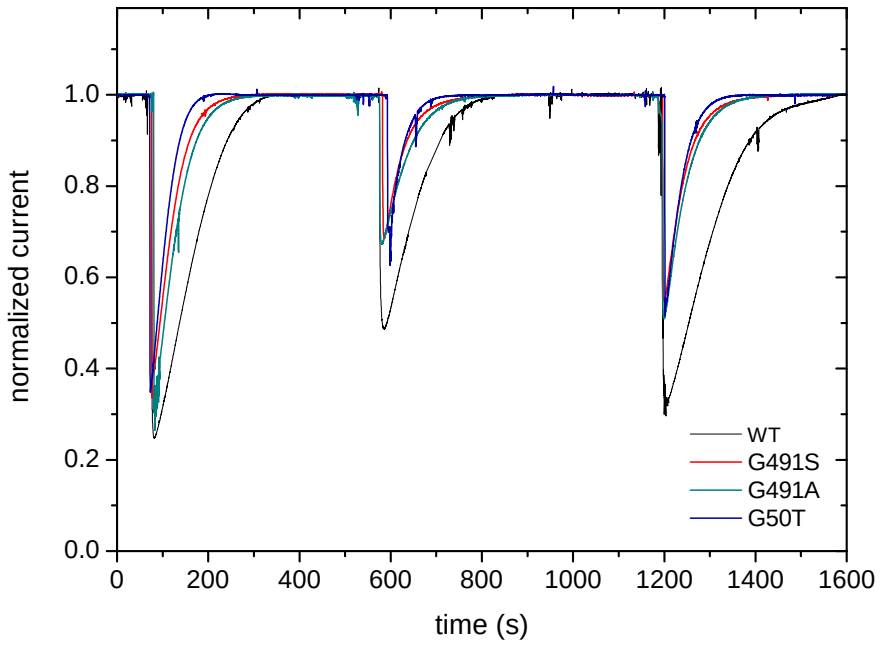

Figure S6. Effect of CO on the H_2 oxidation current of WT [NiFeSe] hydrogenase and variants adsorbed onto a graphite rotating electrode. Experimental conditions: [CO] = 4, 1, 2 µM, E= -0.060 V vs. SHE, 1 bar H_2, pH 7, T= 40°C, electrode rotation rate = 3000 rpm.

Bibliography

Abou Hamdan, A., Burlat, B., Gutiérrez-Sanz, Ó., Liebgott, P.-P., Baffert, C., De Lacey, A. L., … Dementin, S. (2013). O2-independent formation of the inactive states of NiFe hydrogenase. *Nature Chemical Biology*, *9*(1), 15–17. https://doi.org/10.1038/nchembio.1110

Abou Hamdan, A., Liebgott, P.-P., Fourmond, V., Gutiérrez-Sanz, Ó., De Lacey, A. L., Infossi, P., … Léger, C. (2012). Relation between anaerobic inactivation and oxygen tolerance in a large series of NiFe hydrogenase mutants. *Proceedings of the National Academy of Sciences of the United States of America*, *109*(49), 19916–19921. https://doi.org/10.1073/pnas.1212258109

Adams, P. D., Afonine, P. V., Bunkóczi, G., Chen, V. B., Davis, I. W., Echols, N., … Zwart, P. H. (2010). PHENIX: A comprehensive Python-based system for macromolecular structure solution. *Acta Crystallographica Section D: Biological Crystallography*, *66*(2), 213–221. https://doi.org/10.1107/S0907444909052925

Almeida, M. G., Silveira, C. M., Guigliarelli, B., Bertrand, P., Moura, J. J. G., Moura, I., & Léger, C. (2007). A needle in a haystack: The active site of the membrane-bound complex cytochrome c nitrite reductase. *FEBS Letters*, *581*(2), 284–288. https://doi.org/10.1016/j.febslet.2006.12.023

Amara, P., Andreoletti, P., Jouve, H. M., & Field, M. J. (2001). Ligand diffusion in the catalase from Proteus mirabilis: a molecular dynamics study. *Protein Science : A Publication of the Protein Society*, *10*(10), 1927–1935. https://doi.org/10.1110/ps.14201

Baltazar, C. S. A., Marques, M., Soares, C. M., De Lacey, A. L., Pereira, I. A. C., & Matias, P. M. (2011). Nickel-Iron-Selenium Hydrogenases - An Overview. *European Journal of Inorganic Chemistry*, *2011*(7), 948–962. https://doi.org/10.1002/ejic.201001127

Baltazar, C. S. A., Teixeira, V. H., & Soares, C. M. (2012). Structural features of [NiFeSe] and [NiFe] hydrogenases determining their different properties: a computational approach. *Journal of Biological Inorganic Chemistry*, *17*(4), 543–555. https://doi.org/10.1007/s00775-012-0875-2

Barney, B. M., Yurth, M. G., Santos, P. C. Dos, Dean, D. R., Seefeldt, C., & Carolina, N. (2010). A substrate channel in the nitrogenase MoFe protein. *J Biol Inorg Chem*, *14*(7), 1015–1022. https://doi.org/10.1007/s00775-009-0544-2.A

Berman, H., Henrick, K., & Nakamura, H. (2003). Announcing the worldwide Protein Data Bank. *Nature Structural & Molecular Biology*, *10*(12), 980–980. https://doi.org/10.1038/nsb1203-980

Bertrand, P., Dole, F., Asso, M., & Guigliarelli, B. (2000). Is there a rate-limiting step in the catalytic cycle of [Ni-Fe] hydrogenases? *Journal of Biological Inorganic Chemistry*, *5*(6), 682–691. https://doi.org/10.1007/s007750000152

Bertrand, P., Frangioni, B., Dementin, S., Sabaty, M., Arnoux, P., Guigliarelli, B., … Léger, C. (2007). Effects of slow substrate binding and release in redox enzymes: Theory and application to periplasmic nitrate reductase. *Journal of Physical Chemistry B*, *111*(34), 10300–10311. https://doi.org/10.1021/jp074340j

Buhrke, T., Lenz, O., Krauss, N., & Friedrich, B. (2005). Oxygen tolerance of the H2-sensing [NiFe] hydrogenase from Ralstonia eutropha H16 is based on limited access of oxygen to the active site. *Journal of Biological Chemistry*, *280*(25), 23791–23796. https://doi.org/10.1074/jbc.M503260200

Ceccaldi, P., Marques, M., Fourmond, V., Pereira, I. A. C., & Léger, C. (2015). Oxidative inactivation of NiFeSe hydrogenase. *Chemical Communications (Cambridge, England)*, *51*, 14223–14226. https://doi.org/10.1039/C5CC05930E

Chen, V. B., Arendall, W. B., Headd, J. J., Keedy, D. A., Immormino, R. M., Kapral, G. J., … Richardson, D. C. (2010). MolProbity: all-atom structure validation for macromolecular crystallography. *Acta Crystallographica. Section D, Biological Crystallography*, *66*(Pt 1), 12–21. https://doi.org/10.1107/S0907444909042073

Chovancova, E., Pavelka, A., Benes, P., Strnad, O., Brezovsky, J., Kozlikova, B., … Damborsky, J. (2012). CAVER 3.0: A Tool for the Analysis of Transport Pathways in Dynamic Protein Structures. *PLoS Computational Biology*, *8*(10), e1002708. https://doi.org/10.1371/journal.pcbi.1002708

del Barrio, M., Guendon, C., Kpebe, A., Baffert, C., Fourmond, V., Brugna, M., & Léger, C. (2019). A valine-to-cysteine mutation further increases the oxygen tolerance of Escherichia coli NiFe hydrogenase Hyd-1. *ACS Catalysis*, *9*(5), 4084–4088. https://doi.org/10.1021/acscatal.9b00543

del Barrio, M., Sensi, M., Orain, C., Baffert, C., Dementin, S., Fourmond, V., & Léger, C. (2018).

Electrochemical Investigations of Hydrogenases and Other Enzymes That Produce and Use Solar Fuels. *Accounts of Chemical Research*, *51*(3), 769–777. https://doi.org/10.1021/acs.accounts.7b00622

Dementin, S., Burlat, B., De Lacey, A. L., Pardo, A., Adryanczyk-Perrier, G., Guigliarelli, B., … Rousset, M. (2004). A Glutamate Is the Essential Proton Transfer Gate during the Catalytic Cycle of the [NiFe] Hydrogenase. *Journal of Biological Chemistry*, *279*(11), 10508–10513. https://doi.org/10.1074/jbc.M312716200

Diederichs, K., & Karplus, P. A. (1997). Improved R-factors for diffraction data analysis in macromolecular crystallography. *Nature Structural Biology*, *4*(4), 269–275. https://doi.org/10.1038/nsb0497-269

Duché, O., Elsen, S., Cournac, L., & Colbeau, A. (2005). Enlarging the gas access channel to the active site renders the regulatory hydrogenase HupUV of Rhodobacter capsulatus O2 sensitive without affecting its transductory activity. *FEBS Journal*, *272*, 3899–3908. https://doi.org/10.1111/j.1742-4658.2005.04806.x

Durrant, M. C. (2001). Controlled protonation of iron–molybdenum cofactor by nitrogenase: a structural and theoretical analysis. *Biochemical Journal*, *355*(3), 569–576. https://doi.org/10.1042/bj3550569

Emsley, P., Lohkamp, B., Scott, W. G., & Cowtan, K. (2010). Features and development of Coot. *Acta Crystallographica Section D: Biological Crystallography*, *66*(4), 486–501. https://doi.org/10.1107/S0907444910007493

Evans, P. (2006). Scaling and assessment of data quality. *Acta Crystallographica Section D Biological Crystallography*, *62*(1), 72–82. https://doi.org/10.1107/S0907444905036693

Evans, P. R., & Murshudov, G. N. (2013). How good are my data and what is the resolution? *Acta Crystallographica. Section D, Biological Crystallography*, *69*(Pt 7), 1204–1214. https://doi.org/10.1107/S0907444913000061

Fernández, V. M., Hatchikian, E. C., & Cammack, R. (1985). Properties and reactivation of two different deactivated forms of Desulfovibrio gigas hydrogenase. *Biochimica et Biophysica Acta*, *832*(1), 69–79.

Fontecilla-Camps, J. C., Amara, P., Cavazza, C., Nicolet, Y., & Volbeda, A. (2009). Structure-function relationships of anaerobic gas-processing metalloenzymes. *Nature*, *460*(7257), 814–822. https://doi.org/10.1038/nature08299

Fourmond, V. (2016). QSoas: A Versatile Software for Data Analysis. *Analytical Chemistry*, *88*(10), 5050–5052. https://doi.org/10.1021/acs.analchem.6b00224

Fourmond, V., Lautier, T., Baffert, C., Leroux, F., Liebgott, P.-P., Dementin, S., … Léger, C. (2009). Correcting for Electrocatalyst Desorption and Inactivation in Chronoamperometry Experiments. *Analytical Biochemistry*, *10*(11), 928–934. https://doi.org/10.1021/ac8025702

Fritsch, J., Scheerer, P., Frielingsdorf, S., Kroschinsky, S., Friedrich, B., Lenz, O., & Spahn, C. M. T. (2011). The crystal structure of an oxygen-tolerant hydrogenase uncovers a novel iron-sulphur centre. *Nature*, *479*(7372), 249–252. https://doi.org/10.1038/nature10505

Garcin, E., Vernede, X., Hatchikian, E. C., Volbeda, A., Frey, M., & Fontecilla-Camps, J. C. (1999). The crystal structure of a reduced [NiFeSe] hydrogenase provides an image of the activated catalytic center. *Structure*, *7*(5), 557–566. Retrieved from http://www.ncbi.nlm.nih.gov/pubmed/10378275

Gutiérrez-Sanz, Ó., Marques, M., Baltazar, C. S. A., Fernández, V. M., Soares, C. M., Pereira, I. A. C., & De Lacey, A. L. (2013). Influence of the protein structure surrounding the active site on the catalytic activity of [NiFeSe] hydrogenases. *Journal of Biological Inorganic Chemistry : JBIC : A Publication of the Society of Biological Inorganic Chemistry*, *18*(4), 419–427. https://doi.org/10.1007/s00775-013-0986-4

Gutiérrez-Sanz, Ó., Natale, P., Márquez, I., Marques, M., Zacarias, S., Pita, M., … Vélez, M. (2016). H2-fueled ATP synthesis on an electrode: Mimicking cellular respiration. *Angewandte Chemie - International Edition*, *55*(21), 6216–6220. https://doi.org/10.1002/anie.201600752

Kabsch, W. (2010). XDS. *Acta Crystallographica. Section D, Biological Crystallography*, *66*(Pt 2), 125–132. https://doi.org/10.1107/S0907444909047337

Kalms, J., Schmidt, A., Frielingsdorf, S., Utesch, T., Gotthard, G., von Stetten, D., … Scheerer, P. (2018). Tracking the route of molecular oxygen in O2-tolerant membrane-bound [NiFe] hydrogenase. *Proceedings of the National Academy of Sciences*, *115*(10), 2229–2237. https://doi.org/10.1073/pnas.1712267115

Kalms, J., Schmidt, A., Frielingsdorf, S., Van Der Linden, P., Von Stetten, D., Lenz, O., … Scheerer, P. (2016). Krypton Derivatization of an O2-Tolerant Membrane-Bound [NiFe] Hydrogenase Reveals a Hydrophobic Tunnel Network for Gas Transport. *Angewandte Chemie - International Edition*, *55*(18),

5586–5590. https://doi.org/10.1002/anie.201508976

Keller, K. L., Wall, J. D., & Chhabra, S. (2011). *Methods for engineering sulfate reducing bacteria of the genus Desulfovibrio. Methods in enzymology* (1st ed., Vol. 497). Elsevier Inc. https://doi.org/10.1016/B978-0-12-385075-1.00022-6

Kubas, A., Orain, C., De Sancho, D., Saujet, L., Sensi, M., Gauquelin, C., … Léger, C. (2017). Mechanism of O2 diffusion and reduction in FeFe hydrogenases. *Nature Chemistry*, *9*(1), 88–95. https://doi.org/10.1038/nchem.2592

Lamle, S. E., Albracht, S. P. J., & Armstrong, F. A. (2004). Electrochemical potential-step investigations of the aerobic interconversions of [NiFe]-hydrogenase from allochromatium vinosum: Insights into the puzzling difference between unready and ready oxidized inactive states. *Journal of the American Chemical Society*, *126*(45), 14899–14909. https://doi.org/10.1021/ja047939v

Léger, C., Dementin, S., Bertrand, P., Rousset, M., & Guigliarelli, B. (2004). Inhibition and Aerobic Inactivation Kinetics of Desulfovibrio fructosovorans NiFe Hydrogenase Studied by Protein Film Voltammetry. *J Am Chem Soc*, *126*(38), 12162–12172.

Leroux, F., Dementin, S., Burlat, B., Cournac, L., Volbeda, A., Champ, S., … Léger, C. (2008). Experimental approaches to kinetics of gas diffusion in hydrogenase. *Proceedings of the National Academy of Sciences of the United States of America*, *105*(32), 11188–11193. https://doi.org/10.1073/pnas.0803689105

Liebgott, P.-P., Leroux, F., Burlat, B., Dementin, S., Baffert, C., Lautier, T., … Léger, C. (2010). Relating diffusion along the substrate tunnel and oxygen sensitivity in hydrogenase. *Nature Chemical Biology*, *6*(1), 63–70. https://doi.org/10.1038/nchembio.276

Lubitz, W., Ogata, H., Rudiger, O., & Reijerse, E. (2014). Hydrogenases. *Chemical Reviews*, *114 (8)*, 4081–4148. https://doi.org/10.1021/cr4005814

Maroney, M. J., & Hondal, R. J. (2018). Selenium versus sulfur: Reversibility of chemical reactions and resistance to permanent oxidation in proteins and nucleic acids. *Free Radical Biology and Medicine*, *127*, 228–237. https://doi.org/10.1016/j.freeradbiomed.2018.03.035

Marques, M. (2014). PhD Thesis: Structural and functional studies of a high activity NiFeSe Hydrogenase. *Repositório Universidade Nova*. https://doi.org/http://hdl.handle.net/10362/14185

Marques, M., Coelho, R., De Lacey, A. L., Pereira, I. A. C., & Matias, P. M. (2010). The three-dimensional structure of [NiFeSe] hydrogenase from Desulfovibrio vulgaris Hildenborough: a hydrogenase without a bridging ligand in the active site in its oxidised, "as-isolated" state. *Journal of Molecular Biology*, *396*(4), 893–907. https://doi.org/10.1016/j.jmb.2009.12.013

Marques, M., Coelho, R., Pereira, I. A. C., & Matias, P. M. (2013). Redox state-dependent changes in the crystal structure of [NiFeSe] hydrogenase from Desulfovibrio vulgaris Hildenborough. *International Journal of Hydrogen Energy*, *38*(21), 8664–8682. https://doi.org/10.1016/j.ijhydene.2013.04.132

Marques, M., Tapia, C., Gutiérrez-Sanz, Ó., Ramos, A. R., Keller, K. L., Wall, J. D., … Pereira, I. A. C. (2017). The direct role of selenocysteine in [NiFeSe] hydrogenase maturation and catalysis. *Nature Chemical Biology*, *13*(5), 554–550. https://doi.org/10.1038/nchembio.2335

Matthews, B. W. (1968). Solvent content of protein crystals. *Journal of Molecular Biology*, *33*(2), 491–497. https://doi.org/10.1016/0022-2836(68)90205-2

McCoy, A. J. (2007). Solving structures of protein complexes by molecular replacement with Phaser. *Acta Crystallographica. Section D, Biological Crystallography*, *63*(Pt 1), 32–41. https://doi.org/10.1107/S0907444906045975

Montet, Y., Amara, P., Vernede, X., Hatchikian, E. C., Field, M., Frey, M., & Fontecilla-Camps, J. (1997). Gas access to the active site of Ni-Fe hydrogenases probed by X-ray crystallography and molecular dynamics. *Nature Structural Biology*, *4*, 523–526.

Murshudov, G. N., Skubák, P., Lebedev, A. A., Pannu, N. S., Steiner, R. A., Nicholls, R. A., … Vagin, A. A. (2011). REFMAC5 for the refinement of macromolecular crystal structures. *Acta Crystallographica Section D: Biological Crystallography*, *67*(4), 355–367. https://doi.org/10.1107/S0907444911001314

Ogata, H., Nishikawa, K., & Lubitz, W. (2015). Hydrogens detected by subatomic resolution protein crystallography in a [NiFe] hydrogenase. *Nature*, 571–574. https://doi.org/10.1038/nature14110

Parkin, A., Goldet, G., Cavazza, C., Fontecilla-Camps, J. C., & Armstrong, F. a. (2008). The difference a Se makes? Oxygen-tolerant hydrogen production by the [NiFeSe]-hydrogenase from Desulfomicrobium baculatum. *Journal of the American Chemical Society*, *130*(40), 13410–13416. https://doi.org/10.1021/ja803657d

Paulsen, C. E., & Carroll, K. S. (2013). Cysteine-Mediated Redox Signaling: Chemistry, Biology, and Tools

for Discovery. *Chemical Reviews*, *113*(7), 4633–4679. https://doi.org/10.1021/cr300163e

Potterton, E., Briggs, P., Turkenburg, M., & Dodson, E. (2003). A graphical user interface to the CCP4 program suite research papers A graphical user interface to the CCP 4 program suite. *Acta Crystallographica Section D Biological Crystallography*, 1131–1137.

Reisner, E., Powell, D. J., Cavazza, C., Fontecilla-Camps, J. C., & Armstrong, F. a. (2009). Visible light-driven H(2) production by hydrogenases attached to dye-sensitized TiO(2) nanoparticles. *Journal of the American Chemical Society*, *131*(51), 18457–18466. https://doi.org/10.1021/ja907923r

Ruff, A., Szczesny, J., Marković, N., Conzuelo, F., Zacarias, S., Pereira, I. A. C., … Schuhmann, W. (2018). A fully protected hydrogenase/polymer-based bioanode for high-performance hydrogen/glucose biofuel cells. *Nature Communications*, *9*(1), 3675. https://doi.org/10.1038/s41467-018-06106-3

Ruff, A., Szczesny, J., Zacarias, S., Pereira, I. A. C., Plumeré, N., & Schuhmann, W. (2017). Protection and Reactivation of the [NiFeSe] Hydrogenase from Desulfovibrio vulgaris Hildenborough under Oxidative Conditions. *ACS Energy Letters*, 964–968. https://doi.org/10.1021/acsenergylett.7b00167

Sensi, M., del Barrio, M., Baffert, C., Fourmond, V., & Léger, C. (2017). New perspectives in hydrogenase direct electrochemistry. *Current Opinion in Electrochemistry*, *5*(1), 135–145. https://doi.org/10.1016/j.coelec.2017.08.005

Szczesny, J., Marković, N., Conzuelo, F., Zacarias, S., Pereira, I. A. C., Lubitz, W., … Ruff, A. (2018). A gas breathing hydrogen/air biofuel cell comprising a redox polymer/hydrogenase-based bioanode. *Nature Communications*, *9*(1), 4715. https://doi.org/10.1038/s41467-018-07137-6

Tamura, T., Tsunekawa, N., Nemoto, M., Inagaki, K., Hirano, T., & Sato, F. (2016). Molecular evolution of gas cavity in [NiFeSe] hydrogenases resurrected in silico. *Scientific Reports*, *6*(January), 19742. https://doi.org/10.1038/srep19742

Tapia, C., Zacarias, S., Pereira, I. A. C., Conesa, J. C., Pita, M., & De Lacey, A. L. (2016). In Situ Determination of Photobioproduction of H2 by In2S3 -[NiFeSe] Hydrogenase from Desulfovibrio vulgaris Hildenborough Using Only Visible Light. *ACS Catalysis*, *6*(9), 5691–5698. https://doi.org/10.1021/acscatal.6b01512

Teixeira, M., Fauque, G., Moura, I., Lespinat, P. A., Berlier, Y., Prickril, B., … Moura, J. J. G. (1987). Nickel-[iron-sulfur]-selenium-containing hydrogenases from Desulfovibrio baculatus (DSM 1743). *European Journal of Biochemistry / FEBS*, *58*, 47–58. https://doi.org/10.1111/j.1432-1033.1987.tb13302

Teixeira, V. H., Baptista, A. M., & Soares, C. M. (2006). Pathways of H2 toward the active site of [NiFe]-hydrogenase. *Biophysical Journal*, *91*(6), 2035–2045. https://doi.org/10.1529/biophysj.106.084376

Tickle, I., Bricogne, G., Flensburg, C., Keller, P., Paciorek, W., Sharff, A., & Vonrhein, C. (2016). STARANISO anisotropy & amp; Bayesian estimation server. Retrieved May 16, 2019, from http://staraniso.globalphasing.org/cgi-bin/staraniso.cgi

Valente, F., Oliveira, S., Gnadt, N., Pacheco, I., Coelho, A., Xavier, A. V, … Pereira, I. A. C. (2005). Hydrogenases in Desulfovibrio vulgaris Hildenborough: structural and physiologic characterisation of the membrane-bound [NiFeSe] hydrogenase. *Journal of Biological Inorganic Chemistry*, *10*(6), 667–682. https://doi.org/10.1007/s00775-005-0022-4

Volbeda, A., Amara, P., Iannello, M., De Lacey, A. L., Cavazza, C., & Fontecilla-Camps, J. C. (2013). Structural foundations for the O2 resistance of Desulfomicrobium baculatum [NiFeSe]-hydrogenase. *Chemical Communications (Cambridge, England)*, *49*(63), 7061–7063. https://doi.org/10.1039/c3cc43619e

Volbeda, A., Montet, Y., Vernâ, X., Hatchikian, E. C., & Fontecilla-camps, J. C. (2002). High-resolution crystallographic analysis of Desulfovibrio fructosovorans [NiFe] hydrogenase. *International Journal of Hydrogen Energy*, *27*, 1449–1461.

Vonrhein, C., Flensburg, C., Keller, P., Sharff, A., Smart, O., Paciorek, W., … Bricogne, G. (2011). Data processing and analysis with the autoPROC toolbox. *Acta Crystallographica. Section D, Biological Crystallography*, *67*(Pt 4), 293–302. https://doi.org/10.1107/S0907444911007773

Wakerley, D. W., & Reisner, E. (2015). Oxygen-tolerant proton reduction catalysis: much O2 about nothing? *Energy & Environmental Science*, *8*(8), 2283–2295. https://doi.org/10.1039/C5EE01167A

Wombwell, C., Caputo, C. A., & Reisner, E. (2015). [NiFeSe]-Hydrogenase Chemistry. *Accounts of Chemical Research*, *48*, 2858–2865. https://doi.org/10.1021/acs.accounts.5b00326

Zacarias, S., Vélez, M., Pita, M., De Lacey, A. L., Matias, P. M., & Pereira, I. A. C. (2018). Characterization of the [NiFeSe] hydrogenase from Desulfovibrio vulgaris Hildenborough. In *Methods in Enzymology* (Vol. 613, pp. 169–201). https://doi.org/10.1016/bs.mie.2018.10.003

CHAPTER IV

KRYPTON AND OXYGEN PRESSURIZED CRYSTALS OF A [NiFeSe] HYDROGENASE REVEAL GAS ACCESS ROUTES TO THE ACTIVE SITE

Paper in preparation:

Zacarias S, Temporão A, Carpentier P, Pereira I A C, & Matias P M. krypton and oxygen pressurized crystals of a [NiFeSe] hydrogenase reveal gas access routes to the active site.

S.Z purified and crystallized the hydrogenase samples. S.Z, P.M, A.T and P.C. performed the crystals pressurization experiments at the High Pressure Lab of European Synchrotron Radiation Facility. S.Z, P.M. and I.A.C analyze the data and wrote the paper so far.

Abstract

Hydrogenases are metalloenzymes that catalyze both H_2 evolution and uptake. They are gas-processing enzymes with deeply buried active sites, so the diffusion of the gases occurs through channels that connect the active site to the protein surface. The [NiFeSe] hydrogenases are a special class of hydrogenases that contain a selenocysteine as a nickel ligand, and they are more catalytically active and less O_2-sensitive than the standard [NiFe] hydrogenases. Here, crystals of *Desulfovibrio vulgaris* Hildenborough [NiFeSe] hydrogenase were pressurized with krypton and oxygen, disclosing a hydrophobic channel system as the major route for gas diffusion.

1. Introduction

Hydrogenases are gas-processing enzymes with deeply buried active sites, meaning that gases such as H_2 (substrate and product) and inhibitors (O_2 and CO) have to diffuse several nanometers inside the protein interior to reach the active site. A question that emerged as soon as the first hydrogenase structure appeared (Volbeda et al. 1995) is whether the diffusion of gases inside the protein occurs freely at random, or instead in an organized way through specific channels. X-ray crystallographic studies of the interaction of light gases with biomolecules is a challenging task: in the case of hydrogenases, both the substrate and inhibitor, H_2 and O_2, have high mobility, low solubility and low electron density, making their location difficult in electron-density maps. Montet and co-workers (Montet et al. 1997) pioneered tests into the gas accessibility of a hydrogenase using Xenon derivatized crystals of [NiFe] hydrogenase from *Desulfovibrio frutosovorans*, leading to the identification of a hydrophobic channel through which gases can diffuse from the surface of the molecule to reach the active site.

Noble gases, such as Xe and Kr predominantly occupy hydrophobic environments, have Van der Waals diameters of 4.3 Å (Xenon) representing well the dimensions of O_2

molecules (3.0 Å to 4.3 Å) (Bondi 1964) and have high electron densities, thus being easy to detect by X-ray crystallography. However, the use of static crystal structures to study the dynamic interaction of gases and proteins may be insufficient to establish a detailed overview. In the efforts to better understand gas diffusion in hydrogenases, other techniques have been employed, like molecular dynamics simulations (Montet et al. 1997; Teixeira et al. 2006; Cohen, et al. 2005a; 2005b; Wang et al. 2011a; 2011b) and gas diffusion kinetic models (Leroux et al. 2008). These methods have been supporting the use of Xe/Kr as tools for pathway prospections, as they lead to the same conclusions. The importance of studying the structural details of protein channels is to understand their influence on catalytic properties and also how inhibitors diffuse through them. For instance, a narrow bottleneck in the hydrophobic channel system at the entrance of the active site on Regulatory Hydrogenases (RH) is proposed to be one of the reasons for its O_2-tolerance (Volbeda et al. 2002; Duché et al. 2005; Buhrke et al. 2005). Also, a shorter gas tunnel in [FeFe] hydrogenases could be one of the structural motifs for its high turnover rates in comparison with standard [NiFe] hydrogenases (Lubitz et al. 2014). Also, mutations in the residues lining the gas channel in the O_2-sensitive [NiFe] hydrogenase *D. fructosovorans*, confer some degree of O_2 tolerance to this enzyme (Dementin et al. 2006; Liebgott et al. 2011a; 2011b).

The [NiFeSe] hydrogenase of *D. vulgaris* Hildenborough is a very active hydrogenase in both H_2 production and oxidation, and although it is less O_2-sensitive than standard [NiFe] hydrogenases it still suffers from oxygen damage, namely an irreversible oxidation of Cys75, a Ni ligand in the active site, and a reversible oxidation of the proximal FeS cluster (Marques et al. 2010; 2013). Aiming to obtain a comprehensive description of the channel network within the enzyme we tested krypton pressurization on crystals of [NiFeSe] hydrogenase variants. Crystals were also tested for O_2 pressurization in order to explore specific pathways that O_2 might use to reach the active site. The results point to the hydrophobic channel, conserved in all [NiFe] hydrogenases, as the main diffusion path for Kr and O_2. Our results also indicate that the pressurization of crystals causes slight but significant changes in the tunnel inner diameter, indicating that this technique, although valid for disclosing main hydrophobic channels networks, should be complemented with other techniques to allow a broad picture of gas diffusion on narrow or transient channels.

2. Results and Discussion

Hydrogenase crystals were taken to the ESRF in crystallization plates, harvested from their drops, pressurized to 100 bar with Kr for 10 minutes and X-ray diffraction datasets were obtained for WT and G126C variant (mutation in the small subunit described in chapter V). With WT crystals we didn't get good diffraction data and also, few pressurized molecules were found inside the protein (data not shown) so we used hydrogenase crystal of G126C, whose mutation didn't influence the channels predictions. Data was collected at 1.18 Å resolution at beamline ID23-1 (**Table S1**). The structure was determined by molecular replacement and refined (**Table S2**)., and the krypton atomic positions were determined based on strong peaks in difference electron density maps located in regions without hydrogen-bond donor or acceptor atoms. All the krypton atoms are located inside the hydrophobic channels predicted by CAVER, so both methods agree in identifying a hydrophobic channel network as the main route for hydrophobic molecules (**Figure 1**). This hydrophobic channel system if conserved among all [NiFe] hydrogenases (see Figure 10, chapter III). An additional Kr atom is visible on the surface of the large subunit, (**Figure 1**) at the entrance of the hydrophobic branch of the channel recently identified in the *D. vulgaris* Hildenborough [NiFeSe] hydrogenase (Chapter III), (Zacarias et al. 2019). Kr molecules are spherical and bulky, so their diffusion inside this newly identified channel, which is narrow in comparison to the main hydrophobic channel should be difficult, explaining why only one Kr atom was found at the entrance of that tunnel.

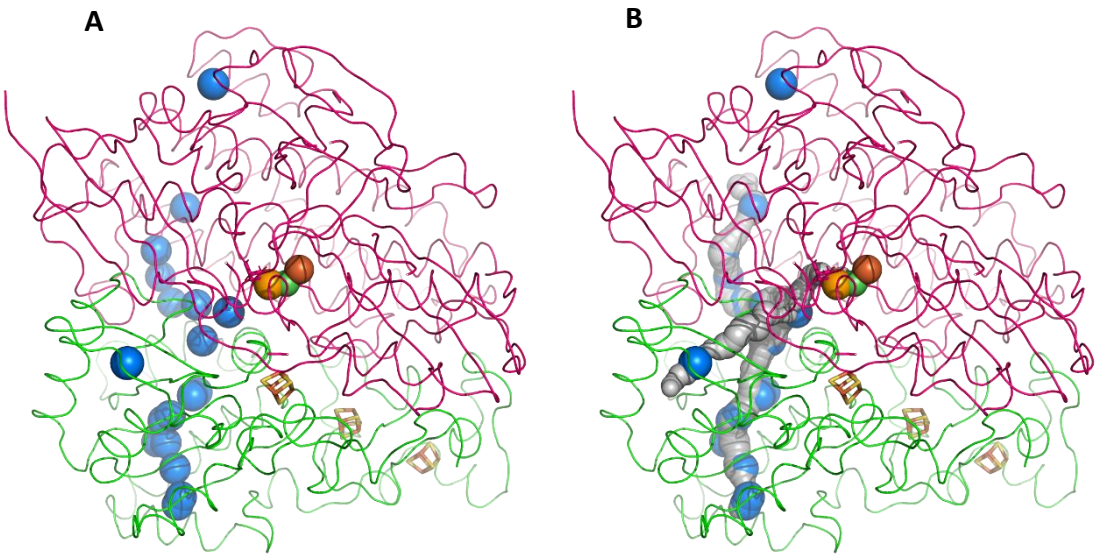

Figure 1. Structure representation of the G126C [NiFeSe] hydrogenase variant crystal structure pressurized with Krypton. **A**: krypton atoms are represented as blue spheres; **B:** Kr atoms are overlaid onto hydrophobic tunnels calculated with CAVER. The large subunit (colored magenta) and the small subunit (colored green) are represented as Cα cartoon tubes. The [NiFeSe] active site is represented as spheres and the FeS clusters as sticks.

Several openings in the protein surface were revealed, through which gases can enter and reach the active site. Interestingly, through CAVER calculations Kalms and co-workers (Kalms et al. 2016) compared the gas channel networks of O_2-tolerant and O_2-sensitive hydrogenases and a pattern was identified: O_2-tolerant hydrogenases have simpler channels with fewer openings than their O_2-sensitive counterparts. This property presumably limits the gas flow rate to the catalytic center, which in turn may contribute to the remarkable O_2 tolerance of these enzymes. However, it could also contribute to fewer H_2 molecules reaching the active site, thereby explaining the lower activities of O_2-tolerant hydrogenases in comparison with O_2-sensitive hydrogenases. The data here presented indicates that the [NiFeSe] hydrogenase from *D. vulgaris* Hildenborough contains a complex channel network with several openings in the protein surface, being more similar to the situation found in O_2-sensitive hydrogenases. The multiple entrances for gases, plus the H_2 reservoirs cavities identified by (Teixeira et al. 2006) might in part explain the high catalytic activities of this hydrogenase.

We also applied the soak-and-freeze method established at the ESRF High-Pressure Lab (Lafumat et al. 2016) to investigate whether O_2 can reach the active site of the [NiFeSe] hydrogenase from *D. vulgaris* Hildenborough through a dedicated channel network. For that, crystals of WT and of the G491A variant in the large subunit were taken to the ESRF in crystallization plates, harvested from their drops, incubated with O_2 at high pressure (just above 75 bar) for varying periods of time and data was collected at ESRF beamlines ID23-1 and ID30B (**Table S1**). Surprisingly, the location of the O_2 molecules in the hydrogenase crystal structures proved to be non-trivial, and it was realized that the intense X-ray beam used under normal data collection conditions led to the reduction of the O_2 molecules by photoelectrons produced in the crystal by the beam. This problem was circumvented by collecting a dataset with very low X-ray dose absorption by the crystal and comparing the resulting electron density map with another dataset recorded with a normal X-ray dose on the same crystal (**Table 1**). These datasets were obtained from a G491A crystal instead of a WT crystal due to lack of suitable WT crystals after the many previous O_2-pressurizing experiments carried out.

Table 1. G491A dataset collected with different X-ray doses

Data Set	%Transmission	MGy	Resolution (Å)	% R-merge	% Completeness
Low Dose (ld)	0.2	0.12	1.59	8.2	97.8
High Dose (hd)	2.0	1.35	1.43	5.4	97.2

The low dose (ld) and high dose (hd) datasets were scaled together with CCP4 SCALEIT (R-factor = 9.0 % to 1.6 Å resolution). An isomorphous difference map, $\mathbf{F_{o,hd} - F_{o,ld}}$ with phases calculated from the **ld** structure, was used to locate the O_2 molecules in the **ld** crystal structure, as negative peaks in the map (**Figure 2A**). The O_2 sites were validated by their location in hydrophobic regions of the structure by comparison with the Kr sites on a previously refined wild-type crystal structure pressurized with krypton gas (**Figure 2B**) and by positive peaks in the $\mathbf{2F_{o,ld} – F_{c,ld}}$ **map**, albeit at contour levels below 1 σ. A total of 6 O_2 molecules were added in this way. Final refinement was carried out with PHENIX (Adams et al. 2010), using the previously refined structure from REFMAC as a starting model (**Table S2**).

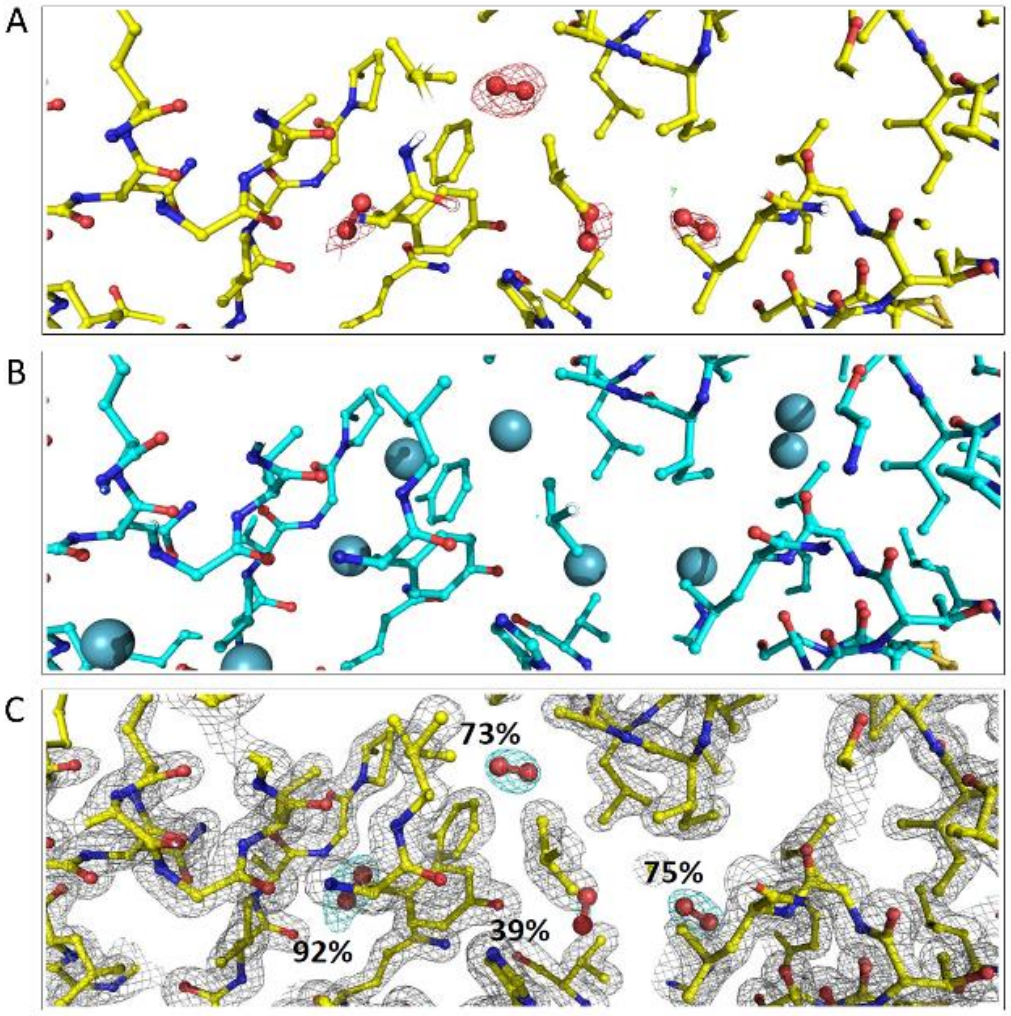

Figure 2: Locating the O_2 molecules in the G491A **ld** structure: (A) Low dose G491A structure with superimposed $|F_{o,hd}|-|F_{o,ld}|$ difference map contoured at 3σ (green mesh) and -3σ (red mesh). The O_2 molecules are displayed in ball-and-stick representation; (B) Structure of the wild type protein pressurized with Kr showing the Kr sites as spheres; (C) Final $2|F_{o,ld}|-|F_{o,ld}|$ map of the G491A structure contoured at 1.5 σ (grey mesh) for the protein and 0.8 σ (cyan mesh) for the O_2 molecules.

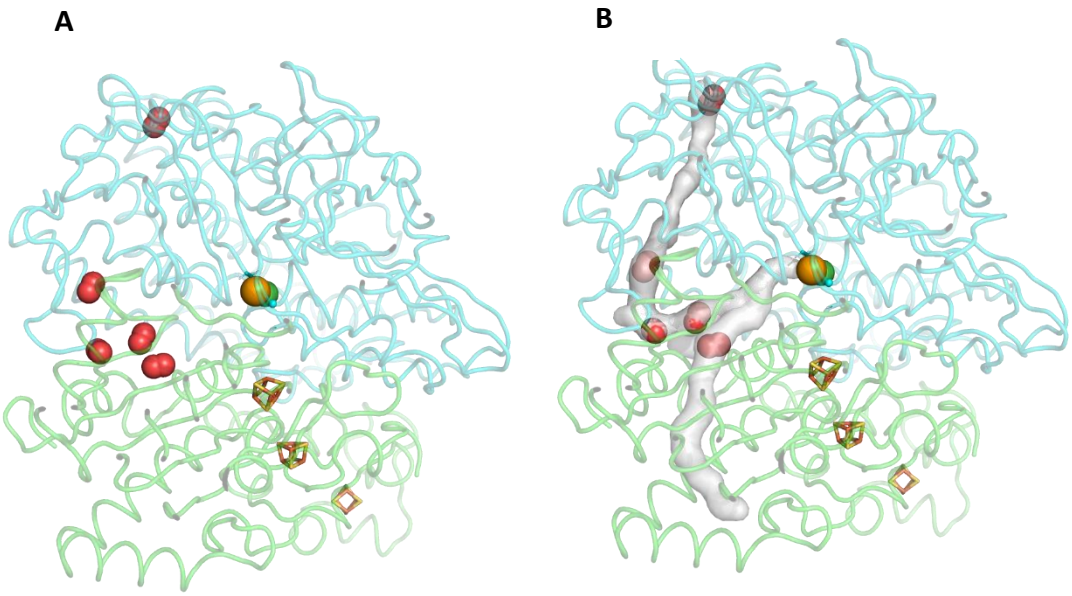

Figure 3: Representation of the G491A [NiFeSe] hydrogenase variant high-dose structure pressurized with O_2. **A:** oxygen atoms are represented as red spheres. **B:** oxygen atoms are overlaid onto hydrophobic tunnels calculated with CAVER. The large subunit (colored light cyan) and the small subunit (colored light green) are represented as Cα cartoon tubes. The [NiFeSe] active site is represented as spheres and the FeS clusters are represented as sticks.

In **Figure 3** we can observe the distribution of the O_2 molecules in the G491A hydrogenase structure, and through a CAVER simulation, we observed that O_2 molecules fit inside the hydrophobic channel (grey).

For a more comprehensive overview of the pressurized gas molecules distribution inside the protein, we overlaid tunnels predicted with CAVER in a WT hydrogenase crystal structure that was not pressurized before cryocooling and than overlaid the gas molecules identified in the Kr and O_2 pressurization experiments (**Figure 4**). It is interesting to note that in the pressurized G491A crystal structure, the channel described in Chapter III and represented here in blue and green (**Figure 4**) begins at Glu28 next to A491 because the pressurization caused a constriction of the channel diameter at A491, below 0.9 Å, the probe radius used in the CAVER calculations.

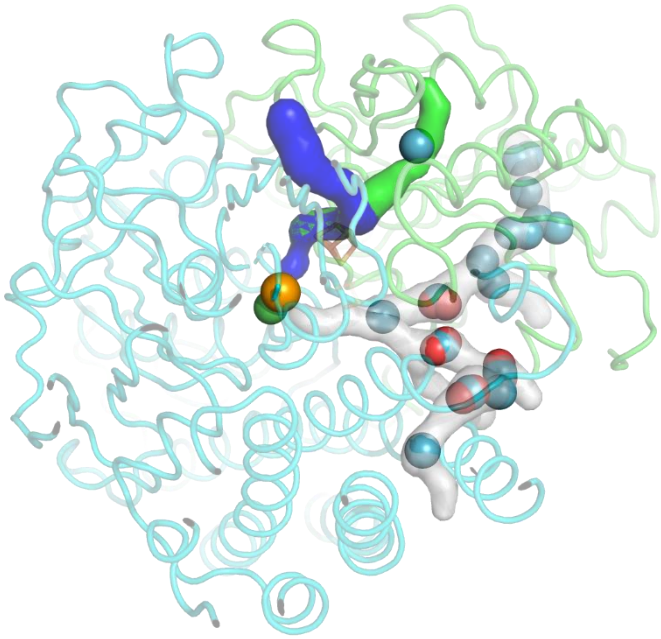

Figure 4: Structure of the [NiFeSe] hydrogenase with channels predicted by CAVER in a non-pressurized WT crystal structure. The main hydrophobic channel is represented in semi-transparent grey color with superimposed Kr atoms (light blue spheres) and oxygen atoms (red spheres), from the pressurization experiments. A Kr atom is placed just inside the hydrophobic branch of the channel described in chapter III. The large subunit (colored cyan) and the small subunit (colored green) are represented as Cα cartoon tubes. The active site is represented as spheres in the middle of the protein structure, the FeS clusters are represented as sticks but are partially hidden from view due to the orientation of the protein structure.

Both pressurization experiments with Kr and O_2 reveal a hydrophobic channel system as the main route for gas access to the active site. The architecture of such tunnels should be analyzed in detail and compared with other hydrogenases. Since the data obtained are based in static crystal structures it should be also complemented with molecular dynamics simulations in order to study dynamic changes of the gas channel networks that likely affect gas access to the active site.

3. Experimental Section:

3.1 Protein and Crystals Preparation:

Protein expression and purification were done as described in Chapter II (Zacarias et al. 2018). Crystals were obtained at 20 °C by the sitting drop vapor diffusion method as previously described in Chapter II (Zacarias et al. 2018). In these studies, crystals of WT and G126C variant (in the small subunit) of the recombinant [NiFeSe] hydrogenase of *D. vulgaris* Hildenborough (Marques et al. 2017) were used for the Kr-pressurization experiments. Crystals of the WT and G491A variant (in the large subunit) of the recombinant [NiFeSe] hydrogenase of *D. vulgaris* Hildenborough were used for the O_2-pressurization experiments. The best results, here presented, for both gases (Kr and O_2) pressurization experiments were obtained from variants hydrogenase, G126C for Kr and G491A variant for O_2.

3.2 High-pressure krypton derivatization

Krypton derivatization was performed using a high-pressure cooling system at the ESRF in Grenoble (Van Der Linden et al. 2014). The G126C crystals were taken to the ESRF High-Pressure Laboratory in crystallization plates, harvested with steel pins topped by polycarbonate tubes of varying diameters according to crystal size and transferred to the high-pressure sample cell. After 10 min of pressurization under 100 bar of krypton gas, the krypton-containing crystals were directly flash-cooled by dropping the pin in the cold end of the cell, at 77 K; then the system was depressurized and the pin mounted on a SPINE base under liquid nitrogen, loaded on a SPINE puck (Van Der Linden et al. 2014) and transferred to beamline ID23-1 for data collection.

3.3 High-pressure Oxygen derivatization

O2-derivatization was performed in a similar fashion. The WT and G491A crystals were taken to the ESRF High-Pressure Laboratory in crystallization plates, harvested with steel pins topped by polycarbonate tubes of varying diameters according to crystal size and transferred to the high-pressure sample cell. After incubation times with O_2 between 5 and 30 minutes at a pressure above 75 bar, the crystals were directly flash-cooled by dropping the pin in the cold end of the cell, at 77 K; then the system was depressurized and the pin mounted on a SPINE base under liquid nitrogen, loaded on a SPINE puck and transferred to beamlines ID23-1 or ID30B for data collection.

3.4 Structure Analysis

A G126C-Kr dataset was collected to 1.18 and integrated with XDS (Kabsch 2010), analyzed with POINTLESS (Evans, 2006) and scaled and merged AIMLESS (Evans et al. 2013). The data collection and processing statistics are listed in **Table S1**. The crystal structure was determined by the molecular replacement method with PHASER (McCoy 2007) via the CCP4 Graphics User Interface (Potterton et al. 2003) The protein chain coordinates of the large and small subunits of *D. vulgaris* Hildenborough [NiFeSe] hydrogenase crystal structure (PDB 2wpn) (Marques et al. 2010) were used as search models. After an initial refinement with REFMAC (Murshudov et al. 2011) and model editing with COOT (Emsley et al. 2010), refinement was continued with PHENIX. (Adams et al. 2010). Hydrogen atoms were included in calculated positions, solvent molecules were added manually in COOT, anisotropic atomic displacement parameters were refined for all non-hydrogen and non-solvent atoms, occupancy factors were refined for disordered residues and the Kr atoms, and anomalous dispersion parameters were refined for the selenium atom in Sec 489. The refined occupancy factors for the 18 Kr atom sites refined ranged between 15% and 90%. The final G126C-Kr refinement statistics are included in **Table S2**.

Several WT-O_2 and G491A-O_2 datasets were collected. Data was integrated with XDS and their crystal structures were determined by the molecular replacement method as

described for the G126C-Kr structure. After an initial refinement with REFMAC the electron-density maps were inspected to locate O_2 molecules. Following several unsuccessful attempts using crystals incubated for different time periods, it was considered that the standard exposure times suggested by the beamline software to minimize radiation damage to the protein crystals might still be too high, and that the photoelectrons produced by the extremely intense X-ray beam might be actually reducing the trapped O_2 molecules *in situ*, with a subsequent random positional shift of the reduced species in the crystal, effectively rendering them invisible to X-ray crystallography.

Two datasets were then measured at beamline ID30B from a G491A crystal incubated for 15 minutes at 75 bar O_2 using transmissions of 0.2% (low dose – ld) and 2.0% (high dose – hd). The data were integrated with XDS (Kabsch 2010) and AutoPROC (Vonrhein et al. 2011), analyzed with POINTLESS (Evans, 2006) and scaled and merged with STARANISO (Tickle et al. 2016) and AIMLESS (Evans et al., 2013). The data collection and processing statistics are listed in **Table S1**. The low dose and high dose datasets were scaled together with CCP4 SCALEIT (R-factor = 9.0 % to 1.6 Å resolution) for difference Fourier map calculations. Both crystal structures were determined by the molecular replacement method as described for the G126C-Kr structure. After an initial refinement of the low dose structure with REFMAC, an $\mathbf{F_{o,hd} - F_{o,ld}}$ isomorphous difference map with phases calculated from the **ld** structure was calculated and used to locate the O_2 molecules in the **ld** crystal structure, as negative peaks in the map (**Figure 2A**).

The **ld** crystal structure was refined in PHENIX using TLS rigid body refinement of atomic displacement parameters, hydrogens in calculated positions, anomalous dispersion parameters for the selenium atom in Sec 489 and manual inclusion of solvent molecules in COOT using $2|F_o|-|F_c|$ and $|F_o|-|F_c|$ maps. The structure was periodically checked and corrected in COOT against $2|F_o|-|F_c|$ and $|F_o|-|F_c|$ maps. Final R-values were 16.1% and 18.4% for R and R-free, respectively, and the occupancies of the six located O_2 molecules refined to 92%, 73%, 75%, 46%, 39% and 40%. The **hd** structure was refined using a similar protocol to final values of 14.6% and 16.4% for R and R-free, respectively. The occupancies of the five O_2 molecules located in the hd structure refined to 64%, 43%, 43%, 33% and 26%. These five molecules match the positions of the first five O_2 molecules in the ld structure. The final refinement statistics are listed in

Table S2. Structure figures were created using the PyMOL Molecular Graphics System, Version 2.1.0 Open Source (Schrödinger, LLC).

3.5 CAVER Tunnel Calculation

CAVER calculations were done using the PyMOL plug-in (Chovancova et al. 2012) with default parameters (minimum probe radius of 0.9 Å, shell depth of 4 Å, shell radius of 3 Å, a clustering threshold of 3.5 and a starting point optimization with 3 Å maximum distance and a desired radius of 5 Å) and atomic coordinates including hydrogen atoms in calculated positions.

Supplementary Information

Table S1. Data collection and processing statistics

Data Collection	*G126C-Kr*	*G491A-O_2 ld*	*G491A-O_2 hd*
Beamline	ESRF ID23-1	ESRF ID30B	ESRF ID30B
Detector	PILATUS 6M	PILATUS 6M	PILATUS 6M
Wavelength (Å)	0.97242	0.97625	0.97625
Space Group	*C* 2	*C* 2	*C* 2
Unit cell parameters:			
a, b, c (Å)	106.21, 62.98, 110.21	106.10 63.50 109.94	106.16 63.42 110.04
β (°)	105.02	104.74	104.78
Data Processing	XDS	AutoPROC / STARANISO	AutoPROC / STARANISO
Resolution limits of ellipsoid fitted to resolution cut-off surface (Å)	n/a	1.66, 1.74, 1.53	1.37, 1.52, 1.47
Resolution, spherical limits (Å)	45.51 – 1.18 (1.20 – 1.18)	51.0 –1.532 (1.667–1.532)	106.4 – 1.37 (1.48 – 1.37)
Nr. Observations	692400 (32688)	202466 (11845)	266160 (15428)
Unique reflections	225011 (10897)	80400 (4020)	115312 (5766)
Multiplicity	3.1 (3.0)	2.5 (2.9)	2.3 (2.7)
Completeness, spherical (%)	97.8 (95.9)	75.7 (17.0)	77.8 (18.4)
Completeness, ellipsoidal (%)	n/a	92.3 (63.6)	91.8 (57.2)
R-merge (%) [b]	4.5 (62.3)	7.7 (72.8)	5.2 (62.5)
R-p.i.m. (%) [c]	2.9 (41.7)	5.9 (50.3)	4.2 (45.9)
<I/σ (I)>	8.6 (1.2)	7.6 (1.4)	9.8 (1.5)
CC $^{1/2}$	0.998 (0.669)	0.992 (0.502)	0.994 (0.566)
ISa	22.7	16.5	21.1
Wilson B (Å^2)	10.1	21.0	20.2
Z [d]	1	1	1
Estimated V_M [e]	2.03	2.05	2.05
Estimated Solvent Content (%) [e]	39.6	39.9	39.9

[a] Values in parentheses refer to the highest resolution shell; [b] R-merge = merging R-factor, $(\Sigma_{hkl} \Sigma_i |I_i(hkl) - \langle I(hkl)\rangle|) / (\Sigma_{hkl} \Sigma_i I(hkl)) \times 100$ %; [c] R-p.i.m. = precision-independent R-factor, $\Sigma_{hkl} [1/(N-1)]^{1/2} \Sigma_i |I_i(hkl) - \langle I(hkl)\rangle| / (\Sigma_{hkl} \Sigma_i I_i(hkl)) \times 100$ % (Diederichs and Karplus 1997). For each unique Bragg reflection with indices (hkl), I_i is the i-th observation of its intensity and N its multiplicity; [d] Nr. molecules in the asymmetric unit; [e] According to (Matthews 1968).

Table S2. Refinement statistics

Dataset	G126C-Kr	G491A-O_2 ld	G491A-O_2 hd
Resolution limits (Å)[a]	45.51 – 1.18 (1.194 – 1.180)	51.0 – 1.532 (1.550 – 1.532)	51.0 – 1.37 (1.385 – 1.370)
R_{work} [b]	0.114 (0.276)	0.161 (0.309)	0.146 (0.257)
R_{free} [c]	0.134 (0.303)	0.184 (0.309)	0.164 (0.495)
ML coordinate error estimate (Å) [d]	0.10	0.13	0.12
Model composition and completeness			
Regions omitted [e]	12B	1A-4A; 12B-13B	1A-4A; 12B-13B
Non-hydrogen protein atoms [f]	6085	5927	5927
Ligand/ion atoms	47	45	45
Solvent molecules	629	279	333
Kr atoms / O_2 molecules	18	6	5
Glycerol molecules	4	1	1
Mean B values (Å²) [g]			
Protein	16.3	24.2	22.9
Ligand/ion	12.4	19.6	17.7
Solvent	29.8	29.5	30.5
Kr atoms / O_2 molecules	27.7	36.2	34.6
Glycerol	42.2	37.8	33.1
Model r.m.s. deviations from ideality			
Bond lengths (Å)	0.012	0.004	0.007
Bond angles (°)	1.601	1.107	1.259
Chiral centers (Å³)	0.101	0.050	0.082
Planar groups (Å)	0.009	0.005	0.006
Model validation [h]			
% Ramachandran outliers	0.13	0.13	0.13
% Ramachandran favored	97.6	97.6	98.01
% Rotamer outliers	0.77	0.64	0.80
C^{β} outliers	2	0	0
Clash score	1.86	1.85	1.51

[a] Values in parentheses refer to the highest resolution shell; [b] $R_{work} = (\Sigma_{hkl} ||F_{obs}(hkl)| - |F_{calc}(hkl)||) / (\Sigma_{hkl} |F_{obs}(hkl)|) \times 100$ %; [c] R_{free} is calculated as above from a random sample containing 5% of the total number of independent reflections measured; [d] Maximum-likelihood estimate by PHENIX; [e] HysA (large subunit) is chain B, HysB (small subunit is chain A); [f] Including atoms in the alternate conformations of disordered groups of residues; [g] Calculated from isotropic or equivalent isotropic B-values; [h] Calculated with MolProbity (Chen et al. 2010).

Bibliography

Adams, P. D., Afonine, P. V., Bunkóczi, G., Chen, V. B., Davis, I. W., Echols, N., … Zwart, P. H. (2010). PHENIX: A comprehensive Python-based system for macromolecular structure solution. *Acta Crystallographica Section D: Biological Crystallography*, *66*(2), 213–221. https://doi.org/10.1107/S0907444909052925

Bondi, A. (1964). Van der waals volumes and radii. *Journal of Physical Chemistry*, *68*(3), 441–451. https://doi.org/10.1021/j100785a001

Buhrke, T., Lenz, O., Krauss, N., & Friedrich, B. (2005). Oxygen tolerance of the H2-sensing [NiFe] hydrogenase from Ralstonia eutropha H16 is based on limited access of oxygen to the active site. *Journal of Biological Chemistry*, *280*(25), 23791–23796. https://doi.org/10.1074/jbc.M503260200

Chen, V. B., Arendall, W. B., Headd, J. J., Keedy, D. A., Immormino, R. M., Kapral, G. J., … Richardson, D. C. (2010). MolProbity: all-atom structure validation for macromolecular crystallography. *Acta Crystallographica. Section D, Biological Crystallography*, *66*(Pt 1), 12–21. https://doi.org/10.1107/S0907444909042073

Chovancova, E., Pavelka, A., Benes, P., Strnad, O., Brezovsky, J., Kozlikova, B., … Damborsky, J. (2012). CAVER 3.0: A Tool for the Analysis of Transport Pathways in Dynamic Protein Structures. *PLoS Computational Biology*, *8*(10), e1002708. https://doi.org/10.1371/journal.pcbi.1002708

Cohen, J., Kim, K., King, P. W., Seibert, M., & Schulten, K. (2005). Finding gas diffusion pathways in proteins: Application to O2 and H2 transport in CpI [FeFe]-hydrogenase and the role of packing defects. *Structure*, *13*(9), 1321–1329. https://doi.org/10.1016/j.str.2005.05.013

Cohen, J., Kim, K., Posewitz, M. C., Ghirardi, M. L., Schulten, K., Seibert, M., & King, P. W. (2005). Molecular dynamics and experimental investigation of H(2) and O(2) diffusion in [Fe]-hydrogenase. *Biochem.Soc.Trans.*, *33*(0300-5127 (Print)), 80–82. https://doi.org/10.1042/BST0330080.Molecular

Dementin, S., Belle, V., Bertrand, P., Guigliarelli, B., Adryanczyk-Perrier, G., De Lacey, A. L., … Léger, C. (2006). Changing the ligation of the distal [4Fe4S] cluster in NiFe hydrogenase impairs inter- and intramolecular electron transfers. *Journal of the American Chemical Society*, *128*(15), 5209–5218. https://doi.org/10.1021/ja060233b

Diederichs, K., & Karplus, P. A. (1997). Improved R-factors for diffraction data analysis in macromolecular crystallography. *Nature Structural Biology*, *4*(4), 269–275. https://doi.org/10.1038/nsb0497-269

Duché, O., Elsen, S., Cournac, L., & Colbeau, A. (2005). Enlarging the gas access channel to the active site renders the regulatory hydrogenase HupUV of Rhodobacter capsulatus O2 sensitive without affecting its transductory activity. *FEBS Journal*, *272*, 3899–3908. https://doi.org/10.1111/j.1742-4658.2005.04806.x

Emsley, P., Lohkamp, B., Scott, W. G., & Cowtan, K. (2010). Features and development of Coot. *Acta Crystallographica Section D: Biological Crystallography*, *66*(4), 486–501. https://doi.org/10.1107/S0907444910007493

Evans, P. (2006). Scaling and assessment of data quality. *Acta Crystallographica Section D Biological Crystallography*, *62*(1), 72–82. https://doi.org/10.1107/S0907444905036693

Evans, P. R., & Murshudov, G. N. (2013). How good are my data and what is the resolution? *Acta Crystallographica. Section D, Biological Crystallography*, *69*(Pt 7), 1204–1214. https://doi.org/10.1107/S0907444913000061

Kabsch, W. (2010). XDS. *Acta Crystallographica. Section D, Biological Crystallography*, *66*(Pt 2), 125–132. https://doi.org/10.1107/S0907444909047337

Kalms, J., Schmidt, A., Frielingsdorf, S., Van Der Linden, P., Von Stetten, D., Lenz, O., … Scheerer, P. (2016). Krypton Derivatization of an O2-Tolerant Membrane-Bound [NiFe] Hydrogenase Reveals a Hydrophobic Tunnel Network for Gas Transport. *Angewandte Chemie - International Edition*, *55*(18), 5586–5590. https://doi.org/10.1002/anie.201508976

Lafumat, B., Mueller-Dieckmann, C., Leonard, G., Colloc'H, N., Prangé, T., Giraud, T., … Carpentier, P. (2016). Gas-sensitive biological crystals processed in pressurized oxygen and krypton atmospheres: Deciphering gas channels in proteins using a novel "soak-and-freeze" methodology. *Journal of Applied Crystallography*, *49*(5), 1478–1487. https://doi.org/10.1107/S1600576716010992

Leroux, F., Dementin, S., Burlat, B., Cournac, L., Volbeda, A., Champ, S., … Léger, C. (2008). Experimental approaches to kinetics of gas diffusion in hydrogenase. *Proceedings of the National Academy of*

Sciences of the United States of America, *105*(32), 11188–11193. https://doi.org/10.1073/pnas.0803689105

Liebgott, P.-P., de Lacey, A. L., Burlat, B., Cournac, L., Richaud, P., Brugna, M., … Dementin, S. (2011). Original design of an oxygen-tolerant [NiFe] hydrogenase: major effect of a valine-to-cysteine mutation near the active site. *Journal of the American Chemical Society*, *133*(4), 986–997. https://doi.org/10.1021/ja108787s

Liebgott, P.-P., Dementin, S., Léger, C., & Rousset, M. (2011). Towards engineering O2-tolerance in [Ni–Fe] hydrogenases. *Energy & Environmental Science*, *4*(1), 33. https://doi.org/10.1039/c0ee00093k

Lubitz, W., Ogata, H., Rudiger, O., & Reijerse, E. (2014). Hydrogenases. *Chemical Reviews*, *114 (8)*, 4081–4148. https://doi.org/10.1021/cr4005814

Marques, M., Coelho, R., De Lacey, A. L., Pereira, I. A. C., & Matias, P. M. (2010). The three-dimensional structure of [NiFeSe] hydrogenase from Desulfovibrio vulgaris Hildenborough: a hydrogenase without a bridging ligand in the active site in its oxidised, "as-isolated" state. *Journal of Molecular Biology*, *396*(4), 893–907. https://doi.org/10.1016/j.jmb.2009.12.013

Marques, M., Coelho, R., Pereira, I. A. C., & Matias, P. M. (2013). Redox state-dependent changes in the crystal structure of [NiFeSe] hydrogenase from Desulfovibrio vulgaris Hildenborough. *International Journal of Hydrogen Energy*, *38*(21), 8664–8682. https://doi.org/10.1016/j.ijhydene.2013.04.132

Marques, M., Tapia, C., Gutiérrez-Sanz, Ó., Ramos, A. R., Keller, K. L., Wall, J. D., … Pereira, I. A. C. (2017). The direct role of selenocysteine in [NiFeSe] hydrogenase maturation and catalysis. *Nature Chemical Biology*, *13*(5), 554–550. https://doi.org/10.1038/nchembio.2335

Matthews, B. W. (1968). Solvent content of protein crystals. *Journal of Molecular Biology*, *33*(2), 491–497. https://doi.org/10.1016/0022-2836(68)90205-2

McCoy, A. J. (2007). Solving structures of protein complexes by molecular replacement with Phaser. *Acta Crystallographica. Section D, Biological Crystallography*, *63*(Pt 1), 32–41. https://doi.org/10.1107/S0907444906045975

Montet, Y., Amara, P., Vernede, X., Hatchikian, E. C., Field, M., Frey, M., & Fontecilla-Camps, J. (1997). Gas access to the active site of Ni-Fe hydrogenases probed by X-ray crystallography and molecular dynamics. *Nature Structural Biology*, *4*, 523–526.

Murshudov, G. N., Skubák, P., Lebedev, A. A., Pannu, N. S., Steiner, R. A., Nicholls, R. A., … Vagin, A. A. (2011). REFMAC5 for the refinement of macromolecular crystal structures. *Acta Crystallographica Section D: Biological Crystallography*, *67*(4), 355–367. https://doi.org/10.1107/S0907444911001314

Potterton, E., Briggs, P., Turkenburg, M., & Dodson, E. (2003). A graphical user interface to the CCP4 program suite research papers A graphical user interface to the CCP 4 program suite. *Acta Crystallographica Section D Biological Crystallography*, 1131–1137.

Teixeira, V. H., Baptista, A. M., & Soares, C. M. (2006). Pathways of H2 toward the active site of [NiFe]-hydrogenase. *Biophysical Journal*, *91*(6), 2035–2045. https://doi.org/10.1529/biophysj.106.084376

Tickle, I., Bricogne, G., Flensburg, C., Keller, P., Paciorek, W., Sharff, A., & Vonrhein, C. (2016). STARANISO anisotropy & amp; Bayesian estimation server. Retrieved May 16, 2019, from http://staraniso.globalphasing.org/cgi-bin/staraniso.cgi

Van Der Linden, P., Dobias, F., Vitoux, H., Kapp, U., Jacobs, J., Mc Sweeney, S., … Carpentier, P. (2014). Towards a high-throughput system for high-pressure cooling of cryoprotectant-free biological crystals. *Journal of Applied Crystallography*, *47*(2), 584–592. https://doi.org/10.1107/S1600576714000855

Volbeda, A., Charon, M.-H., Piras, C., Hatchikian, E. C., Frey, M., & Fontecilla-Camps, J. C. (1995). Crystal structure of the nickel–iron hydrogenase from Desulfovibrio gigas.pdf. *Nature*.

Volbeda, A., Montet, Y., Vernâ, X., Hatchikian, E. C., & Fontecilla-camps, J. C. (2002). High-resolution crystallographic analysis of Desulfovibrio fructosovorans [NiFe] hydrogenase. *International Journal of Hydrogen Energy*, *27*, 1449–1461.

Vonrhein, C., Flensburg, C., Keller, P., Sharff, A., Smart, O., Paciorek, W., … Bricogne, G. (2011). Data processing and analysis with the autoPROC toolbox. *Acta Crystallographica. Section D, Biological Crystallography*, *67*(Pt 4), 293–302. https://doi.org/10.1107/S0907444911007773

Wang, P., Best, R. B., & Blumberger, J. (2011a). A microscopic model for gas diffusion dynamics in a [NiFe]-hydrogenase. *Physical Chemistry Chemical Physics : PCCP*, *13*(17), 7708–7719. https://doi.org/10.1039/c0cp02098b

Wang, P., Best, R. B., & Blumberger, J. (2011b). Multiscale simulation reveals multiple pathways for H2 and O2 transport in a [NiFe]-hydrogenase. *Journal of the American Chemical Society*, *133*(10), 3548–

3556. https://doi.org/10.1021/ja109712q

Zacarias, S., Temporão, A., del Barrio, M., Fourmond, V., Leger, C., Matias, P. M., & Pereira, I. A. C. (2019). A hydrophilic channel is involved in oxidative inactivation of a [NiFeSe] hydrogenase. *ACS Catalysis*. https://doi.org/10.1021/acscatal.9b02347

Zacarias, S., Vélez, M., Pita, M., De Lacey, A. L., Matias, P. M., & Pereira, I. A. C. (2018). Characterization of the [NiFeSe] hydrogenase from Desulfovibrio vulgaris Hildenborough. In *Methods in Enzymology* (Vol. 613, pp. 169–201). https://doi.org/10.1016/bs.mie.2018.10.003

CHAPTER V

[NiFeSe] HYDROGENASE VARIANTS AND O_2 STABILITY

1. Recreating the proximal FeS cluster of an O_2 tolerant hydrogenase in a [NiFeSe] hydrogenase

The crucial impact of the proximal [FeS] cluster on the O_2-tolerant MBHs, led us to attempt to reduce the O_2 sensitivity of the [NiFeSe] hydrogenase from *D. vulgaris* Hildenborough by introducing the two additional Cys residues into the coordination sphere of the proximal [4Fe4S] cluster. For that, we performed single and double mutations on the glycines that correspond to the supernumerary cysteines on the O_2-tolerant MBHs. In the *D. vulgaris* Hildenborough hydrogenase the proximal [4Fe4S] cluster is coordinated by Cys19, Cys21, Cys121 and Cys159 (**Figure 1**). Gly20 forms a peptide bond with Cys21. The Gly126 is in the vicinity proximal FeS cluster (≈ 6 Å).

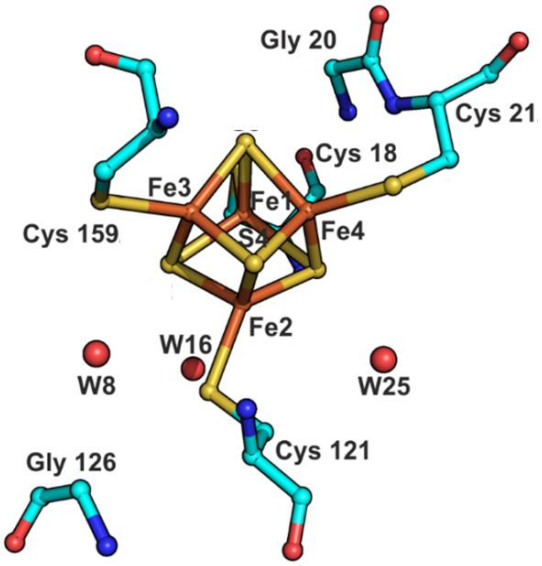

Figure 1: Proximal FeS cluster in the reduced state of the [NiFeSe] hydrogenase from *D. vulgaris* Hildenborough (5JSK). A cubane shaped [4Fe4S] cluster is coordinated by four cysteine residues. Three conserved water molecules in the surroundings of the cluster are also presented.

The variants created were **G126C**, **G20C** and **G126CG20C**. No protein could be obtained for G20C and G126CG20C, but the variant G126C was successfully purified and characterized. It has an H_2 production of 3004 ± 73 s^{-1}, corresponding to 37% of the WT activity. Well diffracting crystals were obtained and a diffraction data set to 1.40 Å

resolution was collected at ESRF beamline ID23-2. The data were integrated with XDS (Kabsch 2010), analyzed with POINTLESS (Evans 2006) and scaled and merged with AIMLESS (Evans et al. 2013). The data collection and processing statistics are listed in **Table V1**. The structure was determined by the molecular replacement as described for the G126C-Kr structure in Chapter IV and refined with PHENIX using isotropic refinement of atomic displacement parameters, hydrogens in calculated positions and manual inclusion of solvent molecules in COOT using 2|Fo|-|Fc| and |Fo|-|Fc| maps. The structure was periodically checked and corrected in COOT against 2|Fo|-|Fc| and |Fo|-|Fc| maps. Final R-values were 12.6% and 15.9% for R and R-free. The final refinement statistics are listed in **Table V2**.

The structure reveals that the introduced Cys126 did not bind to the proximal cluster, not mimicking the situation found in the O_2 tolerant MBHs [NiFe] hydrogenases. Interestingly, one of the conserved waters was displaced by the introduction of this residue (**Figure 2**), leading to a less oxidized FeS cluster in comparison with the wild type structure (13% vs. 25%). All the structural parameters regarding the active site in this variant are similar to the wild type.

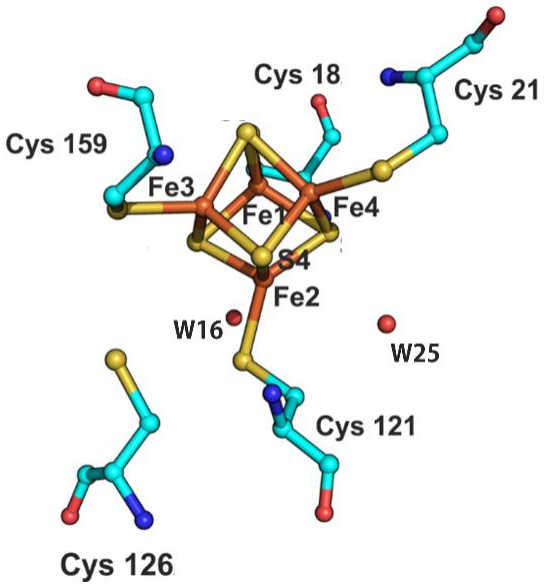

Figure 2: Proximal FeS cluster of the variant G126C. All the aspects of the cluster are similar to the WT, expect the absence of water 8, displaced by the introduction of the Cys126.

No protein could be obtained for variants G20C and G126CG20C. In fact it is known that changing the residues that bind or that are in the vicinity of [FeS] clusters often results in no incorporation of these cofactors or expression problems (Moulis et al. 1996). Attempts to recreated a proximal FeS cluster on the O_2 sensitive [NiFe] from *D. fructosovorans*, also failed to produce viable protein (Liebgott, de Lacey, et al. 2011).

Table V1. Data collection and processing statistics

Data Collection	***G126C***
Beamline	ESRF ID23-2
Detector	PILATUS2 3M
Wavelength (Å)	0.8726
Space Group	*P* 2_1
Unit cell parameters:	
a, b, c (Å)	59.81, 91.13, 63.68
β (°)	105.96
Data Processing	XDS
Resolution (Å)	57.5 – 1.40 (1.43 – 1.40)
Nr. Observations	473017 (20477)
Unique reflections	123932 (5695)
Multiplicity	3.8 (3.6)
Completeness, spherical (%)	96.7 (90.2)
R-merge (%) [b]	10.7 (110.5)
R-p.i.m. (%) [c]	6.3 (66.2)
<I/σ (I)>	8.6 (1.1)
CC [1/2]	0.997 (0.346)
ISa	23.9
Wilson B (Å²)	9.5
Z [d]	1
Estimated V_M [e]	1.90
Estimated Solvent Content (%) [e]	35.4

[a] Values in parentheses refer to the highest resolution shell; [b] R-merge = merging R-factor, $(\Sigma_{hkl} \Sigma_i |I_i(hkl) - \langle I(hkl)\rangle|) / (\Sigma_{hkl} \Sigma_i I(hkl)) \times 100$ %; [c] R-p.i.m. = precision-independent R-factor, $\Sigma_{hkl} [1/(N-1)]^{1/2} \Sigma_i |I_i(hkl) - \langle I(hkl)\rangle| / (\Sigma_{hkl} \Sigma_i I_i(hkl)) \times 100$ % (Diederichs and Karplus 1997). For each unique Bragg reflection with indices (hkl), I_i is the i-th observation of its intensity and N its multiplicity; [d] Nr. molecules in the asymmetric unit; [e] According to (Matthews 1968).

Table V.2. Refinement statistics

Dataset	G126C
Resolution limits (Å)[a]	49.2 – 1.40 (1.42 – 1.40)
R_{work} [b]	0.126 (0.268)
R_{free} [c]	0.159 (0.306)
ML coordinate error estimate (Å) [d]	0.13
Model composition and completeness	
Regions omitted [e]	1A-6A; 12B-14B
Non-hydrogen protein atoms [f]	5855
Ligand/ion atoms	45
Solvent molecules	790
Mean B values (Å²) [g]	
Protein	12.7
Ligand/ion	9.6
Solvent	27.0
Model r.m.s. deviations from ideality	
Bond lengths (Å)	0.010
Bond angles (°)	1.414
Chiral centers (Å³)	0.073
Planar groups (Å)	0.006
Model validation [h]	
% Ramachandran outliers	0.13
% Ramachandran favored	97.5
% Rotamer outliers	0.97
C^{β} outliers	0
Clash score	1.20

[a] Values in parentheses refer to the highest resolution shell; [b] $R_{work} = (\Sigma_{hkl} ||F_{obs}(hkl)| - |F_{calc}(hkl)||) / (\Sigma_{hkl} |F_{obs}(hkl)|) \times 100$ %; [c] R_{free} is calculated as above from a random sample containing 5% of the total number of independent reflections measured; [d] Maximum-likelihood estimate by PHENIX; [e] HysA (large subunit) is chain B, HysB (small subunit is chain A); [f] Including atoms in the alternate conformations of disordered groups of residues; [g] Calculated from isotropic or equivalent isotropic B-values; [h] Calculated with MolProbity (Chen et al. 2010).

2. Role of the medial FeS cluster

As mentioned in the introduction, a significant structural difference between [NiFeSe] hydrogenases and the standard [NiFe] hydrogenases is the medial FeS cluster. In the [NiFeSe] hydrogenases this is a [4Fe4S] cluster with a negative midpoint potential (Teixeira et al. 1990; Valente et al. 2005) and in standard [NiFe] hydrogenases it is a

[3Fe4S] cluster with a very high midpoint potential, appearing to be thermodynamically unfavourable for electron transfer.

To investigate if in fact, the proximal cluster of *D. vulgaris* Hildenborough is more thermodynamically favorable for electron transfer than the [3Fe4S] cluster, we created a variant for Cys259, that is a direct ligand of the FeS cluster, and mutated it to a Pro, the corresponding residue found on standard [NiFe] hydrogenase. However, no stable protein could be obtained, suggesting that this mutation affects the folding of the protein. Additional mutations of residue Cys259 to smaller residues Ala and Gly are now under construction.

3. Role of a His ligand on the distal cluster

In order to test the role of the histidine residue as a coordinating ligand of the distal FeS cluster on [NiFeSe] hydrogenase of *D. vulgaris* Hildenborough we created the variant H208C, in which the hystine is changed to cysteine, the usual coordinating residue of FeS clusters.

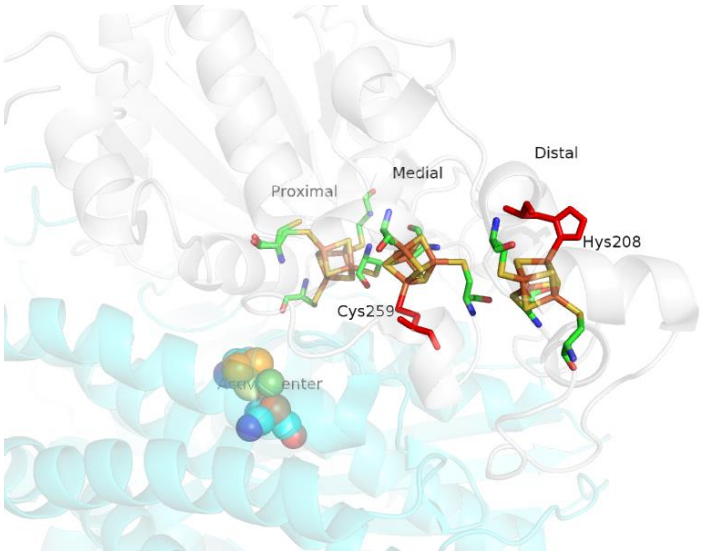

Figure 3: Part of the structure of [NiFeSe] hydrogenase of *D. vulgaris* Hildenborough, empahsing the FeS cluster with the histidine 208 ligating the distal FeS cluster represented in red.

H_2 production of the H208C variant is 4847 ± 163 s^{-1} (59% of the WT) and H_2 oxidation is 4063 ± 208 s^{-1} (92% of the WT) so the bias for H_2 production is not so strong in this variant. Well diffracting crystals of this variant were obtained and the x-ray structure is under analysis.

Electrochemical characterization of the variant on graphite pyrolytic electrodes failed, as no current was detected indicating that the variant could not be attached to this kind of electrode.

4. Tests for evaluating [NiFeSe] hydrogenase stability to O_2

4.1 Observed protection by sulfide on aerobic oxidative inactivation of the [NiFeSe] hydrogenase

We have observed what could be a protective effect of sulfide when the [NiFeSe] hydrogenase (WT and G491A variant) was exposed to air.

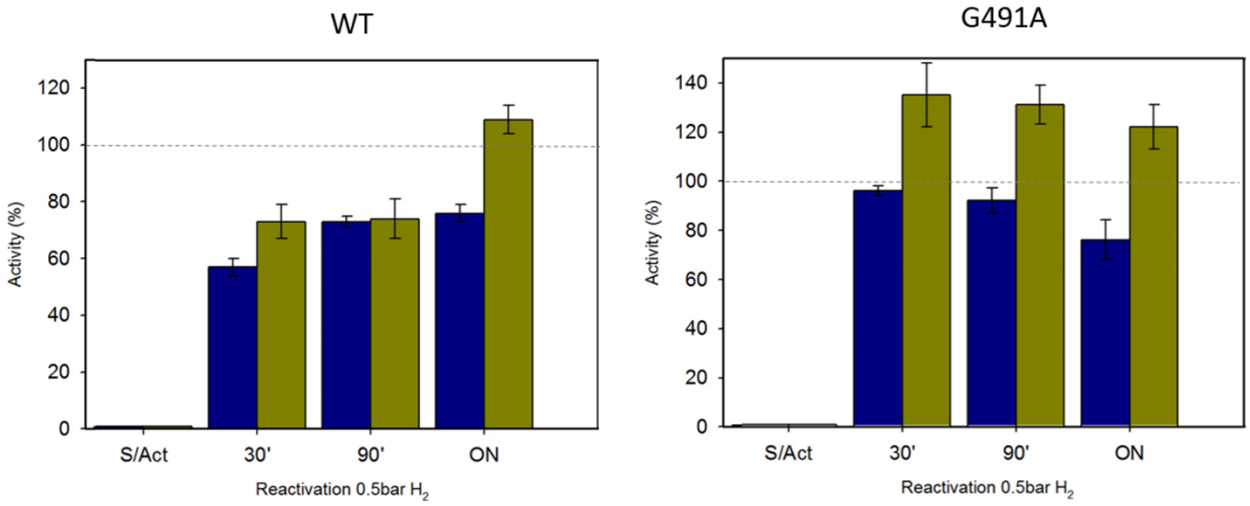

Figure 4: H_2 uptake activity of WT and variants G491A after 4 hours under air (blue) and under air in presence of sulfide (green), followed by different reactivation times under 0.5 bar H_2 (30 and 90 minutes and over-night reactivation), S/act is the control, the protein was not activated with H_2. The activities were normalized by the corresponding maximum activity of each protein.

Like in the experiment presented in chapter 3, figure 8, both enzymes were exposed to air 4 hours and the WT lost around 40% of its activity (blue bars left). The time used for reactivation had little effect on the amount of activity recovered. The G491A variant lost between 10% to 20% activity (blue bars right), also with low variation on the activity recovered with the increased time of reactivation. Both enzymes were exposed to air in the presence of 500 µM of Na_2S buffered with 500 µM Tris-HCl pH 8 (green bars). In the case of the WT it is evident that after an over-night activation the protein could recover its full activity, meaning that the oxidative modifications in that case were not irreversible and the more time spent under reducing conditions could completely reduce them. In the case of the G491A variant, exposure to air in the presence of Na_2S resulted in a state that could be totally reduced even with 30' H_2 reactivation, meaning that no irreversible oxidation took place; actually the enzyme activities after reactivation are above the maximum activities normally obtained for this variant.

A protection confered by Na_2S was report for [FeFe] hydrogenase of *D. desulfuricans* and *C. reinhardtii* (Rodríguez-Maciá et al. 2018). In this protein the Na_2S contributes to the formation of an oxygen stable inactive state that allows the handling of this hydrogenases in air (Rodríguez-Maciá et al. 2018). More studies will be need to understand the observed effect on the [NiFeSe] hydrogenase reactivation after air exposure.

4.2 Activities of prolongued air exposed [NiFeSe] hydrogenase crystals

The majority of oxygen modifications we observed in the structure of [NiFeSe] hydrogenase of *D. vulgaris* Hildenborough took place after prolonged air exposure, that mainly happens during the crystallization process, since the purification protocol (2 days) is faster in comparison with the crystallization of the protein (4 to 6 days, normally).

To have an idea about the structural damages of a longer air exposure, several [NiFeSe] hydrogenase crystals that stood in the crystallization drops for 4 months were dissolved in 20 mM Tris-HCl pH 7.6 and the concentration determined by a UV-Vis (ultraviolet-visible) spectrum.

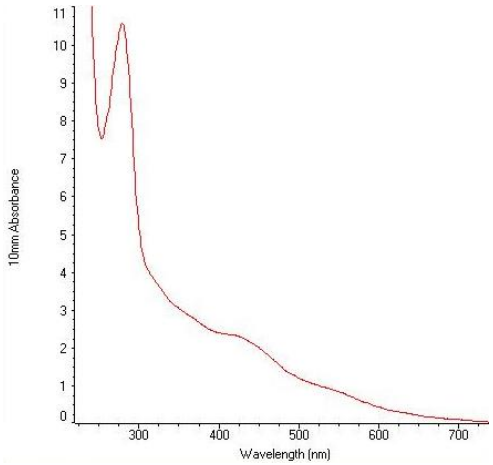

Figure 5: US-Vis spectrum of the [NiFeSe] hydrogenase used to determine the protein concentration based on ε_{410}= 48 000 M^{-1} cm^{-1}, using the protein molecular weight of 88000 g/mol.

The ratio 410 nm / 280 nm was 0.22, below the expected 0.3ratio for the pure protein, indicating that some degradation of the FeS clusters might have occurred.

The H_2 production of the dissolved hydrogenase crystals was 26 ± 9 s^{-1}(corresponding to 0.4% of the initial activity). The H_2 oxidation activity was: 15 ± 1 s^{-1} (0.3% of the initial activity), and an over-nigh reduction under H_2 atmosphere in the presence of MV increased the activity to 45 ± 1 s^{-1} (1.48% of the initial activity). These activities indicate that only a few molecules of hydrogenase survive after prolongued air exposure.

An *in house* x-ray data collection gave a 2 Å diffraction resolution, but to discriminate the oxygen modifications in the structure higher resolution is needed, and so data have to be collected in the synchrotron.

Bibliography:

Chen, V. B., Arendall, W. B., Headd, J. J., Keedy, D. A., Immormino, R. M., Kapral, G. J., … Richardson, D. C. (2010). MolProbity: all-atom structure validation for macromolecular crystallography. *Acta Crystallographica. Section D, Biological Crystallography*, *66*(Pt 1), 12–21. https://doi.org/10.1107/S0907444909042073

Diederichs, K., & Karplus, P. A. (1997). Improved R-factors for diffraction data analysis in macromolecular crystallography. *Nature Structural Biology*, *4*(4), 269–275. https://doi.org/10.1038/nsb0497-269

Evans, P. (2006). Scaling and assessment of data quality. *Acta Crystallographica Section D Biological Crystallography*, *62*(1), 72–82. https://doi.org/10.1107/S0907444905036693

Evans, P. R., & Murshudov, G. N. (2013). How good are my data and what is the resolution? *Acta Crystallographica. Section D, Biological Crystallography*, *69*(Pt 7), 1204–1214. https://doi.org/10.1107/S0907444913000061

Kabsch, W. (2010). XDS. *Acta Crystallographica. Section D, Biological Crystallography*, *66*(Pt 2), 125–132. https://doi.org/10.1107/S0907444909047337

Liebgott, P.-P., de Lacey, A. L., Burlat, B., Cournac, L., Richaud, P., Brugna, M., … Dementin, S. (2011). Original design of an oxygen-tolerant [NiFe] hydrogenase: major effect of a valine-to-cysteine mutation near the active site. *Journal of the American Chemical Society*, *133*(4), 986–997. https://doi.org/10.1021/ja108787s

Matthews, B. W. (1968). Solvent content of protein crystals. *Journal of Molecular Biology*, *33*(2), 491–497. https://doi.org/10.1016/0022-2836(68)90205-2

Moulis, J.-M., Davasse, V., Golinelli, M.-P., Meyer, J., & Quinkal, I. (1996). The coordination sphere of iron-sulfur clusters: lessons from site-directed mutagenesis experiments. *Journal of Biological Inorganic Chemistry*, 13. https://doi.org/10.1007/s007750050017

Rodríguez-Maciá, P., Reijerse, E. J., van Gastel, M., DeBeer, S., Lubitz, W., Rüdiger, O., & Birrell, J. A. (2018). Sulfide Protects [FeFe] Hydrogenases From O2. *Journal of the American Chemical Society*, jacs.8b04339. https://doi.org/10.1021/jacs.8b04339

Teixeira, M., Moura, I., Fauque, G., DerVartanian, D. V, Le Gall, J., Peck, H. D., … Huynh, B. H. (1990). The iron-sulfur centers of the soluble [NiFeSe] hydrogenase, from. *Eur J Biochem*, *386*, 381–386.

Valente, F., Oliveira, S., Gnadt, N., Pacheco, I., Coelho, A., Xavier, A. V, … Pereira, I. A. C. (2005). Hydrogenases in Desulfovibrio vulgaris Hildenborough: structural and physiologic characterisation of the membrane-bound [NiFeSe] hydrogenase. *Journal of Biological Inorganic Chemistry*, *10*(6), 667–682. https://doi.org/10.1007/s00775-005-0022-4

CHAPTER VI

FINAL CONCLUSIONS

Final Conclusions

The work presented in this thesis contributes to a better understanding of [NiFeSe] hydrogenases. We have engineered the *D. vulgaris* Hildenborough [NiFeSe] hydrogenase, aiming to restrict O_2 diffusion to the active site. Others had previously applied a similar rationale in other hydrogenases, restricting the hydrophobic channels (Volbeda et al. 2002; Fontecilla-Camps et al. 2007; Dementin et al. 2009; Liebgott et al. 2010, 2011; Abou Hamdan et al. 2012; Cano et al. 2014), but the problem with that strategy is that O_2 shares the same channel as H_2, so mutations that limit O_2 diffusion had normally a negative impact on the H_2 production/oxidation activity, sometimes abolishing it. We overcame this problem in the [NiFeSe] hydrogenase by performing mutations on a hydrophilic channel found on this hydrogenase that seems to be mainly involved in O_2/ROS diffusion. Although we lost some H_2 production activity, the enzyme variants keep activities above 3500 molecules of H_2 produced per second. However, the strategy of blocking O_2 diffusion inside the protein is most likely insufficient to completely avoid O_2 damages. The complexity of branches and ramification points of the channels, shown here by krypton pressurized crystals, and discussed in previous works based on molecular dynamics simulations (Teixeira et al. 2006; Baltazar et al. 2012), have revealed that transient pathways might be formed through dynamic motions of the protein structure and this could always provide ways for O_2 diffusion. In fact, in the variants present in chapter III, the restriction imposed on O_2 diffusion by mutations G491A and G491S was not sufficient to completely avoid O_2 damages, as Cys75 of G491S variant still presents some degree of oxidation and the proximal FeS cluster of both variants is oxidized. So, other engineering strategies involving different targets besides residues that restrict O_2 access should be considered. Indeed, O_2 tolerance has also been tightly linked to electron transfer reactions involving the proximal FeS cluster (Fritsch et al. 2011; Goris et al.,2011; Lukey et al. 2011; Shomura et al. 2011). Mimicking the coordination arrangement of the proximal FeS cluster found in MBH O_2-tolerant MBH can be theoretically followed as a strategy, although this has not yet been achieved for the *D. vulgaris* Hildenborough [NiFeSe] hydrogenase (chapter IV). Mechanisms involving water molecules and proton transport pathways have also been

suggested to play a role in O_2 tolerance (Sumner et al. 2012; Noth et al. 2015), so exploring their role in [NiFeSe] hydrogenases is also a possibility aiming to further increase its O_2-tolerance.

Because rational mutagenesis may not accurately predict the mutations required to improve oxygen tolerance, random mutagenesis and screening methods are being applied to hydrogenases, namely for [FeFe] hydrogenase, whose maturation machinery is well known (Posewitz et al. 2004) and heterologous expression in *E.coli* is well established (King et al. 2006; Kuchenreuther et al. 2010). Development of high-throughput screening methods is challenging and although there are some descriptions in the literature (Seibert et al. 1998; Wecker et al. 2011; 2014; Ghirardi 2015) including those based on the cell-free technology (Bingham et al., 2012; Koo et al., 2018), screening for both H_2 converting activities and O_2 tolerance has had limited success so far. Applying the principles of directed evolution to the [NiFeSe] hydrogenase is also a possibility but with major challenges to be overcome.

Alternatively to engineering the protein, handling the environment where the hydrogenase is placed has also provided solutions to fight against O_2. Redox polymer hydrogels (Plumeré et al. 2014), chemical treatment with Na_2S (Rodríguez-Maciá et al. 2018), lyophilization (Noth et al. 2015) and protein fusion (Eilenberg et al. 2016) are strategies that have been successfully adopted to protect hydrogenases from O_2-driven damage. Among these options some were already tested for the [NiFeSe] hydrogenase, namely the integration into viologen-based redox polymer hydrogels. This system works as a self-activated catalytic O_2-scavenging mechanism, providing shelter to the electrode-attached hydrogenase from both O_2 attack and high-potential deactivation (Plumeré et al. 2014). The *D. vulgaris Hildenborough* [NiFeSe] hydrogenase was efficiently integrated into such redox hydrogels whose protection allows its application in bioanodes, as a catalyst for H_2 oxidation, achieving high current densities even in presence of 5% O_2 (Ruff et al. 2017). These results paved the way for integrating this hydrogenase as biocatalyst for H_2 oxidation in a H_2/O_2 biofuel cell, in an atmosphere containing between 3% to 5% O_2 (Ruff et al. 2018). Moreover, these authors further enhanced the performance of this hydrogenase, in the same 5% O_2 atmosphere, by applying it on a porous electrode structure that works as gas-diffusion bioelectrodes, allowing high substract fluxes (Szczesny et al. 2018). Overall, these studies represent

incremental steps towards the use of the high performance [NiFeSe] hydrogenase as the biocatalysts for the direct H_2 conversion into electricity, validating the integration of this hydrogenase into the redox hydrogels as a good strategy to overcome its O_2 sensitivity. However, it should be noted that the oxygen levels present in these studies were still lower than atmospheric O_2 partial pressure (~ 21%). Because of the high catalytic activities of [NiFeSe] hydrogenase in both directions, this hydrogenase has also been used in devices for H_2 evolution. Zhao, et al 2019 developed a semi-artificial device for water splitting and concomitant H_2 evolution, with PSI used as light sensitizer providing high energy electrons with the necessary driving force for the H_2 evolution by the [NiFeSe] hydrogenase embedded in the same O_2 protection mechanics made by redox hydrogels (Zhao et al. 2019).

Among the other protective methods mentioned above, chemical treatment with Na_2S on [FeFe] hydrogenase protects this enzyme from O_2 (Rodríguez-Maciá et al. 2018). A protection mechanism provided by sulfide on a [NiFeSe] hydrogenase might also be present and needs to be further explored. Additionally, in that context, the role of a pocket 7 Å away from the active site, whose content has been assigned as an HS^- (mentioned in the introduction), should be further investigated by performing mutations that block the pocket or destabilize the positive charges that hold the negatively charged species.

In conclusion, overcoming the O_2 sensitivity is one of the key challenges for large-scale applications of hydrogenase-based biotechnologies. Here, we provided data that reveal part of the molecular mechanism of the [NiFeSe] hydrogenase inactivation by O_2. Other variants were also created and are being characterized aiming to expand our understanding about the high catalytic activities of this hydrogenase. All these data will provide a deeper understanding of this hydrogenase, which could also lead to inspiring ideas for designing novel biomimetic catalysts.

Bibliography:

Abou Hamdan, A., Liebgott, P.-P., Fourmond, V., Gutiérrez-Sanz, Ó., De Lacey, A. L., Infossi, P., … Léger, C. (2012). Relation between anaerobic inactivation and oxygen tolerance in a large series of NiFe hydrogenase mutants. *Proceedings of the National Academy of Sciences of the United States of America*, *109*(49), 19916–19921. https://doi.org/10.1073/pnas.1212258109

Baltazar, C. S. A., Teixeira, V. H., & Soares, C. M. (2012). Structural features of [NiFeSe] and [NiFe] hydrogenases determining their different properties: a computational approach. *Journal of Biological Inorganic Chemistry*, *17*(4), 543–555. https://doi.org/10.1007/s00775-012-0875-2

Bingham, A. S., Smith, P. R., & Swartz, J. R. (2012). Evolution of an [FeFe] hydrogenase with decreased oxygen sensitivity. *International Journal of Hydrogen Energy*, *37*(3), 2965–2976. https://doi.org/10.1016/j.ijhydene.2011.02.048

Cano, M., Volbeda, A., Guedeney, G., Aubert-Jousset, E., Richaud, P., Peltier, G., & Cournac, L. (2014). Improved oxygen tolerance of the Synechocystis sp. PCC 6803 bidirectional hydrogenase by site-directed mutagenesis of putative residues of the gas diffusion channel. *International Journal of Hydrogen Energy*, *39*(30), 16872–16884. https://doi.org/10.1016/j.ijhydene.2014.08.030

Dementin, S., Leroux, F., Cournac, L., de Lacey, A. L., Volbeda, A., Léger, C., … Rousset, M. (2009). Introduction of methionines in the gas channel makes [NiFe] hydrogenase aero-tolerant. *Journal of the American Chemical Society*, *131*(29), 10156–10164. https://doi.org/10.1021/ja9018258

Eilenberg, H., Weiner, I., Ben-Zvi, O., Pundak, C., Marmari, A., Liran, O., … Yacoby, I. (2016). The dual effect of a ferredoxin-hydrogenase fusion protein in vivo: successful divergence of the photosynthetic electron flux towards hydrogen production and elevated oxygen tolerance. *Biotechnology for Biofuels*, *9*(1), 182. https://doi.org/10.1186/s13068-016-0601-3

Fontecilla-Camps, J. C., Volbeda, A., Cavazza, C., & Nicolet, Y. (2007). Structure/function relationships of [NiFe]- and [FeFe]-hydrogenases. *Chemical Reviews*, *107*(10), 4273–4303. https://doi.org/10.1021/cr050195z

Fritsch, J., Scheerer, P., Frielingsdorf, S., Kroschinsky, S., Friedrich, B., Lenz, O., & Spahn, C. M. T. (2011). The crystal structure of an oxygen-tolerant hydrogenase uncovers a novel iron-sulphur centre. *Nature*, *479*(7372), 249–252. https://doi.org/10.1038/nature10505

Ghirardi, M. L. (2015). Implementation of photobiological H2 production: the O2 sensitivity of hydrogenases. *Photosynthesis Research*. https://doi.org/10.1007/s11120-015-0158-1

Goris, T., Wait, A. F., Saggu, M., Fritsch, J., Heidary, N., Stein, M., … Lenz, O. (2011). A unique iron-sulfur cluster is crucial for oxygen tolerance of a [NiFe]-hydrogenase. *Nature Chemical Biology*, *7*(5), 310–318. https://doi.org/10.1038/nchembio.555

King, P. W., Posewitz, M. C., Ghirardi, M. L., & Seibert, M. (2006). Functional studies of [FeFe] hydrogenase maturation in an Escherichia coli biosynthetic system. *Journal of Bacteriology*, *188*(6), 2163–2172. https://doi.org/10.1128/JB.188.6.2163-2172.2006

Koo, J., & Swartz, J. R. (2018). Improved [FeFe] hydrogenase O2 tolerance suggests feasibility for photosynthetic H2 production. *Metabolic Engineering*. https://doi.org/10.1016/j.ymben.2018.04.024

Kuchenreuther, J. M., Grady-Smith, C. S., Bingham, A. S., George, S. J., Cramer, S. P., & Swartz, J. R. (2010). High-Yield Expression of Heterologous [FeFe] Hydrogenases in Escherichia coli. *PLoS ONE*, *5*(11), e15491. https://doi.org/10.1371/journal.pone.0015491

Liebgott, P.-P., de Lacey, A. L., Burlat, B., Cournac, L., Richaud, P., Brugna, M., … Dementin, S. (2011). Original design of an oxygen-tolerant [NiFe] hydrogenase: major effect of a valine-to-cysteine mutation near the active site. *Journal of the American Chemical Society*, *133*(4), 986–997. https://doi.org/10.1021/ja108787s

Liebgott, P.-P., Leroux, F., Burlat, B., Dementin, S., Baffert, C., Lautier, T., … Léger, C. (2010). Relating diffusion along the substrate tunnel and oxygen sensitivity in hydrogenase. *Nature Chemical Biology*, *6*(1), 63–70. https://doi.org/10.1038/nchembio.276

Lukey, M. J., Roessler, M. M., Parkin, A., Evans, R. M., Davies, R. a, Lenz, O., … Armstrong, F. a. (2011). Oxygen-tolerant [NiFe]-hydrogenases: the individual and collective importance of supernumerary cysteines at the proximal Fe-S cluster. *Journal of the American Chemical Society*, *133*(42), 16881–16892. https://doi.org/10.1021/ja205393w

Noth, J., Kositzki, R., Klein, K., Winkler, M., Haumann, M., & Happe, T. (2015). Lyophilization protects [FeFe]-hydrogenases against O<inf>2</inf>-induced H-cluster degradation. *Scientific Reports*, *5*, 1–10. https://doi.org/10.1038/srep13978

Plumeré, N., Rüdiger, O., Oughli, A. A., Williams, R., Vivekananthan, J., Pöller, S., … Lubitz, W. (2014). A redox hydrogel protects hydrogenase from high-potential deactivation and oxygen damage. *Nature Chemistry*, *6*(September). https://doi.org/10.1038/nchem.2022

Posewitz, M. C., King, P. W., Smolinski, S. L., Zhang, L., Seibert, M., & Ghirardi, M. L. (2004). Discovery of two novel radical S-adenosylmethionine proteins required for the assembly of an active [Fe] hydrogenase. *Journal of Biological Chemistry*, *279*(24), 25711–25720. https://doi.org/10.1074/jbc.M403206200

Rodríguez-Maciá, P., Reijerse, E. J., van Gastel, M., DeBeer, S., Lubitz, W., Rüdiger, O., & Birrell, J. A. (2018). Sulfide Protects [FeFe] Hydrogenases From O2. *Journal of the American Chemical Society*, jacs.8b04339. https://doi.org/10.1021/jacs.8b04339

Ruff, A., Szczesny, J., Marković, N., Conzuelo, F., Zacarias, S., Pereira, I. A. C., … Schuhmann, W. (2018). A fully protected hydrogenase/polymer-based bioanode for high-performance hydrogen/glucose biofuel cells. *Nature Communications*, *9*(1), 3675. https://doi.org/10.1038/s41467-018-06106-3

Ruff, A., Szczesny, J., Zacarias, S., Pereira, I. A. C., Plumeré, N., & Schuhmann, W. (2017). Protection and Reactivation of the [NiFeSe] Hydrogenase from Desulfovibrio vulgaris Hildenborough under Oxidative Conditions. *ACS Energy Letters*, 964–968. https://doi.org/10.1021/acsenergylett.7b00167

Seibert, M., Flynn, T., Benson, D., Tracy, E., & Ghirardi, M. L. (1998). Development of Selection and Screening Procedures for Rapid Identification of H2-Producing Algal Mutants with Increased O2 Tolerance. In *BioHydrogen* (pp. 227–234). Springer US. https://doi.org/10.1007/978-0-585-35132-2_30

Shomura, Y., Yoon, K.-S., Nishihara, H., & Higuchi, Y. (2011). Structural basis for a [4Fe-3S] cluster in the oxygen-tolerant membrane-bound [NiFe]-hydrogenase. *Nature*, *479*(7372), 253–256. https://doi.org/10.1038/nature10504

Sumner, I., & Voth, G. A. (2012). Proton transport pathways in [NiFe]-hydrogenase. *Journal of Physical Chemistry B*, *116*(9), 2917–2926. https://doi.org/10.1021/jp208512y

Szczesny, J., Marković, N., Conzuelo, F., Zacarias, S., Pereira, I. A. C., Lubitz, W., … Ruff, A. (2018). A gas breathing hydrogen/air biofuel cell comprising a redox polymer/hydrogenase-based bioanode. *Nature Communications*, *9*(1), 4715. https://doi.org/10.1038/s41467-018-07137-6

Teixeira, V. H., Baptista, A. M., & Soares, C. M. (2006). Pathways of H2 toward the active site of [NiFe]-hydrogenase. *Biophysical Journal*, *91*(6), 2035–2045. https://doi.org/10.1529/biophysj.106.084376

Volbeda, A., Montet, Y., Vernâ, X., Hatchikian, E. C., & Fontecilla-camps, J. C. (2002). High-resolution crystallographic analysis of Desulfovibrio fructosovorans [NiFe] hydrogenase. *International Journal of Hydrogen Energy*, *27*, 1449–1461.

Wecker, M. S. A., & Ghirardi, M. L. (2014). High-throughput biosensor discriminates between different algal H2-photoproducing strains. *Biotechnology and Bioengineering*, *111*(7), 1332–1340. https://doi.org/10.1002/bit.25206

Wecker, M. S. A., Meuser, J. E., Posewitz, M. C., & Ghirardi, M. L. (2011). Design of a new biosensor for algal H2 production based on the H2-sensing system of Rhodobacter capsulatus. *International Journal of Hydrogen Energy*, *36*(17), 11229–11237. https://doi.org/10.1016/j.ijhydene.2011.05.121

Zhao, F., Wang, P., Ruff, A., Hartmann, V., Zacarias, S., Pereira, I. A. C., … Schuhmann, W. (2019). A photosystem I monolayer with anisotropic electron flow enables Z-scheme like photosynthetic water splitting. *Energy & Environmental Science*, 1–502. https://doi.org/10.1039/C9EE01901D